Journal of Alloys and Compounds 503 (2010) 303–339

Contents lists available at ScienceDirect

Journal of Alloys and Compounds

journal homepage: www.elsevier.com/locate/jallcom

Review

Novel hydrogen storage materials: A review of lightweight complex hydrides

I.P. Jain*, Pragya Jain, Ankur Jain

Centre for Non-Conventional Energy Resources, University of Rajasthan, Jaipur 302004, India

ARTICLE INFO

Article history:
Received 4 March 2010
Received in revised form 23 April 2010
Accepted 28 April 2010
Available online 31 May 2010

Keywords:
Hydrogen storage
Light weight hydrides
Complex hydrides

ABSTRACT

The world is facing energy shortage and has become increasingly depending on new methods to store and convert energy for new, environmentally friendly methods of transportation and electrical energy generation as well as for portable electronics. Mobility – the transport of people and goods – is a socioeconomic reality that will surely increase in the coming years. Non-renewable fossil fuels are projected to decline sharply after 20–30 years. CO_2 emission from burning such fuels is the main cause for global warming. Currently whole world is seeking international commitment to cut emissions of greenhouse gases by 60% by 2050. Hydrogen which can be produced with little or no harmful emissions has been projected as a long term solution for a secure energy future. Increasing application of hydrogen energy is the only way forward to meet the objectives of Department of Energy (DOE), USA, i.e. reducing green house gases, increasing energy security and strengthening the developing countries economy. Any transition from a carbon-based/fossil fuel energy system to a hydrogen based economy involves overcoming significant scientific, technological and socio-economic barriers before ultimate implementation of hydrogen as the clean energy source of the future. Lot of research is going on in the world to find commercially viable solutions for hydrogen production, storage, and utilization, but hydrogen storage is very challenging, as application part of hydrogen energy totally depend on this. During early nineties and now also hydrogen storage as gas, liquid and metal hydride has been undertaken to solve the problem of hydrogen storage and transportation for the utilization as hydrogen energy, but none of these roots could became commercially viable along with the safety aspects for gas and liquid. With the result many new novel materials appeared involving different principles resulting in a fairly complex situation with no correlation between any two materials. In the present review article the fundamental understanding of the physical, chemical and structural properties of light weight hydride materials, e.g. Alanates, Borohydrides, Amide Borohydrides, Amide-Imide system, Amineborane and Alane for hydrogen storage has been presented. Lot of details of these materials has been incorporated such as synthesis, crystal structure, thermodynamics and kinetics of hydrogenation–dehydrogenation processes, reversibility and hydrogen storage capacity has been presented.

Contents

* Corresponding author.
E-mail addresses: ipjain46@sify.com, ipjain46@gmail.com (I.P. Jain), ankurjainankur@sify.com (A. Jain).

0925-8388/$ – see front matter © 2010 Elsevier B.V. All rights reserved.
doi:10.1016/j.jallcom.2010.04.250

1. Introduction

Today the world is facing one of the most serious problems of depleting sources of conventional energy such as fossil fuels (coal, natural gas and petroleum) which when used results in lot of problems, e.g. global warming, acid rains, climate change and pollution, which are degrading our environment resulting in the poor quality of life on this planet. There is constant search of alternate fuel to solve energy shortage which can provide us energy without pollution. Hence most frequently discussed source is hydrogen which when burnt in air produces a clean form of energy. The interest in hydrogen as energy of the future is due to it being a clean energy, most abundant element in the universe, the lightest fuel, richest in energy per unit mass and unlike electricity, it can be easily stored.

Hydrogen gas is now considered to be the most promising fuel of the future for various applications, e.g. it can generate electricity, useful in cooking food, fuel for automobiles, hydrogen powered industries, jet planes, hydrogen village and for all our domestic energy requirements. Hydrogen as a fuel has already found applications in experimental cars and all the major car companies are in competition to build a commercial car and most probably they may market hydrogen fuel automobiles in near future. Hydrogen is already being used as the fuel of choice for space programmes around the world. It will be used to power aerospace transports to build the international space station, as well as to provide electricity and portable water for its inhabitants.

Hydrogen is the simplest and lightest element of our universe with only one proton and one electron [1], not available as element but in the form of compounds such as water needed for survival of human beings and hydrocarbons being used as a fuel today. Hydrogen has potential to solve fuel needs having three times higher energy efficient compared to petroleum. The interest in hydrogen as an energy alternative was initiated in the late 1960s [2] and has grown more and more in the 1990s [3]. There have been tremen-

Table 1
Crystal structure and hydrogenation/dehydrogenation properties of alanates.

S. no.	Materials and their formation/dissociation reaction	Crystal structure; space group; lattice parameters (Å)	Hydrogen capacity (wt%)	Dehydrogenation temperature (°C)	Dissociation enthalpy (kJ mol^{-1} H_2)	Ref.
1.	$NaAlH_4$ $Na + Al + 2H_2 \xrightarrow{T<270-280\,^\circ C;\ P>175\ bar} NaAlH_4$ $NaAlH_4 \Leftrightarrow \frac{1}{3}Na_3AlH_6 + \frac{2}{3}Al + H_2$ $\frac{1}{3}Na_3AlH_6 \Leftrightarrow NaH + Al + \frac{1}{2}H_2$	Tetragonal; $I4_1/a$, $a = 4.9802$, $c = 11.1482$	5.6	210–220 (1st step); >250 (2nd step)	37 (1st step); 47 (2nd step)	[33,41,48]
2.	$LiAlH_4$ $LiH + Al + \frac{3}{2}H_2 \rightarrow LiAlH_4$ $3LiAlH_4 \rightarrow Li_3AlH_6 + 2Al + 3H_2$ $Li_3AlH_6 \rightarrow 3LiH + Al + \frac{3}{2}H_2$ $3LiH + 3Al \rightarrow 3LiAl + \frac{3}{2}H_2$	Monoclinic; $P2_1/C$ $a = 4.8254$ $b = 7.8040$, $c = 7.8968$	7.9	160–180 (1st step); 180–220 (2nd step)	−10 (1st step); 25 (2nd step)	[74,77,89]
3.	$Mg(AlH_4)_2$ $2NaAlH_4 + MgCl_2 \rightarrow Mg(AlH_4)_2 + 2NaCl$ $Mg(AlH_4)_2 \rightarrow MgH_2 + 2Al + 3H_2$ $MgH_2 \rightarrow Mg + H_2$	Trigonal; $P\bar{3}m1$ $a = 5.1949$, $c = 5.8537$	9.3	110–200 (1st step); 240–380 (2nd step)	41 (1st step); 76 (2nd step)	[23,102,108,110]
4.	$KAlH_4$ $KH + Al \xrightarrow{T=270\,^\circ C;\ P>175\ bar} KAlH_4$ $3KAlH_4 \rightarrow K_3AlH_6 + 2Al + 3H_2$ $K_3AlH_6 \rightarrow 3KH + Al + \frac{3}{2}H_2$ $3KH \rightarrow 3K + \frac{3}{2}H_2$	Orthorhombic; $Pnma$ $a = 9.009$ $b = 5.767$ $c = 7.399$	5.7	300 (1st step) 340 (2nd step) 380 (3rd step)	55 (1st step); 70 (2nd step)	[115,118,119]
5.	$Ca(AlH_4)_2$ $4CaH_2 + 2AlCl_3 \xrightarrow{THF} Ca(AlH_4)_2 + 3CaCl_2$ $CaCl_2 + 2NaAlH_4 \rightarrow Ca(AlH_4)_2 + 2NaCl$ $Ca(AlH_4)_2 \rightarrow CaAlH_5 + Al + \frac{3}{2}H_2$ $CaAlH_5 \rightarrow CaH_2 + Al + \frac{3}{2}H_2$	Monoclinic; $P2_1/n$ $a = 8.267$ $b = 10.477$ $c = 14.677$	5.9	127 (1st step) 250 (2nd step)	−7 (1st step); 28 (2nd step)	[123,126,130,132,133]
6.	Na_2LiAlH_6 $2NaAlH_4 + 2LiH \rightarrow Na_2LiAlH_6 + LiAlH_4$ $Na_2LiAlH_6 \rightarrow 2NaH + LiH + Al + \frac{3}{2}H_2$	Cubic; $Fm\bar{3}m$ $a = 7.38484$	3.2	245	53.5 ± 1.2	[135,137,139]
7.	K_2NaAlH_6 $NaAlH_4 + 2KH \rightarrow K_2NaAlH_6$	Cubic; $Fm\bar{3}m$ $a = 8.118$	2.8	325	98	[144]

dous efforts to produce it on a large scale [4]. However, there are still many problems to implement hydrogen economy in daily life, out of which hydrogen storage is major bottleneck. High pressure storage [5] and cryo-storage [6] are not suitable way for practical vehicular application due to their low energy density and also due to safety reasons associated with them. Due to these reasons tremendous efforts have been made to search solid materials which can hold hydrogen reversibly. As a target given by DOE, USA, a solid hydrogen storage material should have few commandments [7] such as: (i) storage capacity to be at least 6.5 wt%, (ii) desorption temperature to be 60–120 °C, (iii) low cost and (iv) low toxicity.

Metal hydrides [8–13], carbon materials [14–16], activated charcoal [17,18] have been tested to fulfill above requirements but unfortunately none of them could show satisfactory performance for commercial vehicular application. Recently, complex hydrides offered a possibility to design a potential hydrogen storage system due to their light weight and number of atoms per metal atom. Complex hydride is termed as a group of materials which are combination of hydrogen and group 1, 2, 3 light metals, e.g. Li, Na, B and Al [19]. Typical complex hydrides include alanates, borohydrides, amides, imides, alane etc. To optimize a material for hydrogen storage one should have knowledge of their structural, thermodynamical and kinetics of hydrogenation properties. This review presents an up-to-date summary of all the complex hydrides one by one.

2. Alanates

The term 'alanate' also known as 'aluminohydrides' refers to a family of compounds consisting of hydrogen and aluminum. $NaAlH_4$ is the most popular material of this family. With the search of reversibility of $NaAlH_4$ by Bogdanovic et al. [20], a lot of methods of preparation have been developed to prepare these aluminohydrides and to study their structural and thermodynamical properties [21,22]. The attractive feature of alanates is related to their easy accessibility. While sodium and lithium alanates are commercially available, magnesium alanate can be easily synthesized from sodium alanate and MgH_2 via a metathesis reaction [23]. Potassium alanate can also be formed from potassium hydride and aluminium under high pressure and temperature [24]. In this section we will explore the structural, and hydrogenation properties and the recent progress for different alanates. Important parameters, viz. crystal structure, hydrogen capacity, dissociation temperature and enthalpy of alanates are summarized in Table 1.

2.1. Sodium alanate

2.1.1. Formation and structure

Sodium alanate was first synthesized in the mid 1950s by Finholt et al. [25]. A direct synthesis of $NaAlH_4$ from sodium hydride, aluminium and hydrogen under pressure in various solvents came into picture in the early sixties [26–28]. The above reaction from elements in the absence of solvents was described by Dymova et al. [24] later on:

$$Na + Al + 2H_2 \overset{T<270-280\ ^\circ C, P>175\ bar}{\longrightarrow} NaAlH_4 \quad (1)$$

Zaluski et al. [29] has introduced a new method, mechanochemical synthesis for the formation of various complex hydrides, which is a combined process of chemical reaction that occurs during mechanical treatment of the reagents.

In the revolutionary work of Bogdanovic [20], $NaAlH_4$ was for the 1st time doped with Ti by a suspension of $NaAlH_4$ in β-$TiCl_3$/ether and $Ti(OBu)_4$/ether. The ether was evaporated and the product was dried until a constant weight was reached.

Wang et al. established an alternative method for the doping of the Ti precursor by direct milling of NaH and Al with few mole percent of off the shelf Ti powder [30]. They claimed superiority of this method over the other methods in terms of kinetics enhancement of the dehydrogenation of Ti doped $NaAlH_4$.

Kang et al. presented a novel two step doping method by first milling Ti with NaH and then milled again after adding Al powder [31]. They found very stable hydrogen capacity and dehydriding kinetics, which was attributed to an optimized dispersion of Ti hydride particles in the NaH/Al matrix.

Thus, on the basis of existing literature one can classify the preparation methods of metal doped $NaAlH_4$ in three categories as classified by Bogdanovic et al. [32]:

1. Ball milling or wet chemical reaction of pre-synthesized $NaAlH_4$ with dopants [33–35].
2. Direct synthesis by ball milling or wet chemical reaction of a mixture of NaH/Al powder and dopants and then hydrogenation of the doped mixture [36–38].
3. One-step direct synthesis by ball milling of a mixture of NaH/Al powder and dopants under hydrogen pressure [39].

The crystal structure of $NaAlH_4$ was first discussed by Lauher et al. [40] using single crystal X-ray diffraction in 1979. The structure was suggested to be tetragonal with space group $I4_1/a$ consisting of isolated $[AlH_4]^-$ tetrahedra. A ball and stick model of structure was presented recently by Ma et al. (Fig. 1a) [41]. Sodium atoms are surrounded by eight nearest $[AlH_4]^-$ tetrahedra (Fig. 1b) with an Al–H bond length of 1.532(7) Å which was found to be inconsistent with the IR data. So another effort was made using a singly crystal and a more realistic bond length, i.e. 1.61(4) Å was calculated [42]. To calculate the coordinates of hydrogen atoms more accurately, a neutron diffraction study was performed on the deuterated compound i.e. $NaAlD_4$ at 8 and 295 K [43]. It was found that no significant change in the Al–D bond length occurred with the change in temperature and it was found to be 1.627(2) Å and 1.626(2) Å at 8 and 295 K, respectively. The two Na–D bond lengths were found to be equal, i.e. 2.403(2) Å and 2.405(2) Å at 8 K and 2.431(2) Å and 2.439(2) Å at 295 K. The shortest distance (Al–Al) was found to be 3.737(1) Å and 3.779(1) Å at 8 and 295 K, respectively. The angles of the $[AlD_4]$ tetrahedron were distorted and equal to 107.32° and 113.86°.

Gross et al. [44] performed in-situ XRD during the decomposition of $NaAlH_4$ in order to understand the phase transition and crystal structure modifications and proposed a very simple schematic representation of restructuring of system as shown in Fig. 2.

The transformation can be achieved by removing one Al and 3H's from two out of every AlH^{4+} complexes in the double columns at the surface. Filling the vacancy left by the Al atom by a Na atom closest to it, will reproduce the Na_3AlH_6 structure in the 1st monolayer at the surface. For this structural change to propagate into the bulk, the remaining Al and 3H's at the surface must be removed and be replaced by an Al and 3H's from the AlH^{4+} complex in the column behind it. Several other techniques have also been employed for the characterization of sodium alanate [45].

2.1.2. Thermodynamics and hydrogenation properties

The thermodynamics of dehydrogenation of undoped $NaAlH_4$ was first studied by Dymova and Bakum [46] in 1969 followed by a detailed TGA and DSC study made by Claudy et al. [47], the thermodynamics of metal doped $NaAlH_4$ was made by Bogdanovic et al. [33]. In the work of Claudy it is found that in addition to the two steps seen in equations (2) and (3), melting of the $NaAlH_4$ occurs and a conversion of monoclinic, α-Na_3AlH_6 into cubic β-Na_3AlH_6

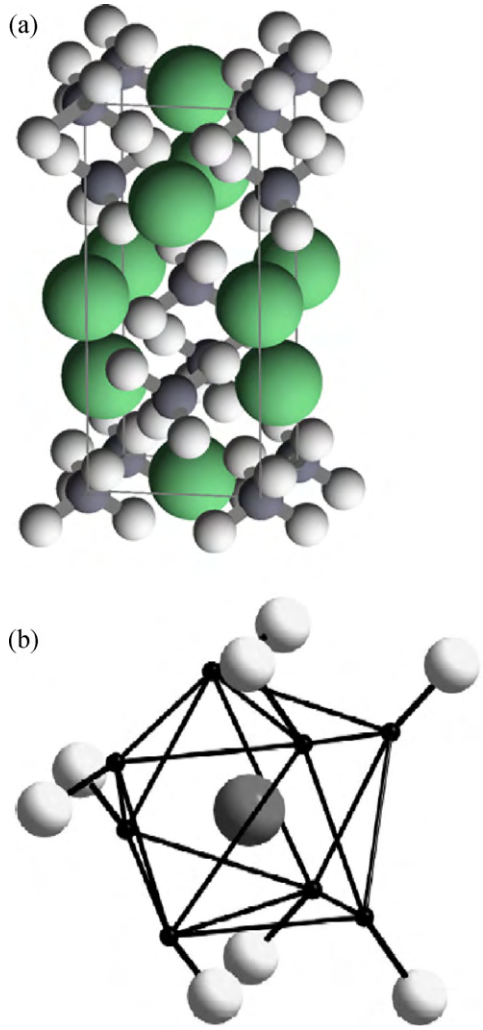

Fig. 1. (a) Equilibrium structure of $NaAlH_4$ and (b) each Na atom is connected to eight $[AlD_4]^-$ tetrahedra in a distorted square antiprism [Reprinted from Ref. [41,43] with permission from Elsevier].

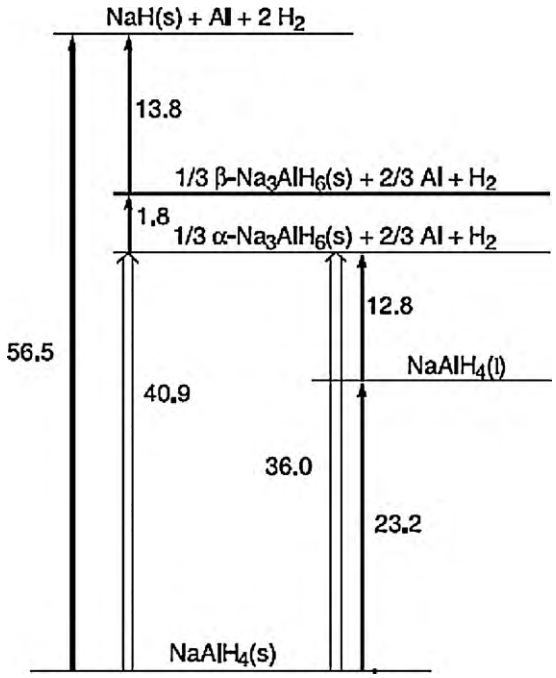

Fig. 3. Enthalpy values (kJ/mol) determined for the processes occurring during the uncatalyzed dehydriding of 1 mole of $NaAlH_4$ [reprinted from Ref. [55] with kind permission from Springer Science].

is taking place. The enthalpies of all the phases are summarized in Fig. 3.

The experimentally determined enthalpies for the 1st and 2nd dissociation step of Ti doped $NaAlH_4$ was found by Bogdanovic et al. [33] to be 37 and 47 kJ/mol, respectively. They also have observed a cooperative synergetic catalytic effect of the combined dopants Ti and Fe, under a constant storage capacity of 4 wt%.

The theoretical reversible storage capacity of $NaAlH_4$ is about 5.5 wt%, although in practice only 5 wt% could be achieved so far. It has been shown that the thermal dissociation of $NaAlH_4$ occurs in two steps: the first step proceeds with the dissociation of $NaAlH_4$ into Na_3AlH_6, Al and hydrogen and in the second step Na_3AlH_6 decomposes into NaH, Al, and hydrogen at relatively higher temperature. Ashby and Kobetz, [48,49] and Dymova et al.

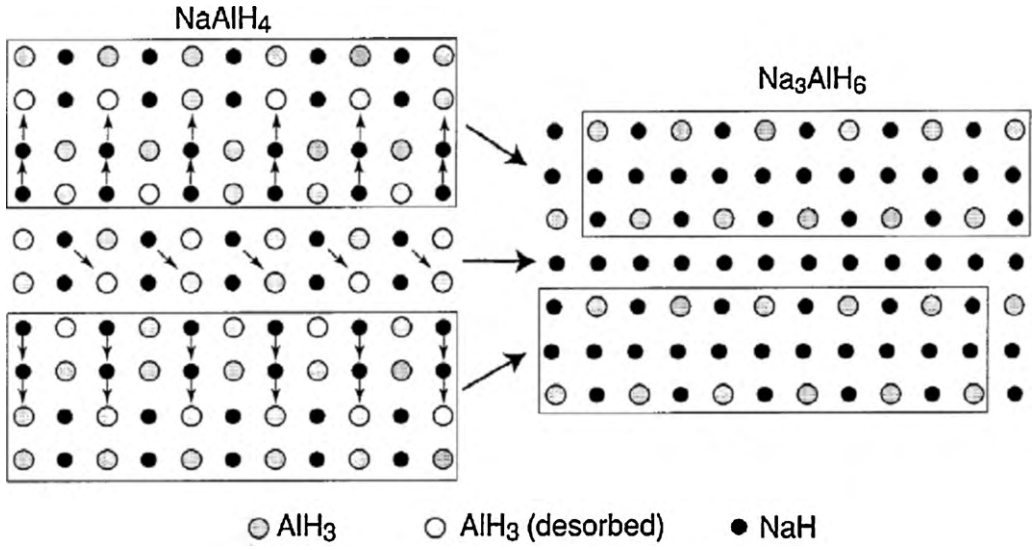

Fig. 2. A schematic representation of a possible mechanism for the crystal structure transformation of $NaAlH_4$ to α-Na_3AlH_6 [Reprinted from Ref. [44] with permission from Elsevier].

[50] proposed the above two steps as:

$$NaAlH_4 \Leftrightarrow \frac{1}{3}Na_3AlH_6 + \frac{2}{3}Al + H_2 \quad (2)$$

$$\frac{1}{3}Na_3AlH_6 \Leftrightarrow NaH + Al + \frac{1}{2}H_2 \quad (3)$$

The NaH formed in eq. (3) can also dissociate to evolute the remaining hydrogen, which would increase the total capacity of the $NaAlH_4$ system upto 7.4 wt%, but this reaction occurs only at temperatures higher than 450 °C, thus being impractical for onboard storage. The equilibrium pressure calculated from the enthalpy values, 37 kJ mol^{-1} H_2 and 47 kJ mol^{-1} H_2 for the first and second step respectively, were found to be 1 bar for the first step at 30 °C and 1 bar for the second step at 100 °C [33]. However, the kinetics of both reactions are very slow for practical applications. Ashby and Kobetz [48] reported that 3.7 wt% hydrogen corresponding to the first step could be released in 3 h at 210–220 °C and the second step occurs at temperatures higher than 250 °C. The condition becomes worst if we talk about re-hydrogenation of this material. Complete conversion to $NaAlH_4$ was achieved by Dymova et al. [24] under 17.5 MPa hydrogen pressure at 270 °C for 3 h. In fact, until the work of Bogdanovic et al. [20,51] it was believed that $NaAlH_4$ is not reversible under practical conditions. In 1997, they first reported [20] the drastic reduction of 50 °C in the dissociation temperature by introducing a small amount of titanium and $NaAlH_4$ could decompose at only 150 °C. Not only dissociation but the re-hydrogenation of this material was also affected by this doping and conversion to $NaAlH_4$ could be achieved at 170 °C under 15.2 MPa. Although this study opened a pathway for the onboard storage, the kinetics of these materials was still not fast enough for practical applications. The capacity was also found to have decreased with the number of cycles. A number of studies employing different catalysts have been undertaken after this discovery.

While extensive efforts were being done all over, a systematic study of the effect of the $TiCl_3$ catalyst level on the hydrogenation properties of $NaAlH_4$ system was presented by Sandrock et al [35]. Although all these studies showed that $TiCl_3$ is the most potent catalyst, Anton [52] studied the effect of number of catalyst, i.e. AgCl, CdCl, $CeCl_3$, $CrCl_3$, CuCl, $FeCl_2$, $FeCl_3$, etc., to observe the primary factor behind the catalysis process. It is concluded in this work that the cation radius is the most important factor affecting the dehydrogenation process. Cations with ionic radii in the range of 0.76 Å, the midpoint between the ionic radii of Al^{3+} and Na^+, were most active. A new mechanism for the dissociation of $NaAlH_4$ was proposed by Walters et al. [53]. According to them thermally activated $NaAlH_4$ initially produce NaH and the alane AlH_3. This alane plays a major role in both the decomposition and the reformation mechanisms rely on its mobility and sorption characteristics. Moreover, since the alane is intimately associated with the bulk aluminium surface, the role of titanium as a catalyst centres on the formation of titanium–aluminium alloys that facilitate the alane formation and sorption dynamics for both decomposition and reformation mechanism. The puzzling behaviours of sodium alanates appear to sort themselves along these mechanistic arguments. The effect of different dopants based on the same cation on the kinetics, when using the same method of preparation, has been shown by Schuth et al. [54], who made a comparison between the three dopants Ti, $TiCl_3$, $Ti(OC_4H_9)_2$ and found differences of more than a factor of ten, as shown in Fig. 4.

Zidan et al. [34] found a significant enhancement in the hydrogenation properties using zirconium doping, which is found to be inferior to titanium for the first step while it is superior to titanium for 2nd reaction. The recyclable capacity of hydrogen absorption/desorption is found to be larger than 4 wt%.

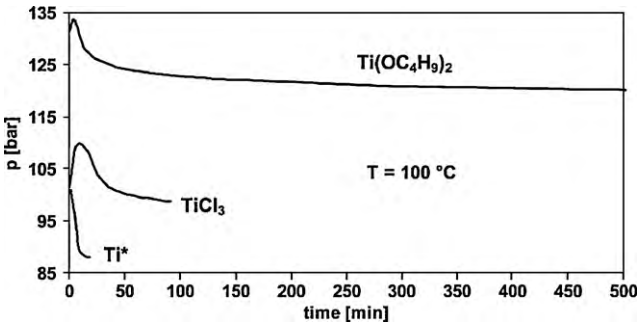

Fig. 4. Rehydrogenation curves for $NaAlH_4$ doped with different doping agents via ball milling [reproduced from Ref. [54] by permission of The Royal Society of Chemistry].

Bogdanovic et al. [32] has extended the one step direct synthesis method from $TiCl_3$ to $ScCl_3$ and $CeCl_3$, and they found superior cycling properties and outstanding kinetics.

Except these, a number of other catalyst has been studied so far for the improvement of $NaAlH_4$ such as Al_3Ti, $ScCl_3$, $CeCl_3$, $PrCl_3$, Mm, VCl_3, $HfCl_4$ [55–65]. Blomquist et al. [59] studied the effect of 3d metal substitution on the dehydrogenation energetic of $NaAlH_4$ by using the supercell electronic structure and gradient corrected density functional theory and concluded that Cr and Fe are much more effective than Ti for hydrogen desorption [59].

A very systematic study of the effect of individual, binary and ternary combination of $TiCl_3$, $FeCl_3$, and $ZrCl_4$ on the dehydrogenation kinetics has been made by Wang et al. [66]. They found that the effect of Ti, Zr and Fe as co-dopants on the second decomposition reaction were not as pronounced as their effects on the first reaction.

A new family of catalyst was introduced when Lee et al. [67] studied the dehydrogenation properties of La_2O_3 doped $NaAlH_4$. They found remarkable improvement in the hydrogen kinetics compare to undoped $NaAlH_4$.

The efforts made to make $NaAlH_4$ a more practical carbon material have also lead to other positive effects, namely to enhance the kinetics and also to maintain the storage capacity. Zaluska et al. [68] succeeded first in accelerating the dehydrogenation kinetics by ball milling with the addition of carbon. Recently Pukazhselvan et al. have shown that $NaAlH_4$ admixed with 8 mol% CNT could recover the storage capacity upto 4.2 wt% [69]. Increased solid–gas surface area due to CNT was considered to be responsible for enhancing the kinetics of the reaction. A theoretical and experimental study made by Berseth et al. [70] explains the role of carbon nano-material as a catalyst for $NaAlH_4$. In this work they have shown the dependence of the stability of $NaAlH_4$ on the charge transfer from Na to AlH_4. This charge transfer promotes the formation of an ionic bond between Na^+ and AlH_4^- and also a covalent bond between Al and H. According to these authors, when $NaAlH_4$ interacts with an electronegative material such as carbon nanotubes, it affects the charge donation ability of Na, thus weakening the Al–H bond which ultimately promotes hydrogen to desorb at lower temperature.

Ball milling without any dopant or any solvent is also an impressive way to enhance the kinetics and to lower the desorption temperature. $NaAlH_4$ ball milled for15 min releases up to 3.1 wt% hydrogen at 160 °C corresponding to the 1st reaction and additional 1.9 wt% at 220 °C corresponds to the 2nd reaction, as shown in Fig. 5 [29]. A relationship between activation energy and particle size of $NaAlH_4$ was established by Balde et al. [71] who claimed a reduction in desorption activation energy from 116 kJ mol^{-1} for 1–10 μm particles to 58 kJ mol^{-1} for 2–10 nm particles and found this value to be lower than that of Ti catalyzed $NaAlH_4$. In the case of absorp-

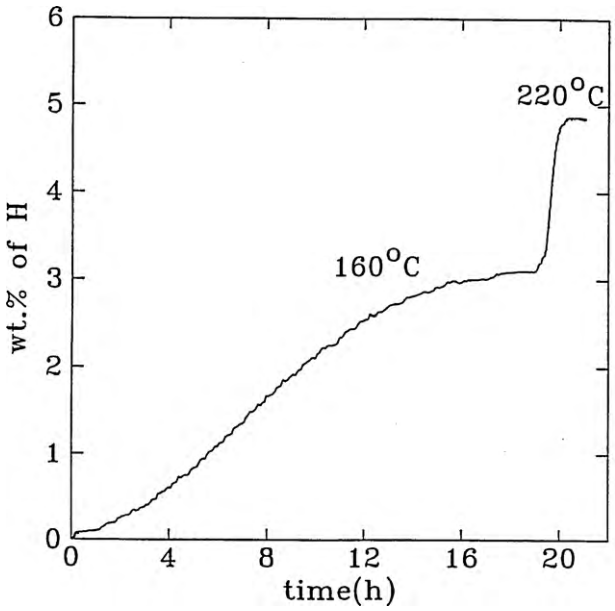

Fig. 5. Decomposition of $NaAlH_4$ at 160 °C (first decomposition stage) and during subsequent heating to 220 °C (second decomposition) [Reprinted from Ref. [29] with permission from Elsevier].

tion, nano-$NaAlH_4$ showed much promise by absorbing hydrogen already at pressures starting from only 20 bar.

2.2. Lithium alanate

2.2.1. Formation and structure

Lithium alanate ($LiAlH_4$) was first synthesized by a treatment of lithium hydride with an ether solution of aluminium chloride in 1947 [72]

$$4LiH + AlCl_3 \xrightarrow{\text{Ether}} LiAlH_4 + 3LiCl \quad (4)$$

But this is a costly process due to the trapping of about 75% lithium in a deep thermodynamic well as LiCl [73]. Ashby et al. [27] and Clasen [28] also proposed a formation method of $LiAlH_4$ using diethyl ether, tetrahydrofuran and diglyme solution. While Clasen [28] used low preassure (30 bar) and temperature (308 K) conditions, Ashby et al. [27] did this experiment with 350 bar pressure of hydrogen at 393 K. Recently Wang et al. [74] proposed a five-step physiochemical pathway for the production of crystalline $LiAlH_4$ from Li_3AlH_6, LiH and Al. A direct synthesis of $LiAlH_4$ from LiH and Al by a mechanochemical reaction was done by Kojima et al. [75]. They proposed milling for 24 h under 1 MPa hydrogen pressure at room temperature, but the yield of $LiAlH_4$ was very small. More recently, a low energy route to form $LiAlH_4$ from LiH and Al was demonstrated by Graetz et al. [73].

The crystal structure of $LiAlH_4$ was first proposed by Sklar and Post [76] by using single crystal XRD and found a monoclinic structure with space group $P2_1/C$. Each aluminium atom is surrounded by 4 hydrogen atoms to form isolated $[AlH_4]^-$ tetrahedra with Al-H bond lengths of 1.55 Å. The lithium ion is surrounded by 5 hydrogen atoms, four at distances between 1.88 and 2.00 Å and a fifth one at 2.16 Å. They suggested to perform neutron diffraction to confirm the slight distortion of the tetrahedra from the ideal configuration as seen from the individual H-Al-H angles. An accurate structure determination was again made by Hauback et al. [77] using XRD and neutron diffraction at 8 K and 295 K. According to these authors, the Li atoms are bonded to one deuterium atom from each of 5 surrounding well separated AlD_4 tetrahedra and adopt trigonal bipyramidal coordination. The distortion in the tetrahedral configuration was found to be as suggested by Sklar and Post [76] and it increases on cooling. The Al–D distances are in the range 1.603–1.633 Å at 295 K and 1.596–1.645 Å at 8 K as shown in Fig. 6.

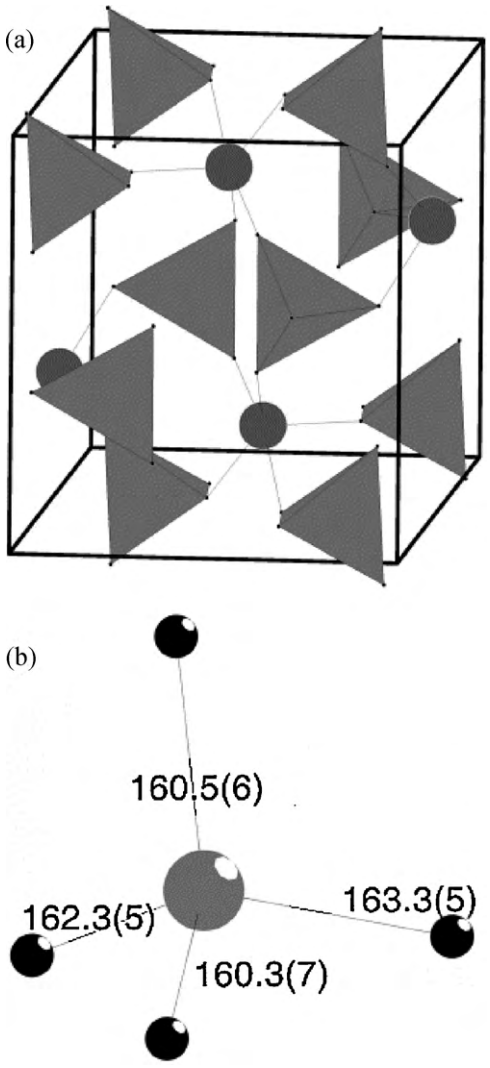

Fig. 6. (a) The crystal structure of $LiAlD_4$; AlD_4 tetrahedra are linked via Li atoms and (b) slightly distorted AlD_4 tetrahedron at 8 K with the Al–D distances[Reprinted from Ref. [77] with permission from Elsevier].

2.2.2. Thermodynamics and hydrogenation properties

The first report on the thermodynamic parameters, i.e. heat of formation, was given by Davis et al. [78] who calculated the value of heat of formation as 28.51 kcal/mole at 25 °C. The detailed analysis, including the free energy of formation, was discussed later by Smith et al. [79]. A number of studies have been performed since then on the thermodynamic properties and reversibility of the reaction $LiAlH_4 \leftrightarrow Li_3AlH_6 \leftrightarrow LiH$ [80–82]. But these all are piecewise and provide very limited information. Recently, Jang et al. have performed a systematic empirical thermodynamic calculation [83] using existing experimental data by means of which they calculated enthalpy and Gibb's energy expressions for the hydride phases $LiAlH_4$, Li_3AlH_6 and LiH. They concluded from this study that more than 10^3 bar of hydrogen pressure is necessary to induce the hydrogen absorption reaction of $Li_3AlH_6 \leftrightarrow LiAlH_4$ above room temperature, and so it is not possible for a reversible reaction between Li_3AlH_6 and $LiAlH_4$ to occur under practical conditions.

Garner and Haycock [84] were the first who investigated the isothermal decomposition of $LiAlH_4$. They proposed a 3-stage reac-

tion consisting of a rapid initial evolution of gas amounting to less than 1% of the ultimate hydrogen evolved, an accelerating reaction corresponding to the formal equation

$$LiAlH_4 \rightarrow LiAlH_2 + H_2, \quad (5)$$

and a slow final step represented formally by

$$LiAlH_2 \rightarrow LiH + Al + \frac{1}{2}H_2 \quad (6)$$

Mikherva et al. [85] investigated the same reactions using differential thermal analysis with simultaneous collection and measurement of the evolved hydrogen. They reported three endothermic maxima in their thermograms, corresponding to the evolution of half of the theoretical hydrogen at 154–160 °C, one quarter at 197–227 °C and the remaining quarter at 580–586 °C. These findings were confirmed in another work of Block and Gray [86] where they re-examined the same reactions with DSC technique. The phase transition was found the same as reported in previous reports, but the results are at little at variance in several aspects. The study of Maycook and coworkers [87] verified the results of Block and Gray but they did not discuss anything about the nature of $LiAlH_2$.

The above findings become contradictory with the proposal of Mikheeva and Arkhipov [88] who discuss the stoichiometry of equation (5) in a different way with the formation of Li_3AlH_6, a complex hydride reported by Ehrlich et al. [89]. They confirmed these results by XRD studies and so the reactions become changed as follows:

$$3LiAlH_4 \rightarrow Li_3AlH_6 + 2Al + 3H_2 \quad (7)$$

$$Li_3AlH_6 \rightarrow 3LiH + Al + \frac{3}{2}H_2 \quad (8)$$

$$3LiH + 3Al \rightarrow 3LiAl + \frac{3}{2}H_2 \quad (9)$$

The first dehydrogenation process of equation (7) occurs exothermically with $\Delta H = -10$ kJ/mol H_2 at 160–180 °C evoluting 5.3 wt% of H_2. The second reaction (equation (8)) occurs endothermically with $\Delta H = 25$ kJ/mol H_2 at 180–220 °C with 2.6 wt% of H_2 evolution. Finally the third reaction (equation (9)) is completed at much higher temperature around at 400 °C with an enthalpy of 140 kJ/mol H_2 and thus is impractical for onboard storage.

Due to the thermodynamic restrictions, this material did not draw much attention until the discovery of Bogdanovic et al. [20] regarding the reversibility of $NaAlH_4$ using Ti catalyst. In 2000, Balema et al. reported that $LiAlH_4$ can be easily transformed into lithium hexahydroaluminate (Li_3AlH_6), Al and H_2 in the presence of a catalytic amount of metallic iron or $TiCl_4$ [90–92]. They demonstrated that the high catalytic activity of $TiCl_4$ is due to the formation of a nano- or microcrystalline Al_3Ti phase formed from $TiCl_4$ and $LiAlH_4$ during milling [92]. It was later shown by Chen et al. [81] that it is possible to achieve reversibility in Li_3AlH_6 by addition of Ti; but they did not find the same effect in $LiAlH_4$. Resan et al. [93] reported that the addition of $TiCl_3$ and $TiCl_4$ to $LiAlH_4$ eliminates the 1st step of hydrogen evolution and lowers the desorption temperature of the second step. In the same work they have shown the effect of various catalysts such as Ti, TiH_2, $AlCl_2$, elemental iron, elemental nickel, elemental vanadium, and carbon black and concluded that these catalysts caused only a slight decrease in the amount of hydrogen released and did not lead to the disappearance of the 1st step of hydrogen evolution. The study of Blanchard et al. [94] showed that ball milling of $LiAlD_4$ and VCl_3 or $TiCl_3 \cdot 1/3AlCl_3$ reduced the decomposition temperature by 50–60 °C. Zheng et al. [95] showed that $Ce(SO_4)_2$ and $LaCl_3$ doping decreased the decomposition temperature by about 30 °C. Kojima et al. [96] doped $LiAlH_4$ with 5 wt% of nano-Ni by ball milling and concluded that the effect of Ni as a catalyst is improved with decrease in particle size. Sun et al. [97] showed further improvement in the dehydrogenation properties by taking $NiCl_2$ as a catalyst in place of Ni and found a reduction of 50 °C in the decomposition temperature. By having a look on the equations it can be understood that the hydrogenation of $Li_3AlH_6 \rightarrow LiAlH_4$ is an endothermic reaction with 9 kJ/mol H_2, i.e. it is a non-spontaneous process and so direct hydrogenation can not be done. But the formation of Li_3AlH_6 from LiH and Al is exothermic and hydrogenation be done under high pressure.

2.3. Magnesium alanate

2.3.1. Formation and structure

Wiberg and Bauer [98–100] were the first who reported a different method of preparation of magnesium alanate based on the following equations:

$$4MgH_2 + 2AlCl_3 \xrightarrow{\text{Diethyl Ether}} Mg(AlH_4)_2 + 3MgCl_2 \quad (10)$$

$$MgH_2 + 2AlH_3 \xrightarrow{\text{Diethyl Ether}} Mg(AlH_4)_2 \quad (11)$$

$$2LiAlH_4 + MgBr_2 \xrightarrow{\text{Diethyl Ether}} Mg(AlH_4)_2 + 2LiBr \quad (12)$$

Later on, Hertwig [101] proposed another reaction to form $Mg(AlH_4)_2$ which is based on hydrogenolysis of Grignard's reagent in diethyl ether followed by aluminium chloride in the reaction product. Afterwards a report [102] came into picture by the reaction of $NaAlH_4$ and $MgCl_2$ in diethyl ether, but the properties of $Mg(AlH_4)_2$ were different from those in previous reports. Plesek and Hermanek [103] confirmed the possibility of the above reaction.

$$NaAlH_4 + MgCl_2 \xrightarrow{\text{THF}} ClMgAlH_4 + NaCl \quad (13)$$

$$ClMgAlH_4 + NaAlH_4 \xrightarrow{\text{THF}} Mg(AlH_4)_2 + NaCl \quad (14)$$

So the reaction is completed in two step; first the formation of soluble $ClMgAlH_4$ and then the insoluble $Mg(AlH_4)_2$. This reaction was repeated in more generalized form by Ashby et al. [104] and they found that the reaction of complex hydrides with magnesium halides in tetrahydrofuran can produce $Mg(AlH_4)_2$ with an exception in the case of MgI_2.

$$MAlH_4 + MgX_2 \xrightarrow{\text{THF}} XMgAlH_4 + MX \quad (15)$$

$$XMgAlH_4 + MAlH_4 \xrightarrow{\text{THF}} Mg(AlH_4)_2 + MX \quad (16)$$

Although a number of efforts have been made, each report mentioned the difficulties to obtain $Mg(AlH_4)_2$ without impurities. In 2002, Fichtner and Fuhr presented a synthesis and purification method for $Mg(AlH_4)_2$ [105] and used the same metathesis reaction of $NaAlH_4$ and $MgCl_2$ as proposed previously [102,103]. The additional purification was done via a Soxhlet extraction process which gave the solvent adduct $Mg(AlH_4)_2$ with a total yield of 81.5% and after removing the solvent they could achieve 95% pure $Mg(AlH_4)_2$. Since then a number of studies have used the same method [106–108]. A mechanochemical preparation of a $Mg(AlH_4)_2$–$MgCl_2$ mixture by ball milling has been described by Dymova et al. [109]:

$$2MgH_2 + AlCl_2 \xrightarrow{\text{Ball milling}} 0.5Mg(AlH_4)_2 + 1.5MgCl_2 \quad (17)$$

Recently Mamatha et al. succeded to prepare $Mg(AlH_4)_2$ by the same mechanochemical synthesis method but they used different starting materials and proposed the following reaction to occur during milling [110]:

$$2NaAlH_4 + MgCl_2 \rightarrow Mg(AlH_4)_2 + 2NaCl \quad (18)$$

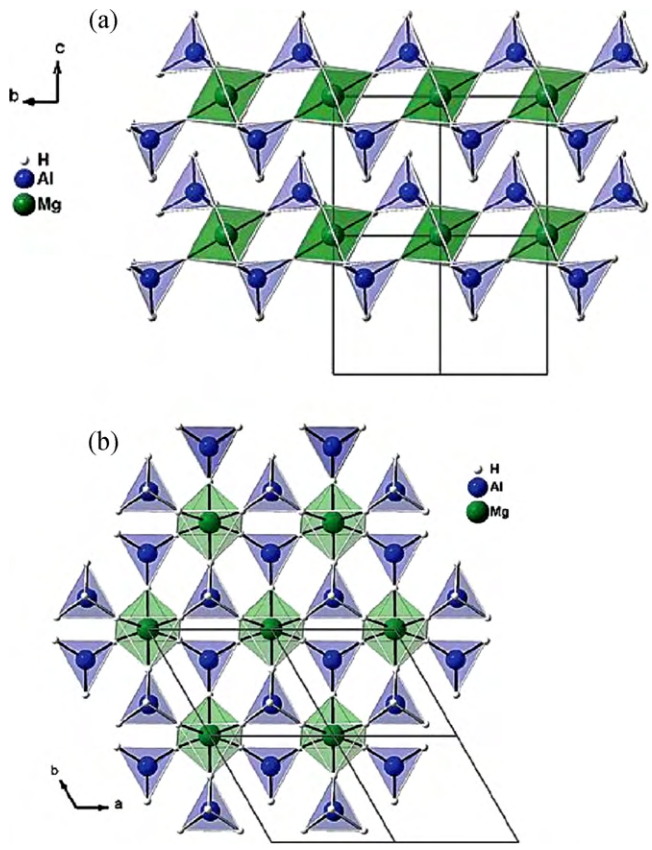

Fig. 7. Trigonal structure of $Mg(AlH_4)_2$, space group $P\bar{3}m1$ (a) Double layer, view along the *a*-axis. (b) Single layer, view along the *c*-axis [Reprinted from ref. [106] with kind permission of American Chemical Society].

In this reaction 2 mol NaCl formed as a by product against 1 mol of $Mg(AlH_4)_2$. They used a wet chemical separation method to remove NaCl from the above solution [111].

The structure of crystalline magnesium alanate was determined by Fichtner et al [106] using powder XRD on the basis of DFT calculations (Fig. 7). A more detailed study of the crystal structure was performed by Fossdal et al. using XRD, PND [108] and synchrotron radiation [107]. They calculated that $Mg(AlH_4)_2$ crystallizes in a trigonal structure with space group $P\bar{3}m1$ consisting of isolated and slightly distorted AlH_4^- tetrahedra that are connected via six coordinated Mg atoms in a distorted octahedral geometry, resulting in a sheet like structure along the crystallographic *c*-axis. The distortion of the AlH_4^- tetrahedra decreases with increasing temperature, whereas the opposite is the case for the MgH_6 octahedra. The Al–H distances are 1.606(10)–1.634(4) Å, 1.602(10)–1.682(3) Å and 1.561 (12)–1.672(4) Å at 8, 111, and 295 K respectively.

2.3.2. Thermodynamics and hydrogenation properties

The formation enthalpy of magnesium alanate and the reaction enthalpy of hydrogen desorption were calculated by Fichtner et al. [106] using quantum chemical calculations which were found to be $\Delta H_f = -64.8$ kJ/mol and $\Delta H_r = +41$ kJ/mol. In another study Fichtner et al. [23] proposed a 3-step thermal decomposition of $Mg(AlH_4)_2$ according to the following equations:

$$Mg(AlH_4)_2 \rightarrow MgH_2 + 2Al + 3H_2 \quad (19)$$

$$MgH_2 \rightarrow Mg + H_2 \quad (20)$$

$$2Al + Mg \rightarrow \frac{1}{2}Al_3Mg_2 + \frac{1}{2}Al \quad (21)$$

The first step occurs at 110–200 °C with 7 wt% H_2 evolution, while in the second step MgH_2 splits into Mg metal and H_2 at 240–380 °C with 2.3 wt% of H_2. The third step occurs due to the reaction between Mg and Al at around 400 °C and it forms the intermetallic compound Al_3Mg_2. In 2005 Wang et al. [111] have performed a study of the effect of Ti doping on the reversibility and kinetics of $Mg(AlH_4)_2$ and found increased kinetics with a very high hydrogen capacity and reasonable dehydrogenation rates at 150 °C. But they did not find any reversibility of $Mg(AlH_4)_2$ under the studied conditions. Several studies have been done so far to increase the kinetics and to reach reversibility [112–114], but as the dehydrogenation of $Mg(AlH_4)_2$ is exothermic, its rehydrogenation is not possible due to thermodynamic reason.

2.4. Potassium alanate

2.4.1. Formation and structure

Potassium alanate was first prepared by direct synthesis in toluene, tetrahydrofuran, and diglyme by Ashby et al. [27]. Among these they found diglyme ideal for preparing $KAlH_4$ as the latter is soluble in diglyme. Other approaches have also been adopted by various workers such as Morioka et al. [115] who synthesized $KAlH_4$ powder directly from KH and Al under high pressure of hydrogen (>175 bar) and high temperature (270 °C). This method was initially proposed by Dymova et al. [24] for the synthesis of other alanates. Recently Hauback et al. [116] prepared $KAlH_4$ using the method of Bastide et al. [117] by adding $LiAlH_4$ to a mixture of KF and $AlEt_3$ in Et_2O and then cleansing of the precipitate with Et_2O. More recently Ares et al. [118] adopted a method reported by Dilts et al. [49], in which $KAlH_4$ is prepared by the interaction of AlH_3 in diglyme with an excess of KH or the interaction of KH with $LiAlH_4$ in diglyme.

The ground state crystal structure of $KAlH_4$ was calculated by Vajeeston et al. [119] using DFT and found it crystallized in the orthorhombic $KGaH_4$ type, i.e. $BaSO_4$ type structure (space group *Pnma*) with unit cell parameters $a = 9.009$ Å, $b = 5.767$ Å, $c = 7.399$ Å at 0 K and ambient pressure (Fig. 8).

These parameters were found to be consistent with those reported in the experimental data [120]. They also predicted that the $KAlH_4$ ground state structure consists of slightly distorted $[AlH_4^-]$ tetrahedra (Fig. 8b) which are separated by intermittent K^+ cations. A more detailed study of the structure of potassium alanate was made by neutron diffraction data of $KAlD_4$ at 8K and 295 K [116]. The authors found that the structure consists of isolated AlD_4^- tetrahedra. Each K atom has 10 D atoms as nearest neighbours from seven different AlD_4^- tetrahedra. The Al–D distances were found to be 1.589–1.659 Å at 8 K and 1.546–1.669 Å at 295 K, whereas the bond angles span the range 106.4–113.3° at 8 K and 106.2–114.6° at 295 K. It means the tetrahedra are quite close to ideal in shape and the distortions decreased with decreasing temperature.

2.4.2. Thermodynamics and hydrogenation properties

$KAlH_4$ is one of the alanate systems which has not been studied by many workers. It attracted the attention of researchers when Morioka et al. demonstrated its reversibility towards hydrogen at low pressure and moderate temperatures without any catalysts [115]. They proposed following reactions to occur in the process on the basis of TPD measurements as shown in Fig. 9:

$$3KAlH_4 \rightarrow K_3AlH_6 + 2Al + 3H_2 \quad (2.9\,wt\%) \quad (22)$$

$$K_3AlH_6 \rightarrow 3KH + Al + \frac{3}{2}H_2 \quad (1.4\,wt\%) \quad (23)$$

$$3KH \rightarrow 3K + \frac{3}{2}H_2 \quad (1.4\,wt\%) \quad (24)$$

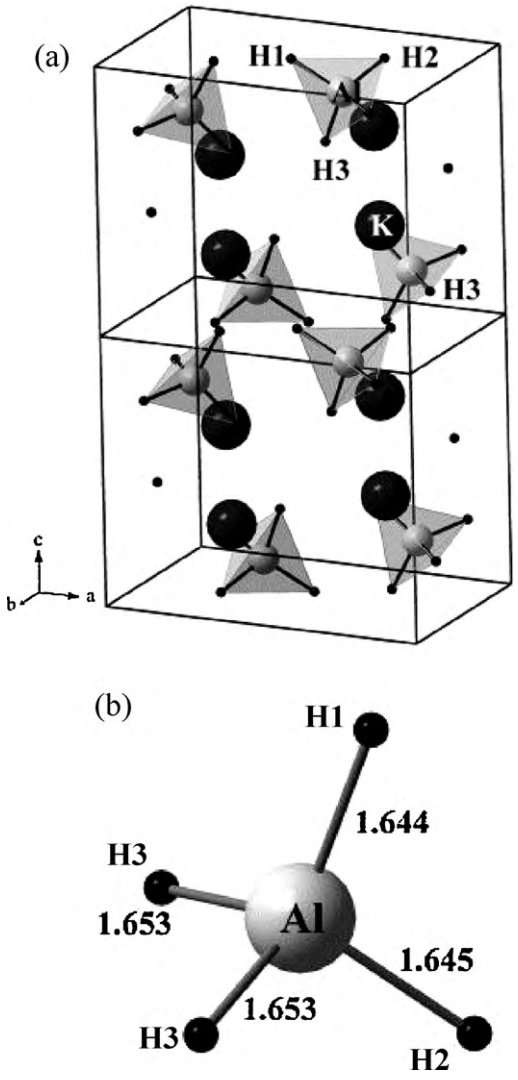

Fig. 8. (a) The ground-state crystal structure of $KAlH_4$. (b) The slightly distorted $[AlH_4]^-$ tetrahedron with the interatomic Al–H distances (in Å) [Reprinted from Ref. [119] with permission from Elsevier].

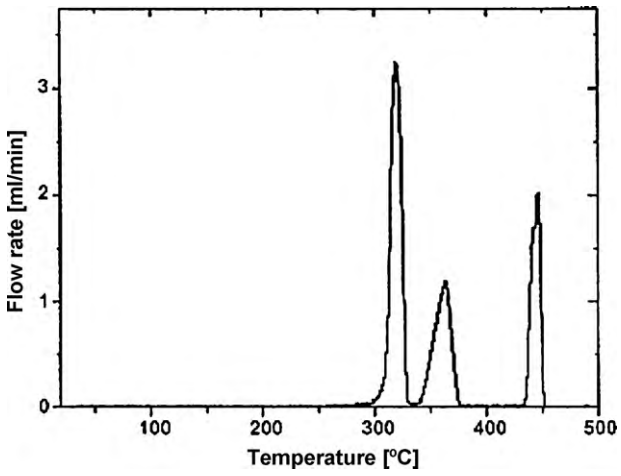

Fig. 9. TPD measurement of $KAlH_4$ dehydrogenation. The sample was heated from room temperature to 500 °C at the rate of 2 °C/min. [Reprinted from Ref. [115] with permission from Elsevier].

As clearly seen from figure, the first dehydrogenation occurred at approximately 300 °C with 2.9 wt%, while the 2nd and 3rd reactions occurred at 340 and 430 °C with 1.4 and 1.4 wt%, respectively. Another measurements obtained by NMR [121,122] suggested an intermediate decomposition species such as AlH_3 and KH. The thermodynamic stability of $KAlH_4$ and its decomposition products K_3AlH_6 and KH were calculated by means of ab initio calculations [118]. The enthalpies of formation of $KAlH_4$ and K_3AlH_6 were found to be −70 and −78.5 kJ/mol, while the enthalpies of decomposition, reactions equations (22) and (23), were determined as 55 and 70 kJ/mol H_2, respectively [118]. Recently, a significant reduction in desorption temperature (∼50 °C) of the reaction $KAlH_4 \rightarrow K_3AlH_6$ was reported due to $TiCl_3$ doping [120]. However, $TiCl_3$ does not affect the decomposition temperature of K_3AlH_6.

2.5. Calcium alanate

2.5.1. Formation and structure

Calcium alanate $Ca(AlH_4)_2$ was first synthesized by Schwab and Wintersberger [123] in 1950s by the following reaction path:

$$4CaH_2 + 2AlCl_3 \xrightarrow{THF} Ca(AlH_4)_2 + 3CaCl_2 \quad (25)$$

The final dried product contains 40% $Ca(AlH_4)_2$ and the rest THF but unfortunately the attempts to purify this solution was not successful. Later on, Finholt et al. [124] reported another attempt repeating the same reaction but with dimethyl ether, but they obtained very little yield of $Ca(AlH_4)_2$.THF. Recently, wet chemical synthesis under inert atmosphere is used to produce almost pure calcium alanate [105,110,125–127]. In this method, first a solvent adduct, e.g. $Ca(AlH_4)_2{\cdot}x$(solvent) is formed, and then the solvent is removed by moderate heating under vacuum. Recently also mechanochemical synthesis using ball milling was proposed as an efficient way to produce calcium alanate in which NaCl was found to be present as a by-product [127,128].

Fichtner et al. [126] reported the structure of $Ca(AlH_4)_2{\cdot}4$THF using powder XRD and found that $Ca(AlH_4)_2{\cdot}4$THF crystallized in the monoclinic space group $P2_1/n$ with two formula units per unit cell. They found a similar molecular structure of $Ca(AlH_4)_2{\cdot}4$THF compared to that of $Mg(AlH_4)_2{\cdot}4$THF [105,129]. It consists of a central calcium ion occupying a crystallographic inversion centre which is octahedrally coordinated by two hydrogen atoms of two $[AlH_4]$ units and four oxygen atoms from four THF molecules.

Attempts were made to predict the crystal structure of solvent free $Ca(AlH_4)_2$, but it proved not to be possible, probably due to rapidly rotating the AlH_4 tetrahedra. Recently, Lovvik [130] proposed a crystal structure of solvent free $Ca(AlH_4)_2$ from DFT calculations (Fig. 10) using different models to optimize the structure and found the most stable structure—the Pbca structure based on CaB_2F_8. Hydrogen is found to be coordinated around Al in slightly distorted tetrahedra with Al–H bond length 161–163 pm and H–Al–H angle between 106.8–113.2°. Ca is eight coordinated to H in distorted square antiprisms, with each corner shared by an AlH_4 tetrahedron. The structure is found to be relatively loose with large voids. Due to this, the barrier of rotation for the tetrahedra is low, this is the reason suggested by Lovvik for the difficulty to confirm the structure experimentally.

The above results were confirmed in another study made by Wolverton and Ozolins [131]. They used a larger set of input structures and thus have a greater confidence in the validity of the structural predictions.

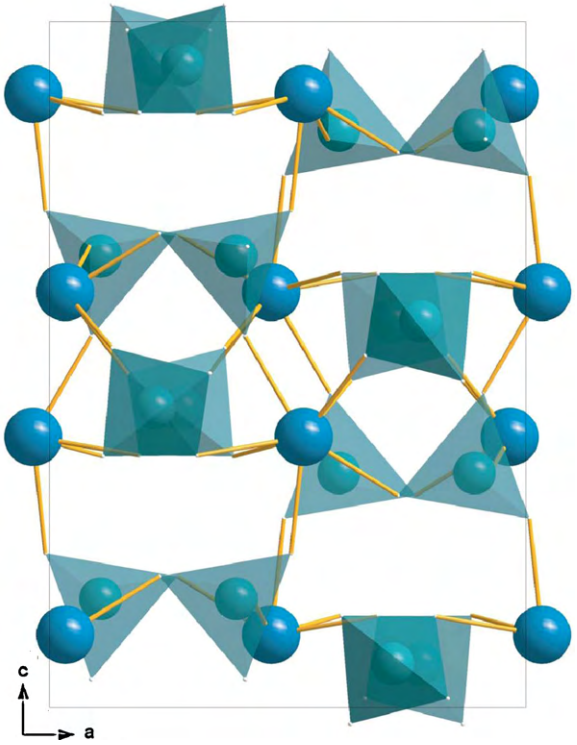

Fig. 10. The proposed crystal structure of $Ca(AlH_4)_2$. The balls and tetrahedra represent the Ca atoms and AlH_4 complexes, respectively [Reprinted from ref. [130] with the permission of American Physical Society].

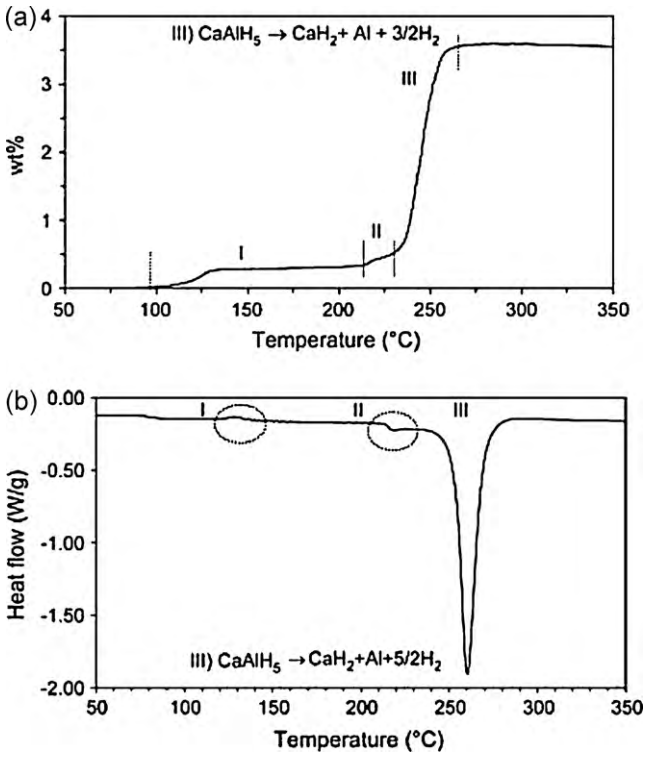

Fig. 11. (a) TPD curve and (b) DSC chart at a heating rate of 2 °C/min for CaH_2/AlH_3 mixtures after ball milling at 400 rpm for 3 h [Reprinted from Ref. [134] with permission from Elsevier].

2.5.2. Thermodynamics and hydrogenation properties

$Ca(AlH_4)_2$ decomposes in two steps with a total 5.9 wt% hydrogen evolution:

$$Ca(AlH_4)_2 \rightarrow CaAlH_5 + Al + \frac{3}{2}H_2 \quad (26)$$

$$CaAlH_5 \rightarrow CaH_2 + Al + \frac{3}{2}H_2 \quad (27)$$

Although CaH_2 can still decompose, the temperature is much higher to be considered for a practical hydrogen storage system.

$$CaH_2 \rightarrow Ca + H_2 \quad (28)$$

The enthalpy of the 1st dehydrogenation reaction (equation (26)) is estimated to be −7 kJ/mol H_2 which shows the metastable nature of $Ca(AlH_4)_2$ [132], while the enthalpy difference for dehydrogenation of $CaAlH_5$ (equation (27)) is found to be 28 kJ/mol H_2 at ambient conditions, which shows that this compound is metastable at ambient conditions. These results are in agreement with those previously reported by Mamatha et al. who used DSC curves [133] and reported that the first reaction occurring at 127 °C is weakly exothermic, while the second reaction occurs at 250 °C is endothermic. These values suggested the $CaAlH_5$ is closer to the targeted values for hydrogen storage systems. The third step occurs at much higher temperature with an endothermic enthalpy of +172 kJ/mol H_2. But this value is suggested to be decreased to +72 kJ/mol H_2, when Al is added to CaH_2 and it form the strongly bound compound $CaAl_2$ [131].

The enthalpy of formation of $Ca(AlH_4)_2$ has been estimated as −214 kJ/mol H_2 using the reaction $CaH_2 + 2AlH_3 \rightarrow Ca(AlH_4)_2$, while the enthalpy of formation of $CaAlH_5$ is estimated as −224 kJ/mol H_2 [133]. Recently a different approach for the decomposition of $CaAlH_5$ has been proposed by Iosub et al. using TPD and DSC experiments [134]. As seen from the TPD curve (Fig. 11), the 1st step starts from 100 °C, the second at 210 °C and the last step occurs at 230 °C. Iosub et al. assumed the last step as a transformation of $CaAlH_5$ to CaH_2 and Al. For the first two steps they proposed the formation of a new intermediate complex $Ca_3(AlH_6)_2$. To confirm these findings they proposed DSC meausrments at different heating rates. The DSC profile comprises 3 peaks. The first peak is exothermic and corresponds to the transformation $Ca(AlH_4)_2 \rightarrow CaAlH_5$. The second peak is endothermic and may represent the formation of small amounts of $Ca_3(AlH_6)_2$. Finally, and the third peak is also endothermic and corresponds to the formation of CaH_2 and Al phase.

However Iosub et al. suggested the need for more thorough investigation as the decomposition of $Ca(AlH_4)_2$ is more complex than other previous reports in literature.

2.6. Other alanates

The alkali alanates discussed above have low kinetics and low enthalpies and thus require very high pressures for the rehydrogenation of the material. These shortcomings led researchers to find some other materials which could retain the high capacity but at ambient condition. This generated the idea of mixed alanates containing more than one alkali or alkaline earth atom. Some important mixed alanates are discussed below in the terms of their synthesis, structure and hydrogenation properties.

2.6.1. Na_2LiAlH_6

Claudy et al. [135] synthesized Na_2LiAlH_6 by a reaction of $LiAlH_4$ with 2 NaH either in toluene or by a solid state reaction at elevated temperature and high hydrogen pressure. Huot et al. first reported the synthesis of solvent free Na_2LiAlH_6 using ball milling [136] of a mixture of NaH, LiH, and $NaAlH_4$ for 40 h. Recently Brinks et al. [137] synthesized Na_2LiAlD_6 by milling of $LiAlD_4$ and $2NaAlD_4$ followed by annealing under 30 bar D_2 pressure at 180 °C.

Claudy et al. [135] proposed a structure having a unit cell of 7.405 Å using PXD data. Later on a systematic determination of

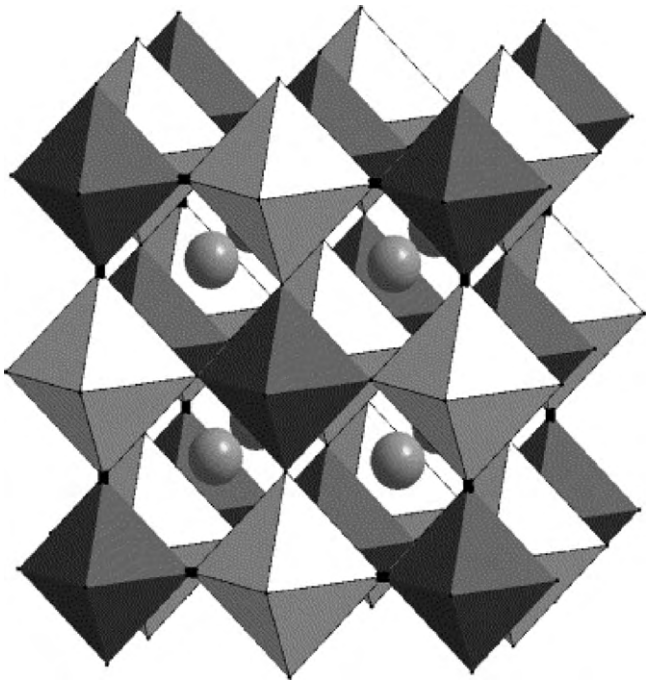

Fig. 12. The crystal structure of Na_2LiAlD_6 at 295 K, showing alternating AlD_6 (dark) and LiD_6 (bright) octahedra in all directions with Na in interstitial 12-coordinated sites [Reprinted from Ref. [137] with permission from Elsevier].

the crystal structure was made from PXD and PND data by Brinks et al. [137] who found that Na_2LiAlD_4 crystallized in an ordered perovskite-type structure with Li and Al in octahedral positions as shown in Fig. 12. The $[LiD_6]^{3-}$ and $[AlD_6]^{3-}$ complex anions are ordered in 3 dimensions such that the neighbouring octahedron is of a different type in all three directions. Na_2LiAlD_6 crystallizes in the cubic space group $Fm\bar{3}m$ with $a = 7.38484(5)$ Å. Brinks et al. also suggested a structure of c.c.p. geometry consisting of AlD_6 entities with Na filling the tetrahedral positions and Li in the octahedral positions. These results are consistent with the prediction on the basis of DFT calculation made by Lovvik et al. [138].

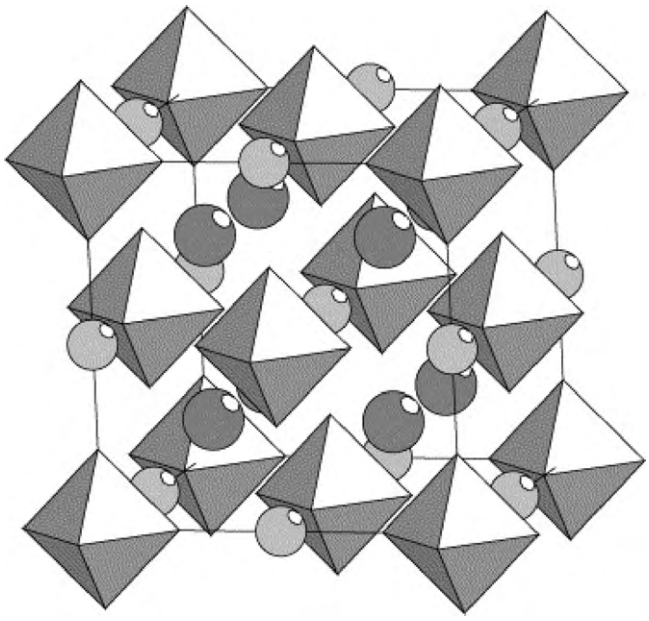

Fig. 13. The crystal structure of K_2NaAlH_6. The large, dark grey spheres are K^+, the smaller, light grey spheres are Na^+ and the octahedra are AlH_6^{3-} [Reprinted from Ref. [144] with permission from Elsevier].

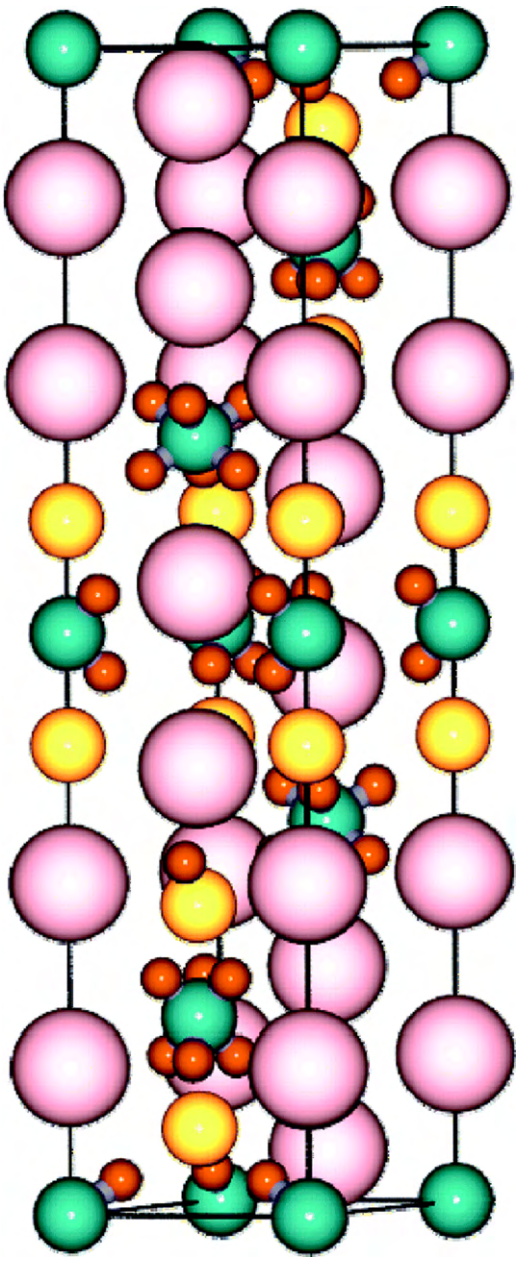

Fig. 14. The crystal structure of K_2LiAlH_6. Potassium is shown in pink, lithium in yellow, and aluminum in green. Atom Al1 is in Wyckoff position (0,0,0), while Al2 is in position (0,0,1/2). The four Al atoms located halfway up the *c*-axis, and one each closest to the plane $z = 0$ and $z = 1$, are in the Al2 position [Reprinted from ref. [145] with kind permission of American Chemical Society].

Only few results of thermodynamics and PCT measurements are reported in the literature [20,29,139–142]. Graetz et al. [139] give a complete set of PCT curves of doped and undoped Na_2LiAlH_6 at different temperatures. The total hydrogen capacity for undoped and doped Na_2LiAlH_6 was found to be 3.2 and 3.0 wt% in the 1st cycle which reduced upto 2.8 and 2.6 wt% in subsequent cycles. The decomposition enthalpy of Na_2LiAlH_6 was also measured using a Van't Hoff plot which is found to be 53.5 ± 1.2 kJ/mol H_2.

2.6.2. K_2NaAlH_6

K_2NaAlH_6 was first synthesized by Bastide et al. [143] under 25 kbar pressure of H_2 at 400 °C. After a long time Sorby et al. [144] synthesized K_2NaAlH_6 using ball milling of KH and $NaAlH_4$ followed by annealing for 18 h at 150 °C under hydrogen pressure of 100 bar.

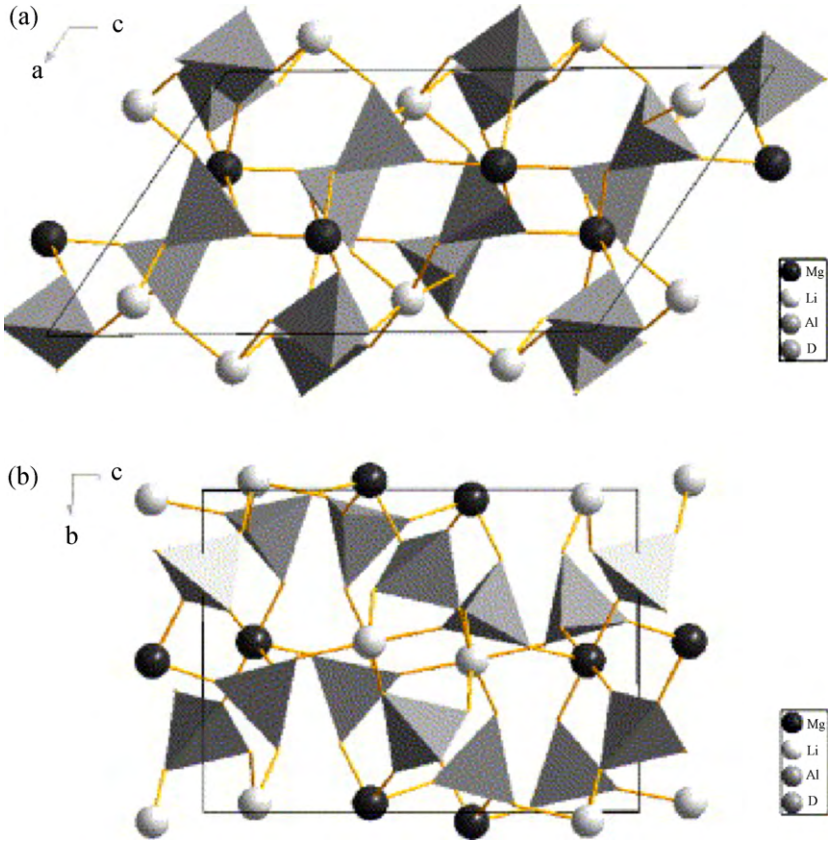

Fig. 15. The crystal structure of $LiMg(AlD_4)_3$. (a) The structure is viewed along *b*-axis. (b) The structure is viewed along the *a*-axis [Reprinted from Ref. [147] with permission from Elsevier].

The crystal structure was determined using PXD and PND data [144]. It was found that K_2NaAlH_6 crystallizes in a cubic ordered perovskite-type structure with space group $Fm\bar{3}m$ ($a = 8.118$ Å) (Fig. 13). The structure could be described as a close packing of isolated octahedral AlH_6^{3-} units with the hydrogen atoms pointing towards the octahedral interstices, which are all filled with K^+ ions that are coordinated with respect to hydrogen.

It is mentioned here that K_2NaAlH_6 and Na_2LiAlH_6 take the same structure type despite the large difference in cation sizes. The K_2NaAlH_6 system has been studied much less. Sorby et al. [144] found that TiF_3-doped K_2NaAlH_6 has a desorption plateau at 176 mbar and it release about 2.8 wt% of H_2 followed by another plateau at slightly lower pressure, namely 93 mbar. The decomposed sample was found to reabsorb hydrogen but less than the full capacity.

2.6.3. K_2LiAlH_6

Another mixed alanate K_2LiAlH_6 is synthesized by mixing K and Li ions using ball milling to mix $LiAlH_4$ and KH in 1:2 ratio followed by heating at 320–330 °C under 100–700 bar for 1–2 days [145]. The structure of K_2LiAlH_6 was determined by Graetz et al. [139] suggesting it to be isostructural with the low temperature form of K_2LiAlF_6, cubic elpasolite ($Fm\bar{3}m$). Lovvik and Swang also predicted the structure by DFT calculations and they found it to be of face centred cubic symmetry in accordance with the low temperature phase of K_2LiAlF_6 [138]. In a more recent study done by Rönnebro and Majzoub [145], it is suggested that K_2LiAlH_6 crystallized in the hexagonal-rhombohedral typestructure with space group $R\bar{3}m$ (Fig. 14). The Li and K cation sites were found mutually exclusive, and no cation mixing was found by Rietveld analysis. There is no report found in literature on the hydriding and thermodynamic characteristics of this mixed alanate.

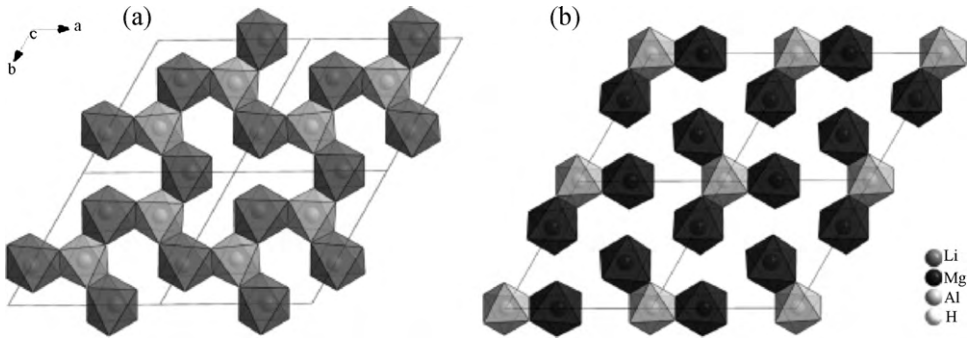

Fig. 16. The different sheets in $LiMgAlD_6$: (a) Li_3Al_2 and (b) Mg_3Al. The sheets are connected in the *c*-direction, giving a three-dimensional structure [Reprinted from Ref. [148] with permission from Elsevier].

2.6.4. $LiMg(AlH_4)_3$ and $LiMgAlH_6$

$LiMg(AlD_4)_3$, was first synthesized from $LiAlH_4$, $NaAlH_4$ and $MgCl_2$ in ether by Bulychev et al. [146] in 1979. Recently Mamatha et al. [110,133] prepared it by ball milling of $LiAlH_4$ and $MgCl_2$ in a molar ratio 3:1.

$$3LiAlD_4 + MgCl_2 \rightarrow LiMg(AlD_4)_3 + 2LiCl \quad (29)$$

$LiMg(AlD_4)_3$ has total 9.7 wt% hydrogen with following decomposition reaction:

$$LiMg(AlH_4)_3 \rightarrow LiMgAlH_6 + 2Al + 3H_2 \quad (30)$$

$$LiMgAlH_6 \rightarrow LiH + MgH_2 + Al + \frac{3}{2}H_2 \quad (31)$$

The first step occurs at 100–130 °C, while the second occurs at 150–180 °C. The enthalpy values for the 1st and 2nd step were calculated using DSC curves [110] as 15.1 kJ/mol (exothermic) and 13.0 kJ/mol (endothermic) respectively. Thus $LiMg(AlH_4)_3$ is not useful for reversible hydrogen storage, while $LiMgAlH_6$ is quite stable by thermodynamic consideration.

The crystal structure of $LiMg(AlD_4)_3$ and $LiMgAlD_6$ was investigated using synchrotron radiation XRD, PND and DFT calculations by Grove et al. [147,148]. $LiMg(AlD_4)_3$ is found to have crystallized in the monoclinic $P2_1/c$ space group. It consists of isolated AlD_4 tetrahedra, connected separately through the four corner D atoms to two Li and two Mg atoms. Each Li and Mg atom is octahedrally coordinated to the corner D atoms of six AlD_4 tetrahedra, so that the structure consists of a corner sharing network of alternating AlD_4 tetrahedra and LiD_6 or MgD_6 octahedra (Fig. 15) [147].

$LiMgAlD_6$ was found to have crystallizing in trigonal space group $P321$, consisting of isolated AlD_6 octahedra connected through octahedrally coordinated Mg and Li atoms. The structure could be described as alternating Mg_3Al and Li_3Al_2 layers as shown in Fig. 16.

In the Li_3Al_2 and Mg_3Al layers, AlD_6 octahedra are sharing edges with three LiD_6 and three MgD_6 octahedron, respectively. Each LiD_6 octahedron is sharing edges with 2 Al-octahedra and forming a two dimensional network, while the Mg – octahedron shares an edge with only one Al octahedron resulting in the formation of isolated Mg_3Al units. These layers are interconnected by corner sharing of the AlD_6^- octahedron and six Mg/LiD_6 octahedra. All corners are connected to Mg, Li and Al octahedra.

3. Borohydrides

Borohydride, sometimes also tetrahydroborate, are the designations for a group of complex hydrides in which hydrogen is covalently bonded to the central atoms in the $[BH_4]^-$ complex anion. Borohydrides have been considered as promising hydrogen storage materials due to their higher gravimetric and volumetric hydrogen capacity. The present section explores the properties of several borohydrides.

3.1. Sodium borohydride

3.1.1. Formation and structure

Several reactions have been reported in the literature to produce sodium borohydride [149–153]. The reaction of sodium hydride with boric oxide has been used for commercial production of $NaBH_4$ [149]:

$$4NaH + 2B_2O_3 \rightarrow NaBH_4 + 2NaBO_2 \quad (32)$$

In another reaction known as Rohm-Haas process, it can be formed with trimethyl borate and sodium hydride reactants [150,151]

$$4NaH + B(OCH_3)_3 \rightarrow NaBH_4 + 3NaOCH_3 \quad (33)$$

This reaction is performed in an autoclave in an inert atmosphere. Another way of $NaBH_4$ production is reacting dehydrated borax and silicon dioxide [152]

$$Na_2B_4O_7 + 16Na + 8H_2 + 7SiO_2 \rightarrow 4NaBH_4 + 7Na_2SiO_3 \quad (34)$$

Sodium hydroxide and diborane reaction is an alternative way of production [154]

$$4NaOH + 2B_2H_6 \rightarrow 3NaBH_4 + NaBO_2 + 2H_2O \quad (35)$$

Since $NaBH_4$ is irreversible chemical hydride and so the byproduct $NaBO_2$ is interesting candiadate to recycle it into $NaBH_4$. Kojima et al. [153] present a method to recycle it by annealing it with MgH_2 or Mg_2Si under high H_2 pressure.

$$NaBO_2 + 2MgH_2 \rightarrow NaBH_4 + 2MgO \quad (36)$$

$$NaBO_2 + Mg_2Si + 2H_2 \rightarrow NaBH_4 + 2MgO + Si \quad (37)$$

The crystal structure of sodium borohydride was first proposed by Soldate in 1947 [155] who predicted that it is based on a face centered cubic lattice and suggested that the structure consisting of tetrahedral BH_4^- ions and Na^+ ions. Abrahams et al. [156] repeated the experiment below the transition point (−83 °C) and demonstrated that sodium borohydride becomes tetragonal at −95 °C. This transition point was according to Stockmayer and Stephenson [157], the result of an order–disorder transition involving different orientations of BH_4^-. Later on, in 1985, Davis and Kennard [158] determined the structure of $NaBD_4$ using neutron diffraction, which was found to have NaCl type structure, in space group $F\bar{4}3m$ with D atoms tetrahedrally oriented about B and along all cube diagonals. This gives a random distribution of BD_4^- tetrahedra in two different configurations. Although in a recent study the structure of $NaBD_4$ was found to belong to space group $P42_1C$ [159] but a later study [160] showed that the high pressure of 6.3 GPa can alter the crystal structure of α-$NaBH_4$ (cubic $Fm3m$) to β-$NaBH_4$ (tetragonal – $P42_1C$), which further undergoes with a transition to an orthorhombic phase (Pnma) at 8.9 GPa, which is stable upto 30 GPa. It is interesting to note that this transition is completely reversible. A more recent study on the destabilization of $NaBH_4$ crystal structure by Ti doping was done by Araujo et al. [161] who predicted by first principle theory that Ti destabilizes the BH_4 cages, which in turn increases the mobility of hydrogen atoms.

This effect is explained by the formation of B-Ti bonds, rather than by the lowering of the BH_4 charge state with site occupancy of the Ti atom as shown in Fig. 17. On the basis of the above predictions Araujo et al. proposed that Ti may act as catalyst for the dehydrogenation of $NaBH_4$.

3.1.2. Thermodynamics and hydrogenation properties

Sodium borohydride is stable in dry air and can be handled easily having a theoretical hydrogen capacity of 10.8 wt% released by hydrolysis of $NaBH_4$. Schlesinger et al. [162] were the first to report 90% hydrogen evolution during the hydrolysis reaction.

$$NaBH_4 + (2 + x)H_2O \rightarrow 4H_2 + NaBO_2 \cdot xH_2O \quad (38)$$

The ΔH values for the above reaction was calculated for different values of x [163] and were found to be −216.7 kJ/mol $NaBH_4$, −250.1 kJ/mol $NaBH_4$ and −272.4 kJ/mol $NaBH_4$ for $x = 0$, 2, 4 values respectively showing that the amount of water is an important factor. DOE has given a target of $x = 0.84$ for the above reaction. To achieve this value the amount of water must be reduced to 1/15th of what is being used today [151]. To achieve hydrogen release with less water a new technique, steam hydrolysis, was proposed by Alfonso et al. [164]. Unlike the reaction in liquid water, 95% yield of hydrogen was obtained with pure steam without a catalyst.

NaOH is another important salt which must be added to the hydrolysis process. Ingersoll et al. investigated the influence of

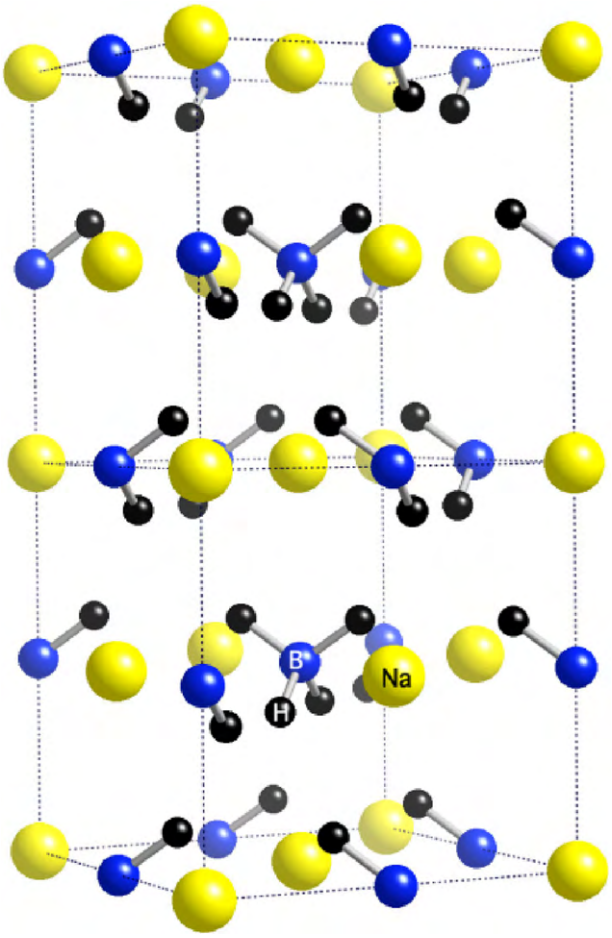

Fig. 17. The supercell geometry used to model the Ti substitutional doping in $NaBH_4$. The yellow (big), blue (medium) and black (small) balls represent the sodium, boron and hydrogen atoms, respectively. The sodium and boron sites that Ti occupies and the hydrogen that was removed are marked by Na, B and H, respectively [Reproduced from ref. [161] with permission from Institute of Physics]. (For interpretation of the color information in this figure legend, the reader is referred to the web version of the article.)

NaOH concentration in $NaBH_4$ solution on the hydrogen generation rate [165]. Mostly researchers suggest 3–5% of NaOH as being sufficient to control H_2 release [166,167]. It is also suggested that the concentration of $NaBH_4$ should be as high as possible in order to improve the fuel energy density [168]. Shang and Chen have shown that the amount of the byproduct $NaBO_2$ formed during hydrolysis also influenced the hydrogen generation rate [169,170]. It is found that the hydrolysis of $NaBH_4$ can be accelerated by the use of catalysts such as metal halides like $NiCl_2$, $CoCl_2$, colloidal platinum, active carbon, Raney nickel, Ru supported on ion exchange resin beds and fluorinated particles of Mg based materials [149,162,171,172]. Kojima et al. suggested metal–metal the oxide catalyst Pt-$LiCoO_2$ as an excellent catalyst in comparison to other reported catalyst [173] and showed that $NaBH_4$ containing 256 mg of Pt-$LiCoO_2$ reacts more than 10 times faster than Ru catalyst [171]. Fig. 18 shows the merits of different metals and metal oxide for the hydrogen generation.

Total hydrogen evolution could be enhanced upto total 6.5 wt% at 45 °C, out of which 4 wt% is at room temperature using a non-noble catalyst Ni_xB [174]. Carbon supported platinum catalyst has been proposed a good catalyst with two effects for the PEM fuel cell. One is for the hydrolysis reaction to generate H_2 and the second is to catalyze the electrochemical reaction of H_2 with O_2 subsequently [175]. The use of Al or Al alloys with $NaBH_4$ is proposed to reduce the

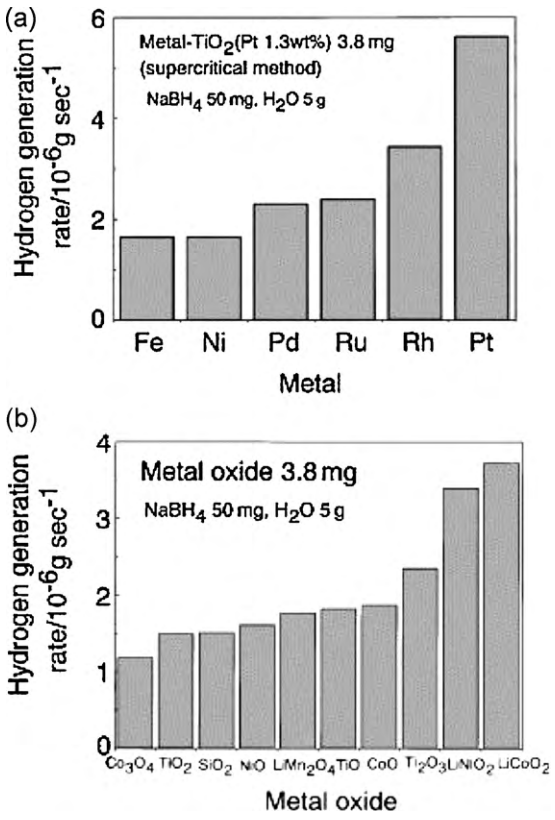

Fig. 18. Hydrogen generation rate using different (a) metals and (b) metal oxides at 20–23 °C [Reprinted from Ref. [173] with permission from Elsevier].

cost of the overall process with an increase in total yield of hydrogen evolution [176]. Soler et al. [176] found that a combination of Al/Si and $NaBH_4$ produces hydrogen with maximum flow and yields as shown in Fig. 19.

A new catalyst made from carbon nanotube paper has been developed by Alonso et al. [177]. This CNT paper was first functionalized with a monolayer of silicon carbonitride and then dispersed with Pt and Pd in picoscale amount. This catalyst is found to be capable of generating hydrogen with a rate of 300 L/min-g_{metal}-$NaBH_4$, one of the highest values reported in the literature. The authors claim to get much better result if the CNT paper is thin-

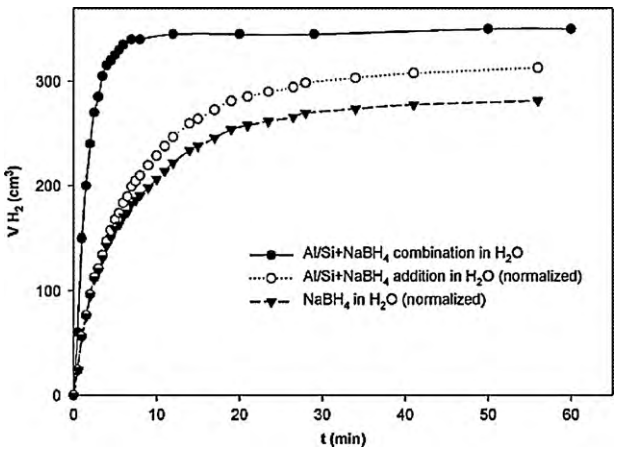

Fig. 19. Comparison of hydrogen production curves obtained in pure water for Al/Si+NaBH4 combination experiment (●) and Al/Si+NaBH4 addition experiments (▼). A synergistic effect was also observed in this case [Reprinted from Ref. [176] with permission from Elsevier].

ner in comparison to 150 μm used in this work. Recently Lee et al. [178] prepared In, Sn, and Sb based catalysts for enhancement of the evolution rate, particularly Sn incorporated into TiO_2 has greater influence on the production of H_2 from the hydrolysis of $NaBH_4$. More recently Demirci et al. [179] claimed to reach the ever highest hydrogen generation rate of about 1000 L min^{-1} g^{-1} (Ru:Al) for $RuCl_3$[50]:$AlCl_3$[50] catalyst system. Mao et al. [180] investigated the effect of various new catalyst such as TiF_3, TiO_2, Zr, Si, and some BCC alloys on the $NaBH_4$-MgH_2 system. They found that by combining $NaBH_4$ with MgH_2, the dehydrogenation temperature is decreased by 40 °C. Moreover, TiF_3 doping lowers the decomposition temperature by 100 °C with faster kinetics. Rehydrogenation upto 5.89 wt% could be possible at 600 °C and 4 MPa H_2 pressure in 12 h.

3.2. Lithium borohydride

3.2.1. Formation and structure

Schlesinger and Brown were the first who synthesized lithium tetrahydroborate ($LiBH_4$) by the reaction of ethyl lithium with diborane (B_2H_6) [181]. In a later study, they proposed the formation of $LiBH_4$ by the reaction of lithium hydride and diborane in the presence of diethyl ether [182]. A direct formation of Li salt from Li metal, boron and hydrogen at 550–700 °C and 3–15 MPa H_2 is proposed and patented by Goerrig [183]. Recently Friedrichs et al. [184] reproduce these results by synthesizing $LiBH_4$ and $LiBD_4$ directly from the elements at 700 °C under H_2/D_2 pressure of 150 bar. They performed intercalation of lithium into boron in argon atmosphere by heating Li and B upto 450 °C.

The first report on the crystal structure of $LiBH_4$ is given by Harris and Meibohm [185] using XRD who suggested the unit cell of $LiBH_4$ as orthorhombic with space group *Pcmn* with each lithium ion associated with four borohydride ions. According to them, the overall structure of lithium borohydride may be described as that of strings of borohydride tetrahedral stacked edge on edge in the b direction of the crystal. Synchrotron XRD technique has been used by Soulie et al. [186] to determine the crystal structure of $LiBH_4$ at RT and at 408 K and they also suggested the same orthorhombic symmetry with space group *Pnma*. The tetrahedral $(BH_4)^-$ anions are aligned along two orthogonal directions and are strongly distorted with respect to bond lengths and bond angles. They also suggested that the structure undergoes a transition to a hexagonal structure with increasing temperature. These results were also confirmed by a first principle study on lithium borohydride by Miwa et al [187] (Fig. 20).

3.2.2. Thermodynamics and hydrogenation properties

The decomposition of $LiBH_4$ was studied by Fedneva et al. [188] using thermal analysis (DTA) and they found 3 endothermic peaks at 108–112, 268–286, and 483–492 °C, which corresponds to the polymorphic transformation of $LiBH_4$, formation of $LiBH_4$ and finally the main evolution (80%) of hydrogen respectively [189]. This study is followed by Stasinevich and Egorenko [190] in hydrogen at pressures upto 10 bar. They suggested one of the following reactions to occur during decomposition with a total yield of hydrogen 18%.

$$LiBH_4 \rightarrow Li + B + 2H_2 \quad (39)$$

Or

$$LiBH_4 \rightarrow LiH + B + \frac{3}{2}H_2 \quad (40)$$

The desorption enthalpy and entropy were calculated as $\Delta H = -177$ kJ/mol and $\Delta S = 238$ J/K mol. These values are in disagreement with those calculated by Davis et al. [78] specially the entropy value as it is very much different from that of hydrogen.

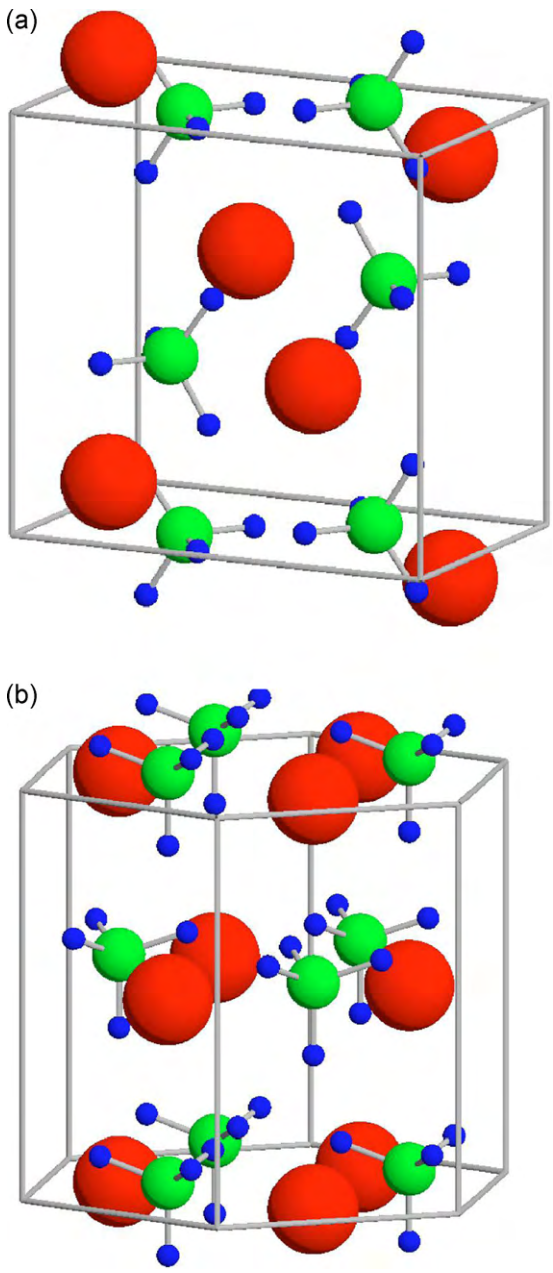

Fig. 20. Crystal structures of $LiBH_4$ in (a) orthorhombic phase at room temperature and (b) hexagonal phase at high temperature. Red (large), green (middle), and blue (small) spheres represent Li, B, and H atoms, respectively [Reprinted from ref. [187] with the permission of American Physical Society].

In a later study, Züttel explained the three possible reactions that occurred during decomposition as shown in Fig. 21 [191].

1. $LiBH_4 \rightarrow LiBH_{4-\varepsilon} + (\varepsilon/2)H_2$: structural transition at 108 °C.
2. $LiBH_{4-\varepsilon} \rightarrow LiBH_2 + (1-\varepsilon/2)H_2$: first hydrogen peak starting at 200 °C.
3. $LiBH_2 \rightarrow LiH + B + (1/2)H_2$: second peak at 453 °C.

Many efforts using additives and partial substitution have been carried out so far to improve the performance of $LiBH_4$ [192–199]. Züttel et al. [191] reported the evolution of 9 wt% H_2 (only $LiBH_4$ weight is taken into account) from 25% $LiBH_4$ ball milled with 75 wt% SiO_2 started from 523 K. The group of Orimo suggested that a reduction in stability is possible by partial cation substitution with higher electronegativity such as Mg, Cu [192,193]. Vajo et al. [194]

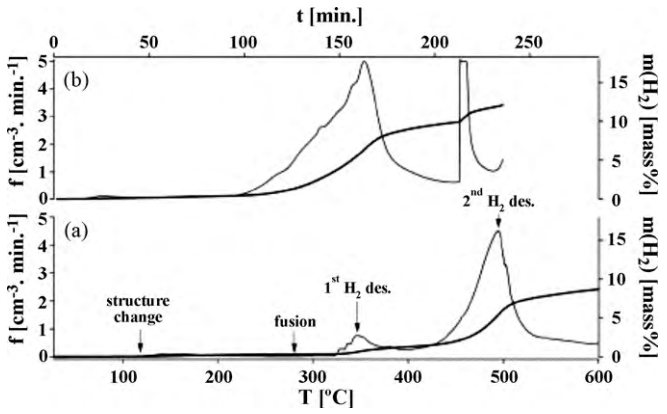

Fig. 21. Thermal desorption spectra of $LiBH_4$. The sample was heated after evacuation at room temperature with a heating rate of 2 K min^{-1}. The gas flow was measured as a function of time and the desorbed hydrogen was computed from the integrated gas flow. (a) Pure $LiBH_4$ and (b) $LiBH_4$ mixed with SiO_2 as catalyst [Reprinted from Ref. [191] with permission from Elsevier].

reported that a mixture of $LiH + 0.5MgB_2 + 0.03TiCl_3$ could absorb 7.84 wt% hydrogen at 350 °C under 100 bar H_2 pressure, while it could desorb 6.96 wt% at 450 °C. They also calculated a reduction in enthalpy of $LiBH_4$ by 25 kJ/mol H_2. Recently Au et al. [195] studied the effect of various oxides and chlorides on the decomposition temperature of $LiBH_4$ as shown in Fig. 22 and found a reduction of 200 °C in the decomposition temperature by adding V_2O_3.

Kojima et al. showed superiority of Pt dispersed $LiCoO_2$ over a mixture of Pt and $LiCoO_2$ to evolute 100% hydrogen [196]. Zhang et al. found a large dehydrogenation capacity (14 wt%) below 600 °C and a reversible capacity of 6.0 wt% H_2 at 350 °C [197] by $LiBH_4$ nanoparticles supported by disordered meso porous carbon. A different approach is adopted by Jin et al. [199] by mixing two complex hydrides $LiBH_4$ and $LiAlH_4$ doped with transition metal halides and they observed a significant enhancement in the dehydrogenation kinetics by this method.

The effective method of hydrogen evolution from $LiBH_4$ is based on the hydrolysis reaction [162]:

$$LiBH_4 + 2H_2O \rightarrow LiBO_2 + 4H_2 \quad (41)$$

The total amount of H_2 generated in this reaction is 13.9 wt% when the weight of water is also considered.

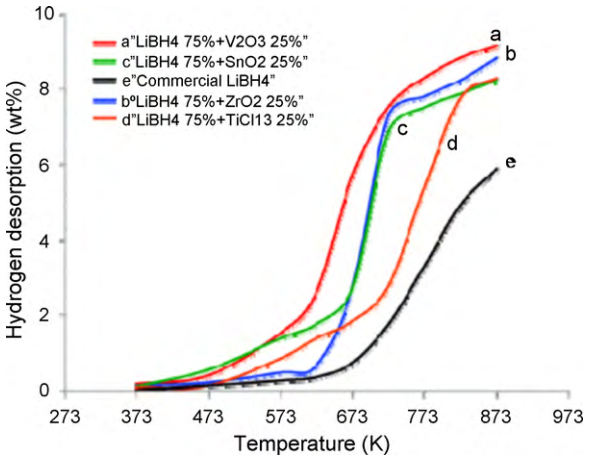

Fig. 22. Comparison of the modified $LiBH_4$ materials with the commercial $LiBH_4$ [Reprinted from ref. [195] with kind permission of American Chemical Society].

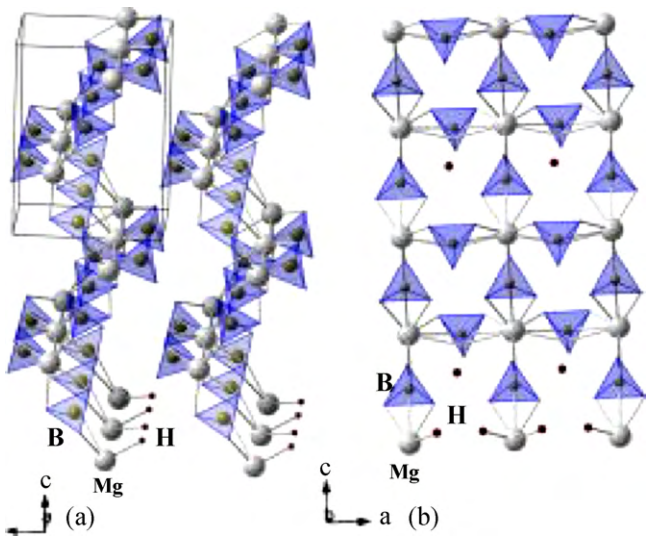

Fig. 23. (a) Three-dimensional view of the proposed crystal structure for $Mg(BH_4)_2$ and (b) projection of the structure along [010]. Atoms are labeled on the illustrations. The tetrahedral BH_4 coordinations are emphasized in all illustrations [Reprinted from ref. [205] with kind permission of American Institute of Physics].

3.3. Magnesium borohydride

3.3.1. Formation and structure

The first report on the synthesis of magnesium tetrahydroborate existing in literature is by Wiberg and Bamer [98], but the product formed in this report was with solvent, and they did not describe any procedure to desolve it without decomposing. In the late 1950s another synthesis route came into picture by the reaction of metal hydride with N-alkylborazanes [200]. A direct synthesis route from the corresponding elements was established in a German patent by Goerrig [183]. About 10 years later, Konoplev et al. [201] reported the synthesis of $Mg(BH_4)_2$ by the reaction of $MgCl_2$ and $NaBH_4$ in diethyl ether:

$$MgCl_2 + 2NaBH_4 \rightarrow Mg(BH_4)_2 + 2NaCl \quad (42)$$

Recently a synthesis by a mechanochemical method was reported by ball milling of $MgCl_2$ and $LiBH_4$ under argon atmosphere [202], however there was no separation mentioned in this method.

A direct wet chemical synthesis method [203] has been developed on the basis of proposition made by Köster et al. [200], in which Mg hydride reacts with an aminoborane as a BH_3 donor was found to be the only method capable of yielding the α-phase of $Mg(BH_4)_2$ and other tetrahydroborates in high purity without any solvents.

Earlier work suggested the existence of two crystalline modifications of $Mg(BH_4)_2$, a low temperature (LT) tetragonal phase and high temperature (HT) cubic phase [204]. Vajeeston et al. [205] predicted the structure of $Mg(BH_4)_2$ on the basis of DFT calculations and they found that $Cd(AlCl_4)_2$ type monoclinic structure proved to have the lowest total energy, however, with a higher symmetry of the orthorhombic space group $Pmc2_1$ (Fig. 23).

Nakamori et al. in another work with similar DFT calculations showed two different modifications, one having a novel ion arrangement and monoclinic symmetry [202]. In contrast to these, Cerny et al. [206] predicted the structure of $Mg(BH_4)_2$ as having hexagonal symmetry with space group $P6_1$ which contains five symmetry independent Mg^{2+} and $[BH_4]^-$ ions connected into a novel three dimensional framework. As shown in Fig. 24 each Mg^{2+} ion is surrounded by four $[BH_4]^-$ tetrahedra arranged in a deformed tetrahedron.

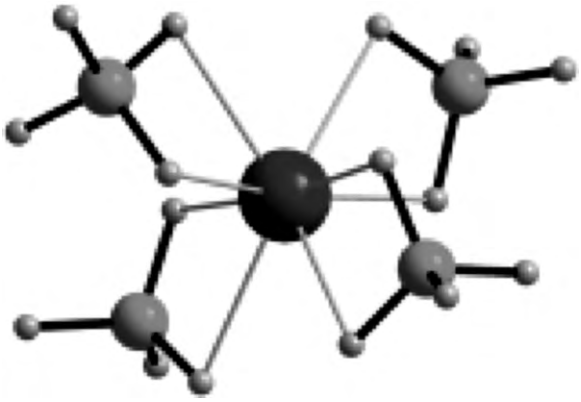

Fig. 24. Structures of $Mg(BH_4)_2$, Mg large, B medium, H small spheres [Reproduced from ref. [206] with permission from Wiley-VCH Verlag GmbH & Co.].

Recetly Her et al. [207] predicted the structure at different temperatures as shown in Fig. 25 and found that as-synthesized unsolvated $Mg(BH_4)_2$ adopts a hexagonal structure with space group $P6_1$, while it transformed to an orthorhombic structure with space group *Fddd* when heated at 453 K. These structures have a surprising level of complexity that is arguably unprecedented for this type of material [206].

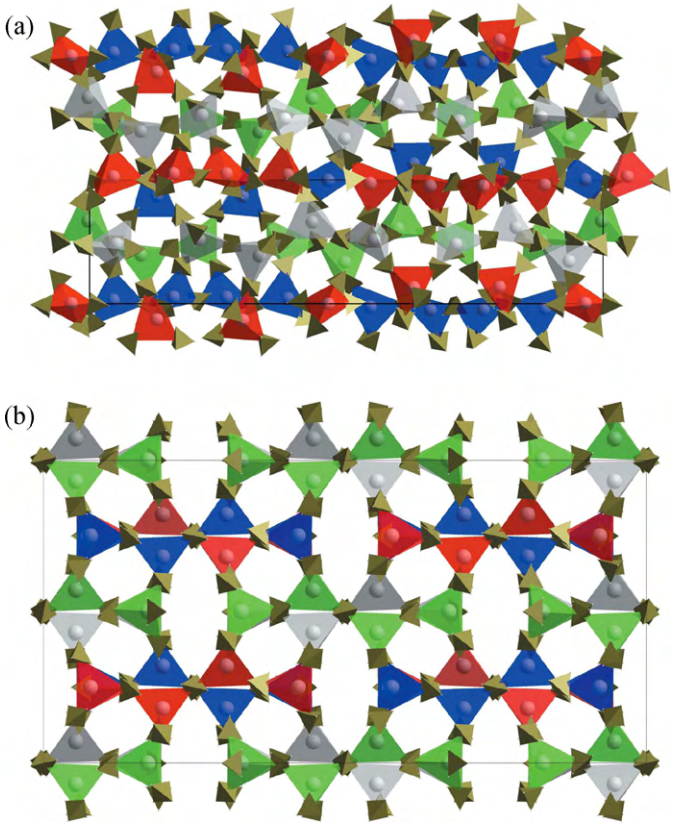

Fig. 25. (a) Structure of the LT $Mg(BH_4)_2$ phase in space group $P6_1$ viewed along the hexagonal a axis, showing two unit cells. The small opaque tetrahedra are BH_4 units; the larger (partially transparent) tetrahedra represent Mg and the four nearest B atoms. MgB_4 tetrahedra are colored according to their projection along a; units centered near 0, 1/4, 1/2, and 3/4 are colored red, green, blue and grey, respectively. (b) Structure of the HT $Mg(BH_4)_2$ phase in the space group *Fddd* viewed along the *c* axis. This is an idealized view that omits the strong antisite disorder discussed in the text. Small opaque tetrahedra are BH_4 units; MgB_4 tetrahedra are colored according to their position along *c*; units centered near 0, 1/4, 1/2, and 3/4 are colored red, green, blue and grey, respectively [Reprinted from ref. [207] with kind permission from IUCr]. (For interpretation of the color information in this figure legend, the reader is referred to the web version of the article.)

Recently George et al. [208] tried to find the effect of high pressure on the structure of $Mg(BH_4)_2$. They found an irreversible structural transition in the structure at 3.35 GPa and this phase was found to be stable under the studied pressure range i.e. upto 11 GPa. They could not solve the structure of this high pressure phase because of low intensity of $Mg(BH_4)_2$ XRD patterns. However, they confirmed that this is different from that of the high temperature orthorhombic (Fddd) phase [207], or the structures predicted by first principle calculations such as trigonal $P\bar{3}m1$, monoclinic ($P2/c$) [202], orthorhombic ($Pmc2_1$) [205], or tetragonal $I\bar{4}m1$ [209].

3.3.2. Thermodynamics and hydrogenation properties

$Mg(BH_4)_2$ has a high gravimetric hydrogen density (14.9 wt%). While the structure of $Mg(BH_4)_2$ has been investigated by several researchers, there are very little attempts to study its dehydriding properties. Hydrogen desorption reaction from $Mg(BH_4)_2$ has been proposed in two steps as follows [201,203]

$$Mg(BH_4)_2 \rightarrow MgH_2 + 2B + 3H_2 \quad (43)$$

$$MgH_2 \rightarrow Mg + H_2 \quad (44)$$

Li et al. [210] performed TG and DTA for the decomposition study of $Mg(BH_4)_2$ and found that the dehydriding reaction initiating at about 535 K with total hydrogen evolution of 13.7 wt% is confirmed upto 800 K. The above reaction is confirmed with two endothermic peaks at 574 and 645 K observed in a DTA experiment.

Matsunaga et al. [211] reported the hydrogen storage properties of $Mg(BH_4)_2$ in detail and confirmed a two step reaction from two flat plateaus observed in the desorption isotherm. They also calculated the enthalpy of the first decomposition, which is found to be −39.3 kJ/mol H_2. A different value of enthalpy change for $Mg(BH_4)_2 \rightarrow MgH_2$ i.e. 57 ± 5 kJ/molH_2 is reported by Li et al. [212] in a later work, but it is not clarified what is the reason for such a big difference in enthalpy for different measurements. They also performed the rehydrogenation of this complex and found that about 6.1 wt% hydrogen can be reversibly stored which is probably only due to the hydrogenation of Mg metal into MgH_2. More recently Soloveichik et al. [213] proposed a four-stage pathway for the thermal decomposition with formation of intermediate magnesium polyboranes that eventually transformed to the most stable magnesium dodecarbonate, and ultimately ends with formation of MgB_2 (Fig. 26).

3.4. Calcium borohydride

3.4.1. Formation and structure

The properties of calcium borohydride was reported in the mid 1950s by making it in a reaction of calcium hydride [214] or alkoxides [215] with a poisonous gas diborane. Later, a preparation method in THF [216] is proposed by Mikheeva et al. and this technique has been adopted commercially for the production of $Ca(BH_4)_2.(THF)_2$. Aduct free $Ca(BH_4)_2$ is obtained by heating $Ca(BH_4)_2.(THF)_2$ at 433 K under vacuum [217]. Recently Barkhordarian et al. [218] proposed an easy way to produce calcium hydride by the reaction of MgB_2 with CaH_2 at 400 °C under 350 bar of H_2, but they obtained MgH_2 also as a byproduct. Nakamori et al. [219] proposed direct synthesis route by ball milling of $LiBH_4$ and $CaCl_2$. More recently Ronnebro et al. proposed a solid state synthesis route by ball milling of CaB_6 and CaH_2 in molar ratio 1:2 followed by heating this mixture at 700 bar of H_2 pressure under 400–440 °C [220]. On the basis of synthesis route and conditions, $Ca(BH_4)_2$ can have different structural modifications namely α, β, and γ $Ca(BH_4)_2$ [221–223].

The first report on the crystal structure of $Ca(BH_4)_2$ is given by Kedrova et al. in the 1970s [224], although they have not given any structural parameters. Miwa et al. [217] predicted and pro-

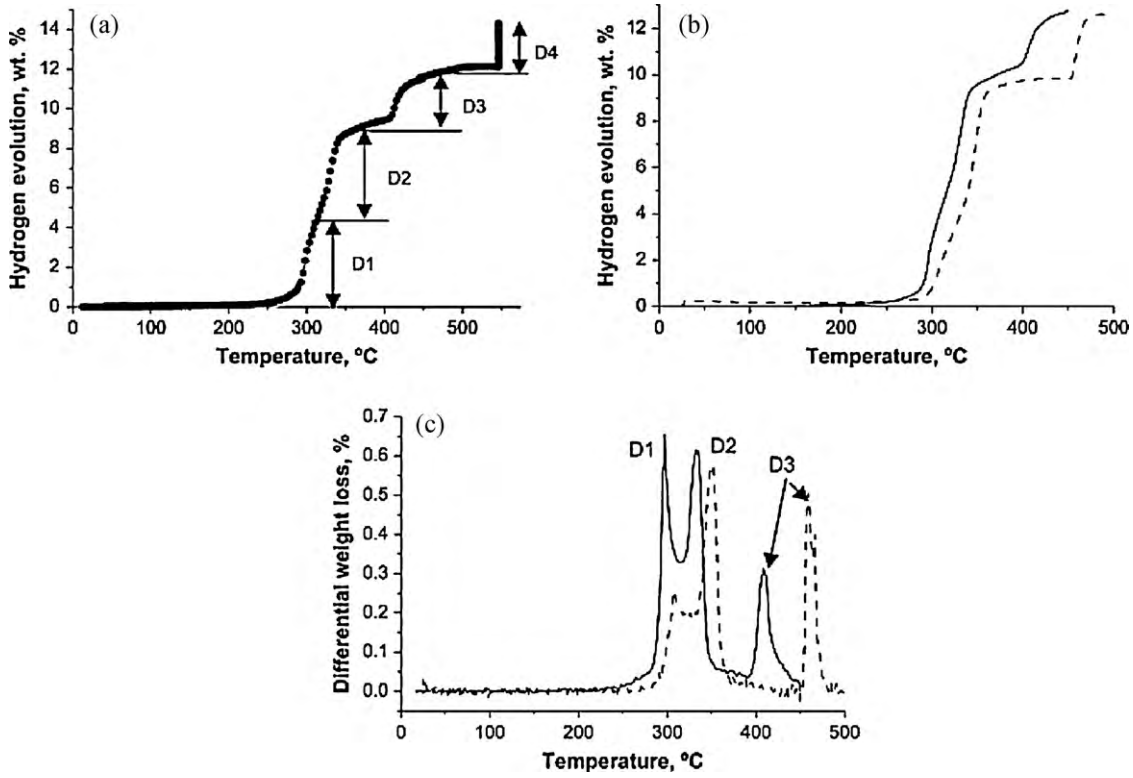

Fig. 26. TPD curve of the first decomposition of $Mg(BH_4)_2$ (a), and integral (b) and differential (c) curves of $Mg(BH_4)_2$ TPD desorption started in vacuum (solid line) and under 30 bar H_2 (dash line) [Reprinted from Ref. [213] with permission from Elsevier].

posed the crystal structure of α-$Ca(BH_4)_2$ using Rietveld analysis and suggested it to be a face centred orthorhombic structure with space group *Fddd* as shown in Fig. 27.

Each Ca^{2+} ion is surrounded by six octahedrally coordinated [BH_4^-] and each [BH_4^-] has three Ca^{2+} neighbours. The above experimental results were verified by theoretical calculations by Vajeeston et al. [225] followed by other researchers using different techniques [220,226]. Riktor et al. [223] found two modifications β-$Ca(BH_4)_2$ and γ-$Ca(BH_4)_2$ having tetragonal and orthorhombic unit cells, respectively. They also studied systematically the effect of temperature on these modifications and found that γ phase transform to β phase upon heating to 330 °C while it again changed to another unknown δ-phase by heating at 500 °C.

A more detailed study on the structure of β phase is done recently by Buchter et al. [221]. The refined structure is found to be tetragonal with space group $P4_2/m$, which is very similar to that of α-phase where Ca ions are coordinated by six (BD_4) tetrahedral as shown in Fig. 28. The BD_4 geometry is slightly distorted with B–D distances in the range 1.02–1.16 Å.

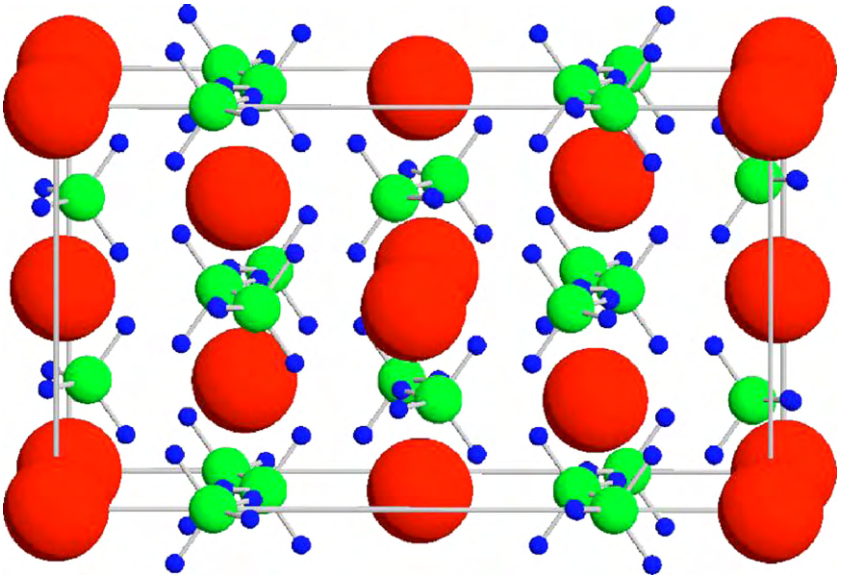

Fig. 27. Crystal structure of $Ca(BH_4)_2$. Red (large), green (middle), and blue (small) spheres represent Ca, B, and H atoms, respectively [Reprinted from ref. [217] with the permission of American Physical Society]. (For interpretation of the color information in this figure legend, the reader is referred to the web version of the article.)

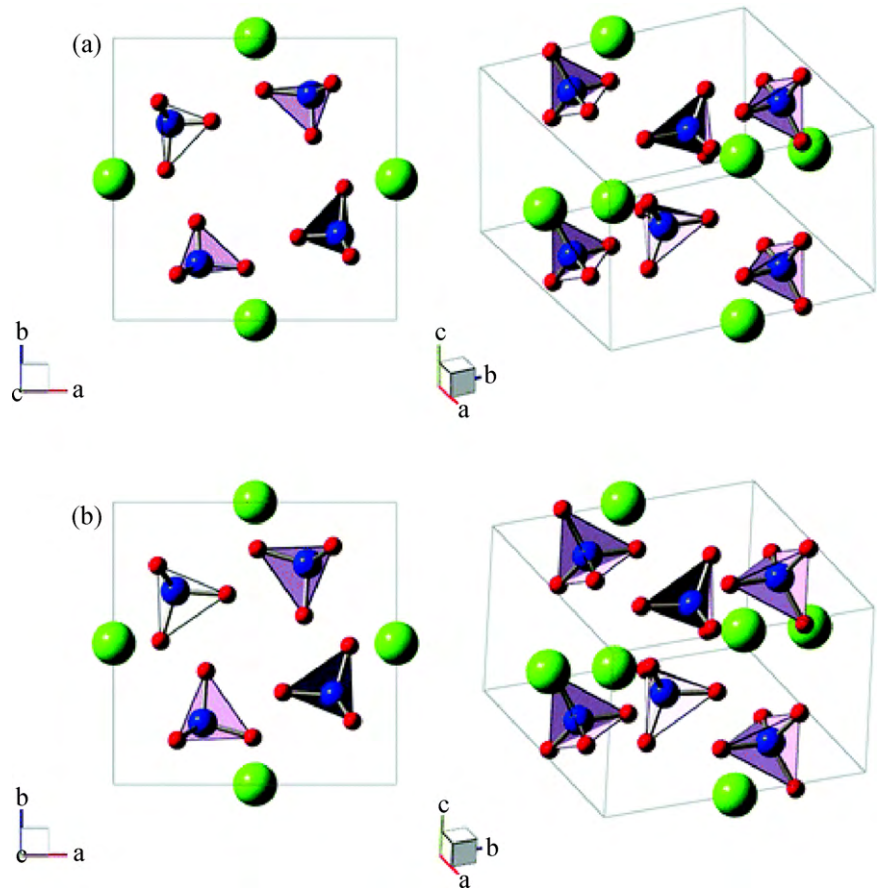

Fig. 28. Structure of experimental and theoretical $Ca(BD_4)_2$ β phase. (a) Experimentaly refined structure. (b) Ab initio calculated structure [Reprinted from ref. [221] with kind permission of American Chemical Society].

In contrast with the above findings, recently Filinchuk et al. [222] showed the formation of an intermediate tetragonal α' phase of space group *I*-42*d*. The space group of α and β modification calculated in this work are also different from those reported previously. They suggested space group *F*2dd and *p*-4 to best fit the structure of the α phase and β phase.

3.4.2. Thermodynamics and hydrogenation properties

As reported by Rönnebro et al [220], $Ca(BH_4)_2$ is formed through the following reaction:

$$CaB_6 + 2CaH_2 + 10H_2 \rightarrow 3Ca(BH_4)_2 \quad (45)$$

The reaction enthalpy of the above reaction is found to be 453 kJ/mol H_2 at $T = 0$K.

The decomposition of $Ca(BH_4)_2$ is first proposed by Miwa et al. according to following reaction with enthalpy change of 32 kJ/mol H_2 [217]:

$$Ca(BH_4)_2 \rightarrow \frac{2}{3}CaH_2 + \frac{1}{3}CaB_6 + \frac{10}{3}H_2 \quad (46)$$

The total yield of hydrogen is 9.6 wt%. The above parameters are in the range of low/medium temperature hydrides and correspond to an equilibrium pressure of 1 bar at temperatures below 100 °C, which suggest this material to be suitable for practical applications [223].

The *P*–*C* isotherm along with a TG/DTA study was reported by Aoki et al. [226] and they found 5.9 wt% hydrogen evolution at 593–650 K and rest 3.5% at around 720 K. Reversibility of $Ca(BH_4)_2$ could be achieved under 90 bar H_2 pressure at 623 K by catalyzing $Ca(BH_4)_2$ by $TiCl_3$, the hydrogen content of the sample was found to be about 3.8% [227]. In another work [228], they tried different catalysts to enhance the hydrogenation properties of $Ca(BH_4)_2$. They found NbF_5 as the best performing catalyst for the rehydrogenation upto 5 wt% of H_2 at 693 K under 90 bar pressure.

3.5. Other borohydrides

There are several other borohydrides having a general formula $M(BH_4)_n$ (M = Mn, Zn, Al, Be, Y, Dy, Gd, Zr, Rb, Cs; $n = 1, 2, 3, 4$) [229–245], but most of them were found to be unsuitable for on board hydrogen storage due to either high decomposition temperature or complete irreversibility. $Zn(BH_4)_2$ is considered a potential candidate due to its highest hydrogen storage capacity of 8.5 wt% and low decomposition temperature ~85 °C.

Zinc tetrahydroborate can be synthesized by two reactions [229–231]:

$$ZnCl_2 + 2MBH_4 \xrightarrow{(C_2H_5)_2O} Zn(BH_4)_2 + 2MCl \quad (47)$$

where M = Li, Na, K, or by

$$B_2H_6 + ZnH_2 \rightarrow Zn(BH_4)_2 \quad (48)$$

The white solid decomposes above 50 °C with a total capacity of 8.5 wt% [1,230,231] and hydrolyzes with water vigorously. But unfortunately there was no further characterization made on this material because it is very difficult to remove the solvent without decomposition of $Zn(BH_4)_2$ itself. Recently mechanochemical synthesis of $Zn(BH_4)_2$ was proposed by Jeon and Cho [232] who used $NaBH_4$ and $ZnCl_2$ as a starting material, milled it for 30 min and found $Zn(BH_4)_2$ with NaCl as a byproduct. They suggested the decomposition of $Zn(BH_4)_2$ as an endothermic reaction

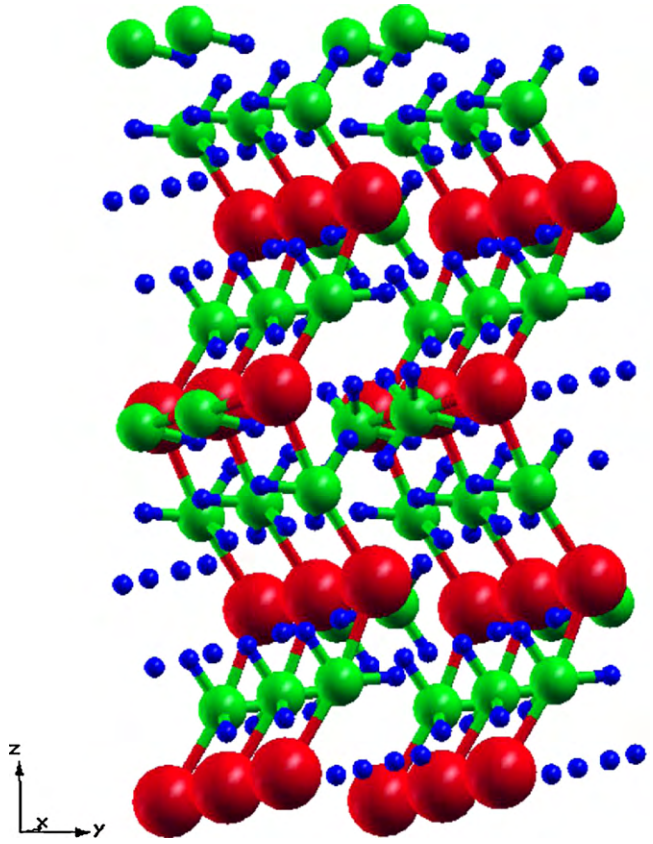

Fig. 29. Orthorhombic structure of space group $Pmc2_1$ of $Zn(BH_4)_2$ [Reprinted from ref. [235] with the permission of American Physical Society].

but it decomposes at room temperature, and so it is not suitable for reversible hydrogen storage. This conclusion is supported by a further study made by Srinivasan et al. [233,234], in which they have studied the effect of various catalysts on the decomposition behaviour. They also suggest the decomposition of $Zn(BH_4)_2$ into several boranes (diborane, tetraborane, pentaborane, hexaborane) and H_2, Zn metal as well, but they found the lack of reversibility of this compound. A contradictory but a hoping claim is made by Choudhary et al. [235] on the basis of DFT calculations, in which they proposed an orthorhombic structure with $Pmc2_1$ symmetry as the most stable structure of $Zn(BH_4)_2$ at finite temperature as shown in Fig. 29.

They also calculated the formation enthalpy of $Zn(BH_4)_2$ as −66.003 kJ/mol H_2 at 300 K and thus suggested a possibility to synthesize this phase. Except this, a number of studies have been devoted in the literature to search for different borohydrides. The different properties of all the borohydrides are summarized in Table 2.

More recently, mixed alkali metal borohydrides came into picture, which are containing dual cations [243–245]. Nickels et al. reported the synthesis of the first mixed borohydride $LiK(BH_4)_2$ by milling $LiBH_4$ and KBH_4 under argon atmosphere followed by heating at 125 °C for 12 h. The structure of $LiK(BH_4)_2$ was identified as having space group *Pnma* which is very similar to that found in orthorhombic $LiBH_4$. The Li–B bond lengths are found to be greater than in $LiBH_4$ but with a narrower range of angles. These larger Li–B separations were considered due to the presence of potassium cations in the structure. The arrangements of BH_4^- units in $LiK(BH_4)_2$ could be best described as monocapped trigonal prisms. These predictions were confirmed by a theoretical study made by Xiao et al. [244] who proposed the structure as shown in Fig. 30.

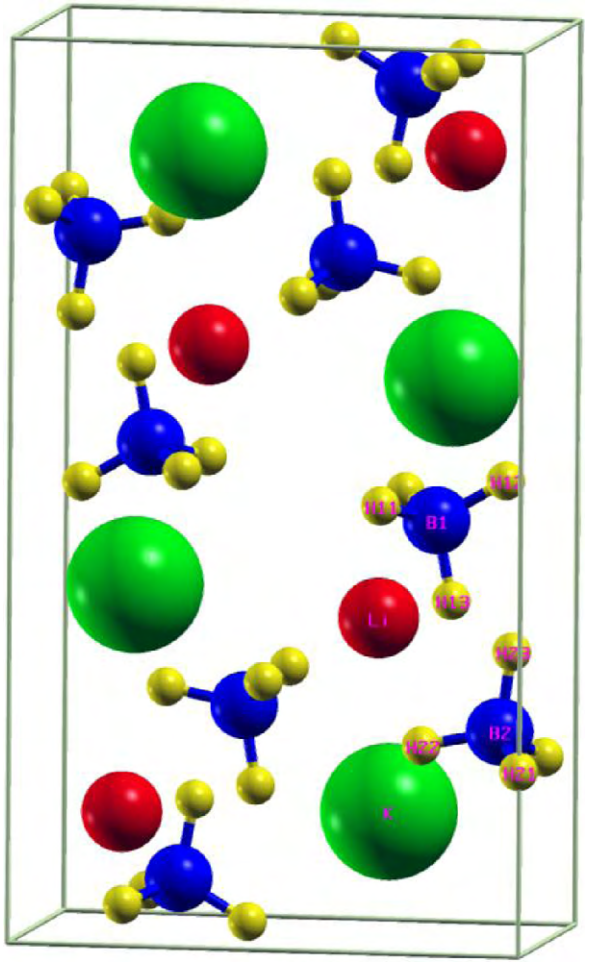

Fig. 30. Crystal structure of $LiK(BH_4)_2$. Hydrogen atoms (small yellow spheres) form tetrahedra around the boron atoms (blue spheres). The red (middle) spheres and green (large) spheres denote lithium atoms and potassium atoms, respectively [Reproduced from ref. [244] with permission from Institute of Physics].

The decomposition temperature of $LiK(BH_4)_2$ lies between those of $LiBH_4$ and KBH_4 which offers the possibility to adjust the decomposition temperature by an appropriate combination of cations [243,244].

On the basis of the above proposed method, recently Seballos et al. [245] tried to synthesize a new mixed borohydride $NaK(BH_4)_2$ from $NaBH_4$ and KBH_4. They found that unlike $LiK(BH_4)_2$ it crystallizes in a completely different rhombohedral symmetry with space group *R*3, which is different from its starting material $NaBH_4$ and KBH_4.

4. Amides and imides

Amides & imides have attracted world wide research interest because of their high hydrogen storage capacity and low operative temperature, but they suffer from poor absorption kinetics limiting their practical use. Mechanical ball milling using catalyst doping can overcome these problems. Hydrogen storage in light weight materials specially Li-N-H systems having lithium imides and amides has shown a new direction for utilization for these materials for practical application and they are very welcome to the specifications of US DOE. Scientist world wide are working in the Li-N-H system to make it useful for material applications. Important parameters, viz. crystal structure, hydrogen capacity, dissociation temperature and enthalpies are summarized in Table 3.

Table 2
Crystal structure and hydrogenation/dehydrogenation properties of borohydrides.

S. no.	Materials and their formation/dissociation reaction	Crystal structure; space group; lattice parameters (Å)	Hydrogen capacity (wt%)	Dehydrogenation temperature (°C)	Dissociation enthalpy ($kJ\,mol^{-1}H_2$)	Ref.
1.	$NaBH_4$	Cubic; $Fm\bar{3}m$	10.8	400	−216.7 to −272.4 for different values of x	[149,153,156,160,162,163,180]
	$4NaH + 2B_2O_3 \rightarrow NaBH_4 + 2NaBO_2$ $NaBO_2 + 2MgH_2 \rightarrow NaBH_4 + 2MgO$ $NaBO_2 + Mg_2Si + 2H_2 \rightarrow NaBH_4 + 2MgO + Si$ $NaBH_4 + (2+x)H_2O \rightarrow 4H_2 + NaBO_2 \cdot xH_2O$	$a = 6.1506$				
2.	$LiBH_4$	Orthorhombic; Pnma $a = 57.17858(4)$, $b = 54.43686(2)$, $c = 6.80321(4)$	13.4	380	−177.0	[181,184,186,187,189,190]
	$2LiH + B_2H_6 \rightarrow 2LiBH_4$ $LiBH_4 \rightarrow LiH + B + \frac{3}{2}H_2$					
3.	$Mg(BH_4)_2$	Different structures are suggested by different authors. See ref. [201–208]	13.7	260–400	−39.3 to −57.0	[201–211]
	$MgCl_2 + 2NaBH_4 \rightarrow Mg(BH_4)_2 + 2NaCl$ $Mg(BH_4)_2 \rightarrow MgH_2 + 2B + 3H_2$ $MgH_2 \rightarrow Mg + H_2$					
4.	$Ca(BH_4)_2$ $CaH_2 + MgB_2 + 4H_2 \rightarrow Ca(BH_4)_2 + MgH_2$ $CaH_2 + B_2H_6 \rightarrow Ca(BH_4)_2$ $Ca(BH_4)_2 \rightarrow \frac{2}{3}CaH_2 + \frac{1}{3}CaB_6 + \frac{10}{3}H_2$	α $Ca(BH_4)_2$ Orthorhombic; Fddd $a = 8.791$ $b = 13.137$ $c = 7.500$ β $Ca(BH_4)_2$ Tetragonal; $P4_2/m$ $a = 6.9468$ $c = 4.3661$ γ $Ca(BH_4)_2$ Orthorhombic; $a = 13.10$ $b = 7.52$ $c = 8.40$	9.6	350	32	[214,217,218,221,223]

4.1. Lithium amide/imide

4.1.1. Formation and structure

The early efforts for the synthesis of amides and imides were made by Gay Lussac and Thernard [246], but these were limited to only $NaNH_2$ and KNH_2. The first report on the synthesis of $LiNH_2$ came in 1894 by Titherley [247]. Later on a number of people proposed a more stabilized and reliable synthesis of $LiNH_2$ by heating Li_3N under hydrogen at 220–250 °C [248,249] and proposed following reaction:

$$Li_3N + 2H_2 \rightarrow LiNH_2 + 2LiH \quad (49)$$

On heating this mixture up to 340–480 °C, this amide converted to amide and ammonia first and then extra lithium hydride reacts with ammonia and form lithium amide again [250]. But no investigation on the reversible reaction was done. Chen et al. [251] were the first who proposed a detailed investigation on the above reaction and gave the following path

$$Li_3N + 2H_2 \leftrightarrow LiNH_2 + 2LiH + H_2 \leftrightarrow LiNH_2 + 2LiH \quad (50)$$

But the enthalpy change of step 1 is too high (148 kJ/mol H_2) and thus impractical for reversible applications. Hence, emphasis is given particularly to step 2. Recently, Shaw et al. [252] milled $LiNH_2$ and LiH in molar ratio 1:1.1 under different conditions to prepare Li_2NH.

4.1.1.1. Crystal structure of $LiNH_2$. The crystal structure of $LiNH_2$ was first demonstrated via XRD by Juza and Opp in 1951 [253] and further reinvestigated by neutron diffraction in 1972 [254]. The compound has tetragonal structure with space group $I\bar{4}$. Two hydrogen atoms form an amide ion with a nitrogen atom, which has a bent shape as shown in Fig. 31(a).

The lattice constants determined by Rietveld analysis of the X-ray powder diffraction experiment are $a = 0.5031$ nm and $c = 1.0210$ nm [254]. First principle calculations have been made by different groups [255–257] to investigate the fundamental properties i.e structural, electronic, dielectric and vibration properties. Results predict that the calculated structural parameters agree well with the experimental data except for the hydrogen positions [255,256]. Miwa et al. [255] analyzed the electronic structure and the Born effective charge tensor indicating an ionic feature between L^+ and $(NH_2)^-$. The internal bonding of $(NH_2)^-$ anion is primarily covalent. They also showed that the internal N-H binding and stretching vibrations of $(NH_2)^-$ anion yield Γ-phonon modes around 1500 and 3000 cm^{-1}, respectively. More recently, a careful structural study on the protonated sample by neutron diffraction

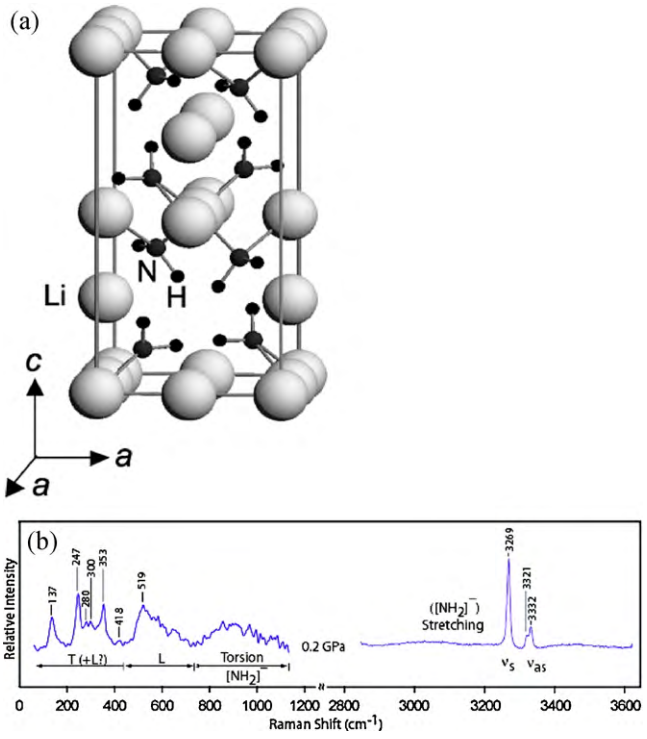

Fig. 31. (a) Atomic Structure of $LiNH_2$ [reprinted from ref. [256] with kind permission from Springer Science]; (b) Raman mode assignments of the as-loaded (~0.2 GPa) $LiNH_2$ sample. The lattice translational (T) and librational (L) are prominent and as discussed in the text; the translational and librational motions may be coupled. The internal torsional modes wagging (ö), rocking (F), and twisting (ô) appear as unresolved broad peaks (beyond 800 cm^{-1}); however, not much activity was observed in this region with increasing pressure, so the internal torsional assignment is tentative. The N-H stretching modes (îs and îas) are well-resolved [Reprinted from ref. [259] with kind permission of American Chemical Society].

confirmed the earlier studies [258] Further, Chellappa et al. [259] performed high pressure in situ Raman spectroscopy of $LiNH_2$ (shown in Fig. 31(b)) to reveal a structural phase transition from ambient pressure α-phase to β-phase at 298K and showed that orientation ordering of $(NH_2)^-$ ion occurs in the β-phase.

4.1.1.2. Crystal structure of Li_2NH. There have been several reports [260,261] on the structure of lithium imide. Noritake et al. [260] used X-ray diffraction to show that Li_2NH is face-centered-cubic with $Fm\bar{3}m$ symmetry and lattice parameter 0.5074 nm (Fig. 32). The Li, N, and H atoms occupy the 8*c* (0.25, 0.25, 0.25), 4*a* (0, 0, 0), and 48*h* (0.11, 0.11, 0.0) positions, respectively. In another report, neutron powder diffraction showed that the symmetry of crystalline Li_2NH is $F\bar{4}3m$, with a lattice parameter $a = 0.507\,69$ nm. The positions 4*c* (0.25, 0.25, 0.25) and 4*d* (0.75, 0.75, 0.75) are occupied by the Li atoms, and the 4*a* (0, 0, 0) position by the N atom. The H atom prefers the 16e (0.093, 0.093, 0.093) position [261]. The common features of the models suggested for this phase are that it is cubic with lattice parameter 0.50742 nm and that the hydrogen atoms are disordered. Song et al. [257] calculated the total energy for both the models and suggested $F\bar{4}3m$ to be the stable structure. However, early reports based on NMR investigation by Forman [262] and more recently diffraction measurements by Balogh et al. [263] found an order-disorder structural phase transition in lithium imide that occurs above room temperature (360 K) [262] While the low-temperature structure can be described as a fully ordered orthorhombic structure, the high temperature structure is still cubic (space group $Fm\bar{3}m$) with D atoms randomized over the 192l sites [262]. Since the lattice parameters of both phases in the *ab* plane are similar and the *c* direction in lithium amide

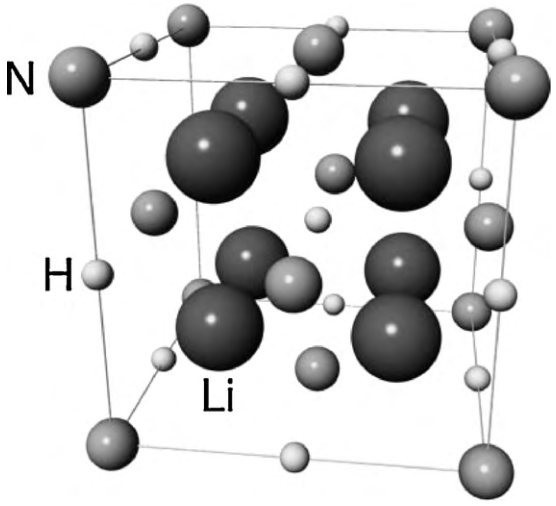

Fig. 32. Crystal structure of Li_2NH [Reproduced from ref. [261] with kind permission of Journal of the Physical Society of Japan].

is doubled, the strongest peaks from both phases appear at close *d*-spacings, which add difficulty in identifying the phases.

4.1.2. Thermodynamics and reaction mechanism

The dehydrogenation reaction of lithium amide and hydride is expressed as

$$LiNH_2 + LiH \rightarrow Li_2NH + H_2 \quad (51)$$

This reaction can theoretical absorb/desorb 6.5 wt% hydrogen and its reaction heat is 44.5 kJ/mol^2 H_2. Chen et al. [251,264] first suggested that $LiNH_2$ might directly react with LiH to generate hydrogen as defined by reaction (51). However, based on the results from a subsequent temperature programmed mass spectrometry study using two-layer materials consisting of $LiNH_2$ and LiH powders, it has been proposed by Hu and Ruckenstein [265] that reaction (51) proceeds via two elementary reactions, namely,

$$LiNH_2 \rightarrow \frac{1}{2}Li_2NH + \frac{1}{2}NH_3 \quad (52)$$

$$\frac{1}{2}NH_3 + \frac{1}{2}LiH \rightarrow \frac{1}{2}LiNH_2 + \frac{1}{2}H_2 \quad (53)$$

As shown in reactions (52) and (53), reaction (51) proceeds by decomposition of $LiNH_2$ to Li_2NH and NH_3 first, followed by reaction of LiH with NH_3 to form H_2 and $LiNH_2$. The newly formed $LiNH_2$ decomposes again and repeats the cycle of reactions (52) and (53). Such successive reactions continue until all $LiNH_2$ and LiH completely transform to Li_2NH and H_2. It has been shown that reaction (53) takes place very fast in the order of less than 25 ms. However, even with such high-reaction rates, escape of NH_3 from the hydrogen storage system has been reported [266–268] and used as an indirect evidence to support the mechanism defined by reactions (52) and (53) [255]. Several recent studies [269,270] have also provided evidence supporting the two-step elementary reaction mechanism. Recently, Hu et al. [271] investigated the reaction mechanism of a $LiNH_2$ + LiH mixture using variable temperature in situ ^1H NMR spectroscopy and observed NH_3 release at a temperature as low as 30 °C with the rapid reaction between NH_3 and LiH at 150 °C. The transition from NH_3 release to H_2 appearance accompanied by disappearance of NH_3 confirmed the 2-step reaction pathway proposed earlier. Shaw et al. [252] proposed a model describing the major steps of the dehydriding reaction of the mixture and related them to the evidence obtained from the X-ray diffraction and specific surface area measurements of the mixture before and after 10 isothermal cycles at 285 °C. The study revealed

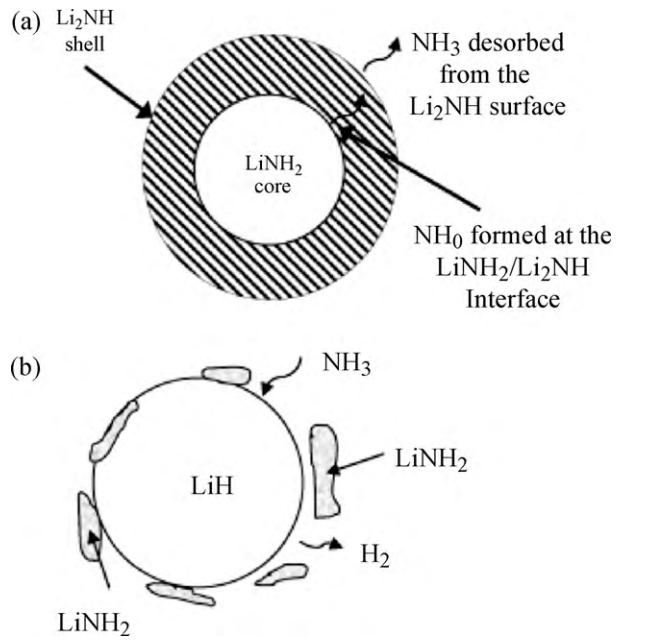

Fig. 33. Schematic of the hydrogen release pathway of the $LiNH_2$ + LiH mixture: (a) the Li_2NH product forms a continuous shell outside the $LiNH_2$ shrinking core, leading to a reaction rate controlled by NH_3 diffusion through the Li_2NH product layer, and (b) the $LiNH_2$ product flakes off continuously, resulting in direct reaction between NH_3 and constantly regenerated new LiH surface [Reprinted from Ref. [252] with permission from Elsevier].

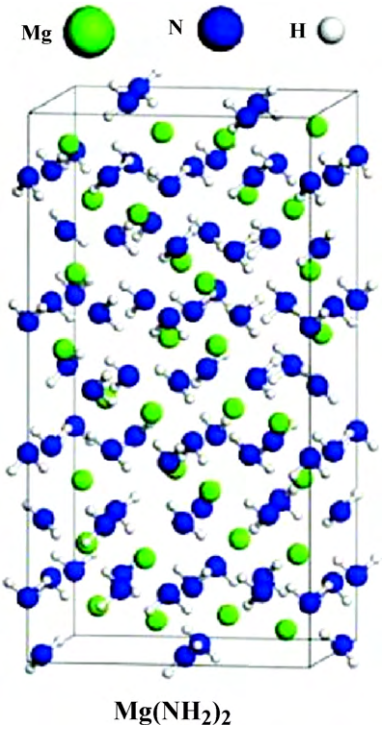

Fig. 34. Unit cell of $Mg(NH_2)_2$ with green, blue and grey spheres representing Mg, N and H [Reprinted from ref. [276] with kind permission of American Chemical Society].

that dehydrogenation of the mixture is diffusion controlled and the rate limiting step is NH_3 diffusion through the Li_2NH product layer outside the $LiNH_2$ shrinking core as shown in Fig. 33.

4.2. Magnesium amide/imide

4.2.1. Formation and structure

Initially magnesium amide $Mg(NH_2)_2$ was synthesized by a reaction of magnesium nitride Mg_3N_2 or Mg with ammonia and the time taken for the completion was of the order of ages [272,273]. Recently Nakamori et al. [274] prepared the Mg amide and imide by a gas–solid reaction of MgH_2 with ammonia. The MgH_2 was placed in a Mo crucible, sealed and connected to the reaction tube for NH_3 introduction at 0.5 MPa. The crucible was then heated upto a temperature of 603–653 K for 1 week. X-ray diffraction profile at varying temperatures indicated the formation of single phase $Mg(NH_2)_2$ upon heating the sample to 613 K by the following reaction:

$$MgH_2 + 2NH_3 \rightarrow Mg(NH_2)_2 + 2H_2 \quad (54)$$

$$Mg + 2NH_3 \rightarrow Mg(NH_2)_2 + H_2 \quad (55)$$

Jacobs et al. [272] first reported the crystal structure of Mg $(NH_2)_2$ in 1969. Mg $(NH_2)_2$ is characterized by tetragonal unit cell belonging to space group No. 142 $I4_1/acd$, $a = 10.37$ Å, $c = 20.15$ Å. The unit cell contains three crystallographically different amide $(NH_2)^-$ units and the H–N–H angle varies between 104.1° and 129.6°. In a recent report, Sorby et al. [275] used neutron powder diffraction (NPD) to demonstrate the same space group for Mg $(ND_2)_2$ with little difference in lattice parameters, which are $a = 10.3758$ Å and $c = 20.062$ Å respectively. Wang et al. [276] used both the above experimental structures to compute the total energy of $Mg(NH_2)_2$: (−1589.2606 eV/formula unit for the former and −1589.2866 eV/formula unit for the latter, respectively) and thus concluded that the latter structure is more likely to be the stable structure for $Mg(NH_2)_2$ as shown in Fig. 34.

4.2.2. Thermodynamics and reaction mechanism

Magnesium amide $Mg(NH_2)_2$, a lightweight amide, decomposes to magnesium imide (MgNH) and ammonia at elevated temperatures [277]. The generation of ammonia starts at about 200 °C. Nakamori et al. investigated the thermal behavior of the mixture of $Mg(NH_2)_2$ with MgH_2 by means of thermogravimetry-differential thermal analysis (TG-DTA). Instead of the expected interaction between amide and hydride, they only observed the self-decomposition of $Mg(NH_2)_2$ [274]. However, Hu et al. [278,279] showed that hydrogen desorption from $Mg(NH_2)_2$ and MgH_2 (at either a 1:1 or 1:2 molar ratio) can occur under a mechanochemical reaction condition, i.e. energetic ball milling, as shown by the reactions [278,279]:

$$Mg(NH_2)_2 + MgH_2 \rightarrow 2MgNH + H_2 \quad (56)$$

$$Mg(NH_2)_2 + 2MgH_2 \rightarrow Mg_3N_2 + 4H_2 \quad (57)$$

Hu et al. [279] showed that a total of 7.4 wt% of hydrogen was released from the mixture of magnesium amide and magnesium hydride at a molar ratio of 1:2 by mechanical ball milling. Fourier Transform Infrared Spectroscopy (FTIR) and X-ray diffraction (XRD) characterizations along with the amount of hydrogen released at different stages of ball milling (shown in Fig. 35) reveal that magnesium imide was first formed in the reaction. The imide then reacted continuously with magnesium hydride and was converted to magnesium nitride and hydrogen.

$$Mg(NH_2)_2 + 2MgH_2 \rightarrow 2MgNH + MgH_2 + 2H_2 \quad (58)$$

$$2MgNH + MgH_2 \rightarrow Mg_3N_2 + 2H_2 \quad (59)$$

The overall reaction is given by reaction (57).

Thermodynamic analysis revealed that the average heat of desorption is ~3.5 kJ/mol H_2 [279] for reaction (57), indicating that Mg_3N_2 can hardly be converted to $Mg(NH_2)_2$ and MgH_2 under normal hydrogenation conditions. It took 72 h to complete the hydrogen desorption even if the dehydrogenation was allowed

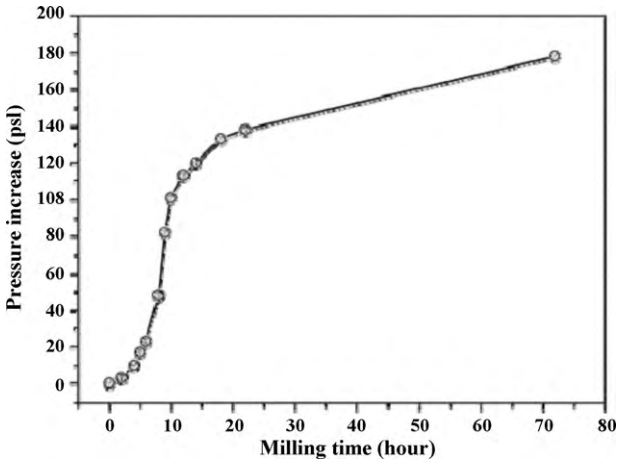

Fig. 35. Time dependence of the hydrogen pressure increase in the milling jar [Reprinted from ref. [279] with kind permission of American Chemical Society].

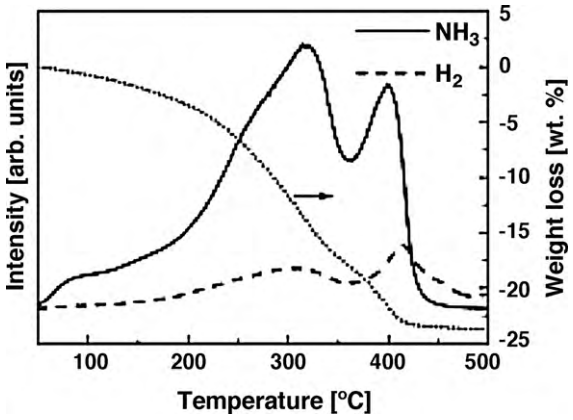

Fig. 37. Thermal desorption mass spectra (TDMS) and thermogravimetry (TG) analysis for $Ca(NH_2)_2$ in the heating process up to 500 °C under a He gas flow atmosphere at a heating rate of 5 °C/min. Here, the solid line indicates NH_3 desorption, the dashed line shows H_2 desorption and the dotted line shows weight loss [Reprinted from Ref. [284] with permission from Elsevier].

thermodynamically. Therefore, the overall kinetics for hydrogen desorption should be rather slow, which might be the reason why investigations by other researchers have failed to detect the reaction between $Mg(NH_2)_2$ and MgH_2 [274].

4.3. Calcium amide/imide

4.3.1. Formation and structure

Two different approaches for the preparation of calcium amide were used [280–284].

4.3.1.1. Ball milled Ca_3N_2. Kojima et al. [281] performed a mechanochemical reaction by ball milling calcium nitrides Ca_3N_2 in H_2 atmosphere at a pressure of 1 MPa and room temperature. The XRD pattern indicated the presence of orthorhombic CaH_2 [282] along with CaNH or Ca_2NH because the unit cell of both the imides is cubic and their diffraction patterns are similar.

The only difference is that the N-H bond is present in CaNH while absent in Ca_2NH. The crystal structure of CaNH and Ca_2NH is given in Fig. 36 w.r.t. generation of a possible N–H bond.

It was shown by the infra red absorption spectra that ball milled Ca_3N_2contains CaNH.

Thus, the reaction of Ca_3N_2 and H_2 is expressed as:

$$Ca_3N_2 + 4H_2 \leftrightarrow 2CaNH + CaH_2 + 2H_2 \quad (60)$$

$$2CaNH + CaH_2 + H_2 \rightarrow Ca(NH_2)_2 + 2CaH_2 \quad (61)$$

4.3.1.2. Ball milled CaH_2. Leng et al. and coworkers [283,284] prepared Ca amide by mechanical milling of CaH_2 in NH_3 atmosphere for 18 h. The atmosphere was replaced to pure NH_3 every 2 h milling so as to realize the gas–solid reaction completely.

$$CaH_2 + 2NH_3 \rightarrow Ca(NH_2)_2 + 2H_2 \quad (62)$$

4.3.2. Decomposition behavior of $Ca(NH_2)_2$

Juza and Schumacher [285] performed partial decomposition studies of $Ca(NH_2)_2$ (up to 67.7%) and regarded the decomposed phase as cubic calcium imide (CaNH) phase through XRD analysis. Recently Leng and co-workers [283,284] investigated the thermal decomposition behavior of calcium amide up to 500 °C. The thermal decomposition mass spectroscopy (TDMS) profile indicated that $Ca(NH_2)_2$ decomposed to CaNH in the heating process up to 500 °C. The starting temperature of the decomposition is about 60 °C as shown in Fig. 37.

The XRD profile shows that CaNH produced agrees with the cubic CaNH phase up to 350 °C, but changes to an unknown phase up to 500 °C. The H_2 desorption process from the mixture of Ca $(NH_2)_2$ and CaH_2 with 1:3 molar ratio was carefully examined.

Hino et al. [284] indicated that the H_2 desorption reaction can be described by the following two reactions:

$$Ca(NH_2)_2 + CaH_2 \rightarrow 2CaNH + 2H_2 \quad (63)$$

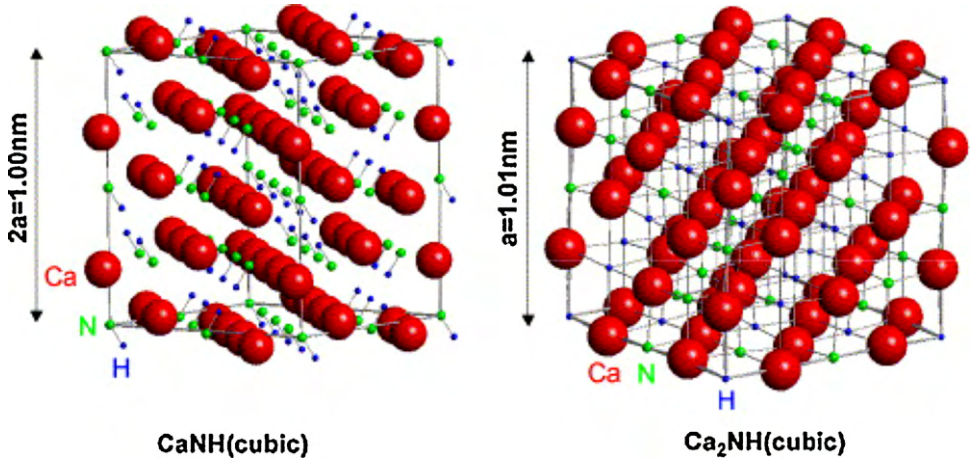

Fig. 36. Crystal structures of CaNH and Ca_2NH [Reprinted from Ref. [281] with permission from Elsevier].

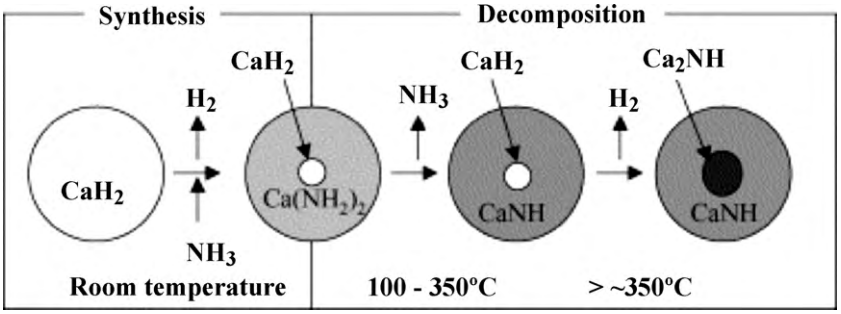

Fig. 38. Schematic diagram for the synthesis and decomposition processes of $Ca(NH_2)_2$. Synthesis: CaH_2 reacts with ammonia to produce $Ca(NH_2)_2$ during milling, but still exists in a core part. Decomposition: $Ca(NH_2)_2$ decomposes to CaNH by heating, then CaNH reacts with CaH_2 in the core part at high temperatures and desorbs H_2 [Reprinted from Ref. [284] with permission from Elsevier].

and

$$CaNH + CaH_2 \rightarrow Ca_2NH + H_2 \quad (64)$$

where the former and the latter reactions are exothermic and endothermic, respectively.

Hino et al. [284] explained the H_2 desorption occurs due to a direct solid–solid reaction [251] between CaNH and CaH_2, where CaH_2 still remains in the core part of $Ca(NH_2)_2$ after reaction (62) (Fig. 38).

4.4. Other amides/imides

4.4.1. Li-Mg-N-H

Among these systems, the Li-Mg-N-H system shows promising characteristics for onboard vehicular application as it significantly decreases the enthalpy of reaction and thus favors reversible hydrogen storage near ambient conditions. Studies on various Mg:Li ratios have been reported in the literature [286–291] and can be summarized as:

- Mg:Li = 1:2 (cf. Luo and Sickafoose [287,288], Xiong [289,290])

$$3Mg(NH_2)_2 + 6LiH \leftrightarrow 3Li_2Mg(NH)_2 + 6H_2 \quad (65)$$

- Mg:Li = 3:8 (Luo and Ichikawa [287,291])

$$3Mg(NH_2)_2 + 8LiH \leftrightarrow 4Li_2NH + Mg_3N_2 + 8H_2 \quad (66)$$

- Mg:Li = 1:4 (cf. Orimo et al. [274,256])

$$3Mg(NH_2)_2 + 12LiH \rightarrow 4Li_3N + Mg_3N_2 + 12H_2 \quad (67)$$

The trend is that the reversible capacity increases when decreasing the Mg content. The capacity reaches 7.0 and 9.2 wt% for reactions (66) and (67), but a high temperature (up to 500 °C) is required to achieve full hydrogen desorption for these reactions, due to the stability of the transitory imide phases. Consequently, the most promising material concerns Mg:Li = 1:2 ratio, with both a high capacity (5.6 wt%) and a relatively low operating temperature (about 200 °C).

4.4.1.1. Formation and structure. Two methods have been described for the formation of the dehydrided phase, $Li_2Mg(NH)_2$, starting from $LiNH_2$ and MgH_2 [289,292].

$$2LiNH_2 + MgH_2 \rightarrow 3Li_2Mg(NH)_2 + 6H_2 \quad (68)$$

One method involves direct dehydriding (at 300 °C) under vacuum of a mechanically milled mixture of $LiNH_2$ and MgH_2 in a 2:1.1 molar ratio [289]. According to this method, removal of hydrogen gas through evacuation should presumably facilitate the formation of the dehydrided mixed imide phase, $Li_2Mg(NH)_2$. However, a second competitive reaction can also occur under these conditions, involving the decomposition of $LiNH_2$ into NH_3 and Li_2NH [253,265,269]:

$$2LiNH_2 \rightarrow Li_2NH + NH_3 \uparrow \quad (69)$$

Thus, when the milled mixture of $LiNH_2$ and MgH_2 is initially heated under vacuum, it is possible for the decomposition reaction (69), to occur prior to or in parallel with the reaction (68). The competition between reactions (68) and (69) is important, since any contribution of reaction (69) would result in a permanent decrease in the reversible storage capacity for this system.

The second route suggested by Luo et al. [287,288] involves the formation of the mixed imide phase is a two-step process, wherein $LiNH_2$ and MgH_2 are initially transformed to Mg $(NH_2)_2$ and LiH

$$2LiNH_2 + MgH_2 \rightarrow Mg(NH_2)_2 + 2LiH \quad (70)$$

and these products are reversibly decomposed to form $Li_2Mg(NH)_2$ according to

$$Mg(NH_2)_2 + 2LiH \rightarrow Li_2Mg(NH)_2 + H_2 \quad (71)$$

This second activation route is achieved under heat at static, positive hydrogen or inert gas pressure to prevent decomposition of $LiNH_2$ according to reaction (69).

The crystal structure of mixed imide $Li_2Mg(NH)_2$ was first examined by Rijssenbeek et al. [293] using in situ X-ray diffraction. The structure at ambient conditions is characterized by a tetragonal unit cell with space group No. 45 (*Iab*2), and lattice parameters $a = 9.7871$ Å, $b = 4.9927$ Å and $c = 20.15$ Å respectively. Their study showed that $Li_2Mg(NH)_2$ undergoes progressive disordering of the cations and the cation vacancies as temperature increases, resulting in two disordering transitions at elevated temperatures. The corresponding three phases at and above room temperature are determined, via a combination of X-ray and neutron powder diffraction, to be orthorhombic (α), primitive cubic (β) and face-centered cubic fcc (γ) phases. In all three phases, the N-atom lattice resembles a slightly distorted fcc lattice similar to the arrangement in lithium imide/amide and magnesium amide [263,275]. The Li/Mg cations are located at the tetrahedral interstitial sites of this fcc lattice. Not all of the tetrahedral interstitial sites are occupied. In the room temperature (α) phase, 25% of the tetrahedral sites are ordered vacancies, while Li and Mg occupy the remaining tetrahedral sites in a disordered fashion (Fig. 39).

As temperature is raised above 350 °C, the (α) phase converts into the (β) phase, where some of the tetrahedral sites (3c) are disorderly occupied by Li and Mg, and some others (3d) are partially occupied by Li, leading to disordered arrangement of both cation and cation vacancy. A fraction of the tetrahedral sites is still orderly occupied by either Li or vacancies. When temperature is raised above 500 °C, the (β) phase converts into the (γ) phase, where all the tetrahedral sites are disorderly occupied by Li, Mg,

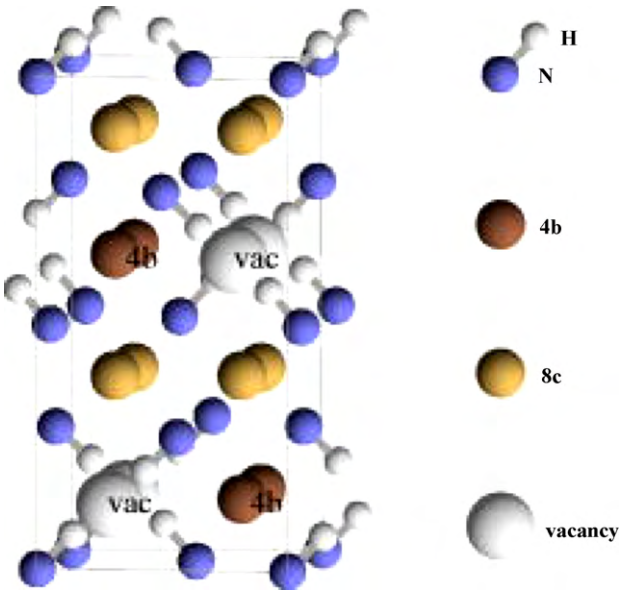

Fig. 39. Ball and Stick models for $\alpha Li_2Mg(NH_2)_2$. The origin is set at a *n* atom. The large light spheres represent cation vacancies. The figure shows the specific cation disordered figure of the Li-Mg mixed amide [Reprinted from ref. [296] with kind permission of American Institute of Physics].

and vacancies. Wang et al. [294] used pseudo potential density functional calculations to identify important local orderings for the experimentally observed disordered phase at room temperature. Velikokhatnyi et al. [295] calculated the electronic structure and density of states as well as vibrational properties of the mixed imide and showed that GGA approximation to the exchange correlation potential allows obtaining the calculated structural parameters of the material within the accuracy of ~1.5–2%. Recently, Maa et al. [296] proposed an ordered structure at low temperature with Mg atoms placed at face-diagonal arrangements on the "cubes" formed by tetrahedral interstitial sites of an fcc lattice, and arrange themselves in alternating face-diagonal directions on opposite faces of two adjacent cubes (Fig. 40).

4.4.1.2. Thermodynamics and reaction mechanism. Luo [292] first reported that the mixture $2LiNH_2 + 1.1MgH_2$ desorbs hydrogen at 30 bar H_2 pressure at 200 °C with the hydrogen capacity

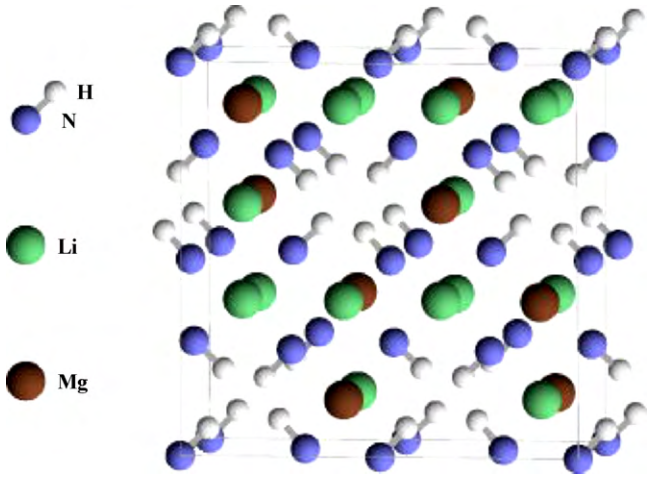

Fig. 40. A low-energy crystal structure proposed for $Li_2Mg(NH)_2$ at low temperature [Reprinted from ref. [296] with kind permission of American Institute of Physics].

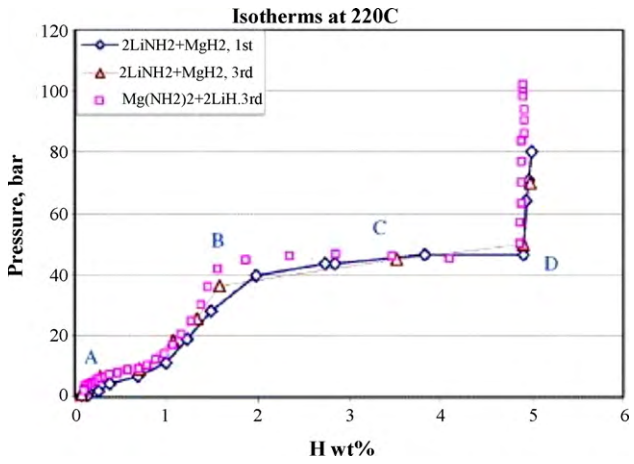

Fig. 41. Desorption pressure-composition isotherms at 220 °C for first and third desorption of the $(2LiNH_2 + MgH_2)$ sample. Desorption isotherm for $(Mg(NH_2)_2 + 2LiH)$ is included. Letters A, B, C and D mark hydrogen contents (weight percent) in the solid: Hwt.% is 0 at point A; Hwt.% is 1.5 at point B (the beginning of plateau); Hwt.% is 3.2 at point C (the mid-point of the plateau); Hwt.% is 5 at point D (the end of plateau) [Reprinted from Ref. [288] with permission from Elsevier].

of 4.5 wt% and enthalpy of reaction 39 kJ/mol. It was supposed that the reaction during the absorption/desorption for the system is reversible between $2LiNH_2 + MgH_2$ and $Li_2Mg(NH)_2 + 2LiH$.

This assumption is partially correct since the rehydriding material is not $2LiNH_2 + MgH_2$ but $Mg(NH_2)_2 + 2LiH$. Gross and Luo [297] further performed a cycle life test and showed that the system looses only 11% capacity after 100 cycles. Based on the information of pressure-composition isotherms, powder XRD and FTIR, Luo et al. [288] proposed a mechanism for the sorption reactions (Fig. 41).

There are two different processes, which take place in the sorption isotherm. In the sloping part of the isotherm a single solid-phase reaction takes place. In this step no more than one hydrogen-atom is inserted into each formula unit of $Li_2MgN_2H_2$, forming $Li_2MgN_2H_3$ with $-NH_2$ bonded to Li. Upon the completion of the single phase reaction, a multiple solid phase reaction takes place which corresponds to the plateau region. In this reaction three more hydrogen atoms are added to each formula unit of $Li_2MgN_2H_3$ which leads to the formation of the new species, $Mg(NH_2)_2$ and LiH as shown in Fig. 42.

Recently Yang et al. [298] suggested that although the hydrogen released temperature for the system is projected to be 90 °C at 1 bar but the reaction kinetics is quite slow (at 180 °C absorbing <2 wt%). Thus additional work is required to develop and incorporate an effective catalyst to overcome the current kinetic barriers and decrease the hydriding/dehydriding reaction temperature to there thermodynamically predicted values.

Recently, Alapati et al. [299] predicted the $LiNH_2$ and MgH_2 in 1:1 molar ratio could be energetically favorable by first principles density function theory (DFT) calculations.

$$LiNH_2 + MgH_2 \leftrightarrow LiMgN + 2H_2 \quad (72)$$

This reaction yields 8.19 wt% hydrogen at completion with a calculated reaction enthalpy of 9.7 kJ/mol H_2 at 0K using the ultrasoft pseudo potential (USPP) approach. Furthermore, Akbarzadeh et al. [300] inferred that the 1:1 mixture of $LiNH_2$ and MgH_2 would decompose according to the following sequential reactions by the modern first-principles calculations of total energies and vibra-

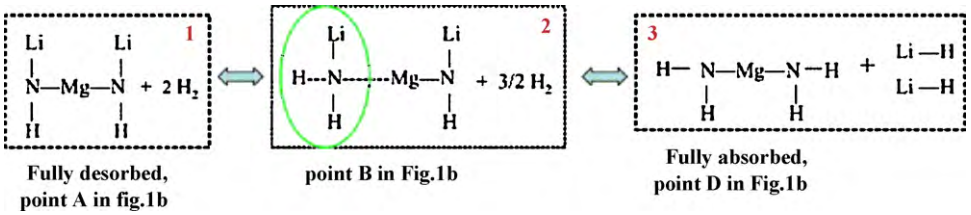

Fig. 42. Proposed mechanism for the sorption reactions [Reprinted from Ref. [288] with permission from Elsevier].

tional free energies:

$$LiNH_2 + MgH_2 \rightarrow \frac{1}{2}Mg(NH_2)_2 + LiH + \frac{1}{2}MgH_2 \rightarrow \frac{1}{4}Mg(NH_2)_2 + \frac{1}{4}Mg_3N_2 + LiH + H_2 \rightarrow \frac{1}{4}Li_2MgN_2H_2 + \frac{1}{4}Mg_3N_2 + \frac{1}{2}LiH + \frac{3}{2}H_2 \rightarrow LiMgN + 2H_2 \quad (73)$$

Interestingly enough, instead of the predicted reactions 1 and 3 of equation (73), Osborn et al. [301] found experimentally the presence of a new product, $Li_2Mg_2(NH)_3$, after dehydrogenation of the $LiNH_2$-MgH_2 mixture at 210 °C as expressed in the following reaction:

$$LiNH_2 + MgH_2 \rightarrow \frac{1}{3}Li_2Mg_2(NH)_3 + \frac{1}{3}LiH + \frac{1}{3}MgH_2 + H_2 \quad (74)$$

Thermodynamic analysis made by Liu et al. [302] showed that the 1:1 molar ratio of $LiNH_2$-MgH_2 system desorbs 6.1 wt% hydrogen in an endothermic reaction, and the overall heat of reaction was calculated as 45.9 kJ/mol of H_2.

4.4.2. Li-Ca-N-H

Xiong et al. [289] first reported that the mixture of $LiNH_2$ and CaH_2 with a 2:1 molar ratio desorbs hydrogen from 70 °C and takes a hydrogen desorption peak at 206 °C at the heating rate of 2 °C/min in the temperature programmed desorption (TPD) profile. Furthermore, Hino et al. [284] have explained the thermal desorption mass spectra (TDMS) of calcium amide $Ca(NH_2)_2$ in detail and clarified that $Ca(NH_2)_2$ decomposes into Ca(NH) and emits NH_3 at a lower temperature Tokoyoda et al. [303] proposed the reversible hydrogen storage reaction for Li-Ca-N-H as:

$$CaH_2 + 2LiNH_2 \rightarrow CaNH + Li_2NH + 2H_2 \leftrightarrow Ca(NH_2)_2 \quad (75)$$

According to this reaction equation the system possesses a theoretical hydrogen storage capacity of 4.5 wt%. More recently, Wu et al. [304] used X-ray diffraction to understand the intermediate products formed at different dehydrogenation stages (shown in Fig. 43) and proposed the structure for ternary compound $Li_2Ca(NH)_2$ using neutron powder diffraction. Rehydrogenation of this product does not lead to the initial mixture ($2LiNH_2 + CaH_2$) (Fig. 44).

4.4.3. Li-Al-N-H

Investigations on metal-N-H system reveals that mixtures of amide and binary hydrides of alkali and alkaline earth metals are capable of releasing hydrogen due to Coulombian attraction between $H^{\delta+}$ in amide and $H^{\delta-}$ in hydrides. Based on this interpretation, studies have been made on the amide-complex hydride systems such as $NaAlH_4$, $LiAlH_4$ and $LiBH_4$.

Attempts have been made by different groups for hydrogen release from $LiNH_2$-$LiAlH_4$ and $NaNH_2$-$LiAlH_4$ systems [305,306]. Fast hydrogen release was observed by Xiong et al. [307] from the mixture of $NaNH_2$ and $LiAlH_4$ upon ball milling, i.e; 4-H atoms per ($1NaNH_2$-$1LiAlH_4$) were detached from the mixture within 10 min. Unfortunately the reaction was exothermic which is irreversible for the release process of hydrogen under practical conditions.

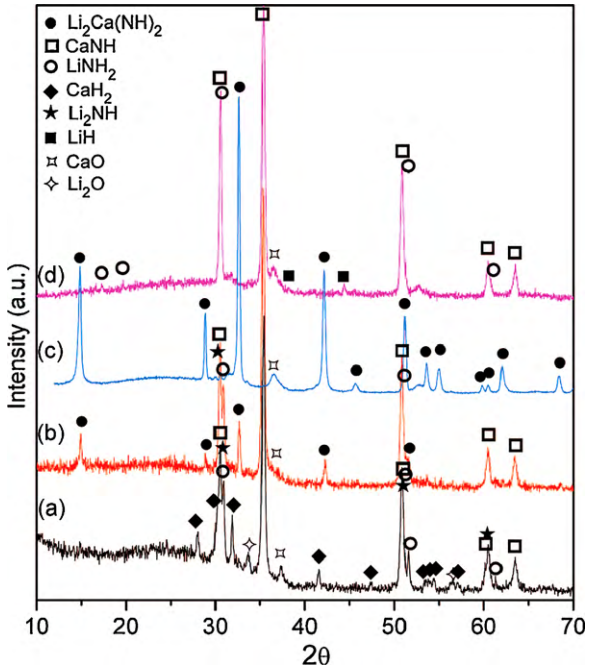

Fig. 43. XRD pattern of products at varios dehydrogenation/hydrogenation stages of $2LiNH_2 + CaH_2$. (a) Desorption during heating ramp to 300 °C, products: CaNH, Li_2NH, $LiNH_2$, and CaH_2; (b) desorption at 300 °C for 30 min, products: CaNH, Li_2NH, $Li_2Ca(NH)_2$, and small amount of $LiNH_2$; (c) desorption at 300 °C for 5 h, product:$Li_2Ca(NH)_2$; (d) hydrogenation of $Li_2Ca(NH)_2$ at 200 °C, products: $LiNH_2$, LiH and CaNH [Reprinted from ref. [304] with kind permission of American Chemical Society].

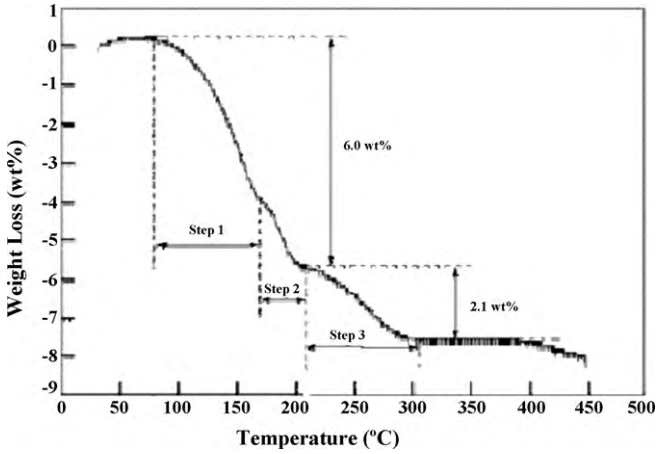

Fig. 44. TGA curves of $2LiAlH_4 + LiNH_2$ under atmospheric argon and a heating rate of 2 °C/min [Reprinted from ref. [309] with kind permission of American Chemical Society].

Table 3
Crystal structure and hydrogenation/dehydrogenation properties of amides/imides.

S. no.	Materials and their formation/dissociation reaction	Crystal structure; space group; lattice parameters (Å)	Hydrogen capacity (wt%)	Dehydrogenation temperature (°C)	Dissociation enthalpy (kJ mol^{-1} H_2)	Ref.
1.	Li imide/amide $Li_3N + H_2 \rightarrow Li_2NH + LiH + H_2$ $Li_2NH + LiN + H_2 \leftrightarrow LiNH_2 + LiH + H_2$	Li_2NH: Cubic, $Fm\bar{3}m$ $a = 5.046$ Å LiNH2: Tetragonal $a = 5.031$ Å $c = 10.210$ Å	5.4 6.5	 280	148 45	[251]
2.	Mg imide/amide $Mg(NH_2)_2 + 2MgH_2 \rightarrow Mg_3N_2 + 2H_2$	$I4_1/acd$ $a = 10.3779$ Å $c = 20.065$ Å	7.4	200	~3.5	[275,279]
3.	Ca imide/amide $Ca(NH_2)_2 + CaH_2 \rightarrow 2CaNH + 2H_2$ $2CaNH + 2H_2 \rightarrow Ca_2NH + H_2$	$P2_1/a$ $a = 6.30$ Å $b = 7.257$ Å $c = 7.2434$ Å	3.5 2.1	350 500		[284,286]
4.	Li-Mg-N-H $2LiNH_2 + MgH_2 \rightarrow 3Li_2Mg(NH)_2 + 6H_2$ $Li_2Mg(NH)_2 + H_2 \leftrightarrow Mg(NH_2)_2 + 2LiH$	$Li_2Mg(NH)_2$: Tetragonal, 45(Iab2) $a = 9.7821$ Å $b = 4.9927$ Å $c = 20.15$ Å $Mg(NH_2)_2$: Tetragonal,142 ($I4_1/acd$) $a = 10.37$ Å $c = 20.15$ Å	4.5	200	39	[293]
5.	Li-Ca-N-H $2LiNH_2 + CaH_2 + H_2 \rightarrow CaNH + Li_2NH \leftrightarrow Li_2Ca(NH)_2$ $Li_2Ca(NH)_2 + 2LiH \rightarrow 4LiNH_2 + Ca_3N_2 + 2H_2$	$Li_2Ca(NH)_2$: Trigonal, $P\bar{3}m1$ $a = 3.5664$ Å $c = 5.9540$ Å	5	300	102.6	[307]
6.	Li-Al-N-H $3LiAlH_4 \rightarrow Li_3AlH_6 + 2Al + 3H_2$ $Li_3AlH_6 \rightarrow 3LiH + Al + \frac{3}{2}H_2$ $2LiAlH_4 + LiNH_2 \rightarrow 2Al + Li_2NH + 4H_2$	–	4 2 2.1	85 165 200		

The reaction between $LiNH_2$-$LiAlH_4$ (1:1 molar ratio) is a mildly endothermic process liberating approximately 4H atoms per ($1LiNH_2$-$1LiAlH_4$) after 10 h of ball milling. However, the recharging of the dehydrogenated sample was unsuccessful at H_2 pressures upto 80 bar [308]. Recently, Jun and Fang [309] investigated a mixture of $LiNH_2$ and $LiAlH_4$ in 1:2 molar ratios by thermo gravimetric analysis (TGA) and indicated that a large amount of hydrogen (~8.1 wt%) can be released between 85 and 320 °C under the heating rate of 2 °C/min in three dehydrogenation reaction steps given by:

$$3LiAlH_4 \rightarrow Li_3AlH_6 + 2Al + 3H_2 \quad (76)$$

$$Li_3AlH_6 \rightarrow 3LiH + Al + \frac{3}{2}H_2 \quad (77)$$

$$2LiAlH_4 + LiNH_2 \rightarrow 2Al + Li_2NH + LiH + 4H_2 \quad (78)$$

It was also reported that $LiNH_2$ effectively destabilizes $LiAlH_4$. More recently, Xiong et al. [310] performed nuclear magnetic resonance (NMR) measurements along with XRD and FTIR to indicate that a Li-Al-N-H intermediate with chemical composition $Li_3AlN_2H_4$ forms after ball milling which reversibly store 5 wt% hydrogen.

5. Amino borane

Amino boranes are compounds of borane groups having ammonia addition as indicated from their name. Among all the known amino boranes [311], ammonia borane is considered as promising candidate for chemical hydrogen storage applications due to their low molecular weight and high hydrogen content of 19.6 wt%. The present section will explore detailed review on its synthesis, crystal structure and their hydrogen uptake reaction.

5.1. Formation and structure

The first report on synthesis of NH_3BH_3 is given by Shore and Parry [312] in 1955 using the following reactions:

$$LiBH_4 + NH_4Cl \xrightarrow{\text{DiethylEther}} LiCl + NH_3BH_3 + H_2 \quad (79)$$

Table 4
Comparative structural information of ammonia borane obtained by different groups [Reproduced from ref. [326] with permission from Institute of Physics].

Temperature (K)	Structure	Space group	a (Å)	b (Å)	c (Å)	Volume (Å^3)
295	Tetragonal	$I4mm$ (C^9_{4V})	5.240 ± 0.005		5.028 ± 0.008	138.0 ± 0.2
110	Orthorhombic	$Pmn2_1$ (C^7_{2V})	5.517 ± 0.001	4.742 ± 0.001	5.020 ± 0.001	131.33 ± 0.03
RT	Tetragonal	$I4mm$ (C^9_{4V})	5.255		5.048	139.4
RT	Tetragonal	$I4mm$ (C^9_{4V})	5.234		5.027	137.7
	Orthorhombic (face-centered)		7.22	7.38	5.23	278.7

$$2LiBH_4 + (NH_4)_2SO_4 \xrightarrow{DiethylEther} Li_2SO_4 + 2NH_3BH_3 + 2H_2 \quad (80)$$

$$[H_2B(NH_3)_2^+][BH_4^{2-}] + NH_4Cl \xrightarrow{\text{Diethyl Ether, trace of } NH_3} [H_2B(NH_3)_2{}^+][Cl^{2-}] + NH_3BH_3 + H_2 \quad (81)$$

Later on Mayer [313] suggested that $[H_2B(NH_3)_2]BH_4$ may convert to H_3BNH_3 without H_2 evolution in polyether solution:

$$[H_2B(NH_3)_2][BH_4] \xrightarrow{\text{Poly Ether, } B_2H_6 \text{ small amount}} 2NH_3BH_3 \quad (82)$$

Except these, a number of studies has been performed for the preparation of ammonia borane using ammonium salts such as chloride [314], sulfate [315], carbonate [316] for salt metathesis. Direct reaction of ammonia with B_2H_6 [311,317,318], $BH_3.SMe_2$ [319], or BH_3.THF [320] gives satisfactory amount of ammonia borane. Recently Ramachandran and Gagare [321] obtained high yield ~96% of ammonia borane and suggested that a low concentration of the reaction medium is necessary for the purity and yield of the product. More recently, Heldebrant et al. [322] proposed that ammonium borohydride, NH_4BH_4 can be induced to decompose in an organic ether to yield AB in near quantitative yield. They found the purity of this AB is sufficient to meet the thermal stability requirements for on board hydrogen storage.

Lippert and Lipscomb [323] were the first who proposed tetragonal structure of ammonia borane with lattice parameter a = 5.234 Å, c = 5.027 Å using XRD. This was supported by a theoretical study made by Hughes [324] in the same year. In a later study by Sorokin et al. [325] the structure was suggested as face centered orthorhombic. Thus a detailed structural information was needed for clarifying this difference in suggested structure, which was attempted by Hoon and Reynhardt in 1983 [326]. They found a first order rotational order–disorder phase transition at 225 K. The low temperature structure is orthorhombic, while in high temperature tetragonal phase, the space group permits twelve-fold reorientation of BH_3 and NH_3 groups. Table 4 shows comparative structural information obtained by different groups.

The solid state structure of ammonia borane exhibits short BH–HN contacts, the hydridic hydrogen atoms on boron are 2.02 Å away from the protic hydrogen atoms on nitrogen of an adjacent molecule, a distance lower than the Vander Waals distance of 2.4 Å, an interaction constituting a dihydrogen bond [327–329], while B-N bond distance is 1.564(6) Å in solid state ammonia borane [330], it is significant longer ~1.6722(5) Å in gas phase structure as determined by microwave spectroscopy [331,332].

5.2. Thermodynamics and hydrogenation properties

There are several methods of dehydrogenation of ammonia borane in literature, which can be broadly divided in two categories namely (1) thermolysis and (2) hydrolysis.

5.2.1. Thermolysis

Thermolysis of ammonia borane has been widely studied [333–347]. The thermal dehydrogenation of ammonia borane occurs in 3 steps [333,334] as follows:

$$NH_3BH_3(s) \rightarrow (NH_2BH_2)_n(s) + nH_2(g) \quad (83)$$

$$(NH_2BH_2)_n(s) \rightarrow (NHBH)_n(s) + nH_2(g) \quad (84)$$

$$NHBH(s) \rightarrow (BN)_n(s) + nH_2(g) \quad (85)$$

The first step starts at ~90 °C and reaches a maximum at ~110 °C, which results in the release of one molar equivalent of hydrogen gas, but at very slow rates because of the long induction period prior to hydrogen release [333]. The second molar equivalent of H_2 is released at temperatures around 150 °C. The final step can occur only at high temperature ~500 °C, which gives the third final molar equivalent H_2. The reaction enthalpy for H_2 release from ammonia borane is found to be −21 kJ/mol [335], which is suitable for onboard hydrogen storage application. The only disadvantage associated with the thermal dehydrogenation is the long induction time ~200 min at 80 °C before the hydrogen release [336]. Number of methods have been suggested to overcome this problem using silica scaffolds [333], Metal catalyst [334], Ionic liquids [337,338] etc. The use of a 1:1 mixture of ammonia borane and mesoporous silica SBA-15, as a scaffold, enabled the release of 1 equivalent of hydrogen at 50 °C in only 85 min as reflected from DSC results shown in Fig. 45.

The addition of ionic liquids to ammonia borane make the dehydrogenation possible at 95 °C [337,338] after 22 h heating. It was reported that $Ni_{0.88}Pt_{0.12}$ hollow sphere catalyzed NH_3BH_3 can release upto 2.2 equivalent of H_2 upto 453 K [339]. In organic solvents, acid catalyzed [340] or transition metal complex catalyzed [341–343] dehydrogenation can also control hydrogen release and 18 wt% of hydrogen is released at 333 K. Benedetto et al. [344] have shown that mechanical milling with metal catalysts enhances

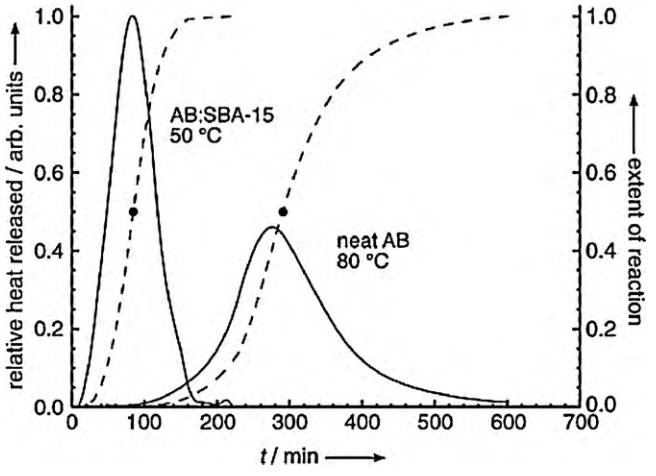

Fig. 45. Scaled exotherms (solid lines) from isothermal DSC experiments that show the time-dependent release of H_2 from AB and AB:SBA-15 (1:1 wt/wt). The area under the curve for neat AB corresponds to $\Delta H_{rxn} = -21$ kJ mol^{-1}, and the area under the curve for AB:SBA-15 corresponds to $\Delta H_{rxn} = -1$ kJ mol^{-1}. The release of hydrogen from AB proceeds at a more rapid rate and at lower temperatures in SBA-15. The dashed line (–) is the integrated signal intensity; (●) is the point at which the reaction is 50% complete [Reproduced from ref. [333] with permission from Wiley-VCH Verlag GmbH & Co.].

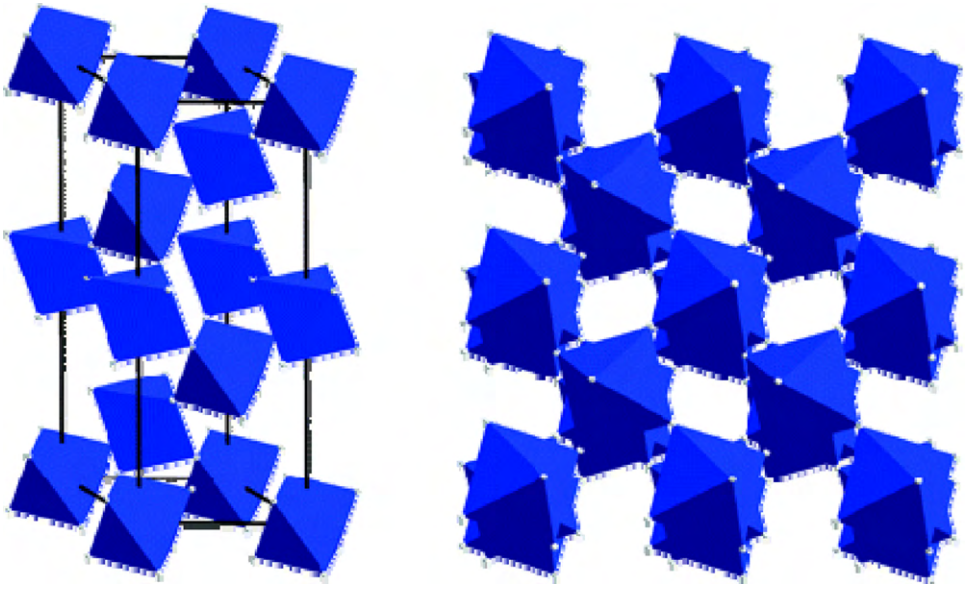

Fig. 46. Crystal structure of α-AlD_3. The unit cell is shown to the left, and the connectivity of the octahedra is illustrated to the right. Each octahedron is sharing one corner with one other octahedron, building a distorted primitive Al sublattice [Reprinted from ref. [360] with kind permission of American Chemical Society].

hydrogen release in solid state ammonia borane. Recently, the addition of trace quantities of diamoniate of diborane to ammonia borane could also reduce the induction time and onset temperature of hydrogen release as well [345]. It is found that nanophase boron nitride has also the same effect as above to reduce the onset temperature [346,347].

5.2.2. Hydrolysis

The second option for hydrogen generation from NH_3BH_3 is its hydrolysis or alcoholysis, a name given to the reaction with water and alcohol, respectively. Amonnia borane is relatively stable in neutral water and alcohol at room temperature [348]. Hydrolysis of NH_3BH_3 releases hydrogen rapidly in the presence of metal catalysts or solid acids via the reaction [339,349–352]:

$$NH_3BH_3 + 2H_2O \rightarrow NH_4^+ + BO_2^- + 3H_2 \quad (86)$$

The reaction is exothermic with $\Delta H = -156$ kJ/mol [350,351] and provides 9.1 wt% hydrogen based on ammonia borane and reacted H_2O. The reaction rate significantly depends on the catalysts used. Pt based catalysts were found to be best in this category, by which the above reaction could be completed within 2 min [349,352]. Another important catalyst for the hydrolysis of NH_3BH_3 is amorphous Fe nanoparticles, having a hydrogen release H_2/NH_3BH_3 of 3 in 8 min [353]. Other important catalysts are summarized in a recent review article by Umegaki et al. [353].

6. Alane

6.1. Formation and structure

Al hydride was first synthesized by Finholt et al. by the ethereal reaction of lithium aluminium hydride ($LiAlH_4$) with aluminium

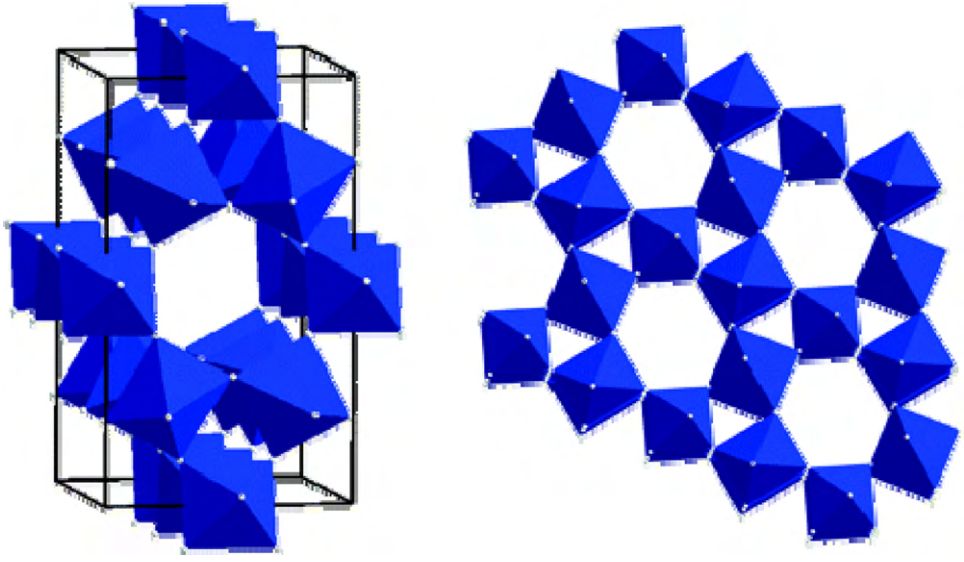

Fig. 47. Crystal structure of α'-AlD_3. The unit cell is shown to the left, and the pores through the whole structure are highlighted to the right [Reprinted from ref. [360] with kind permission of American Chemical Society].

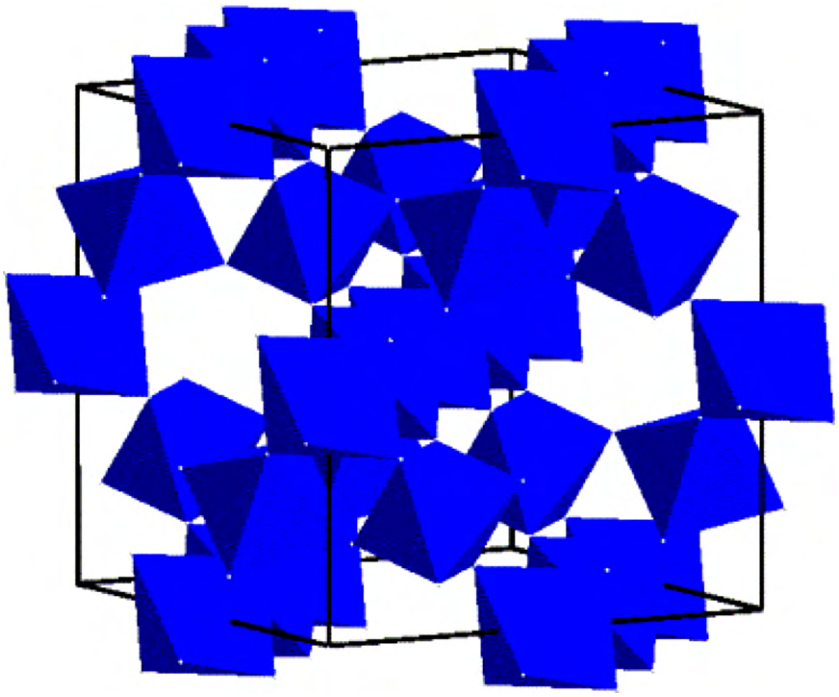

Fig. 48. The atomic arrangement of β-AlD_3 in the unit-cell [Reprinted from Ref. [361] with permission from Elsevier].

chloride ($AlCl_3$) [72]:

$$3LiAlH_4 + AlCl_3 \xrightarrow{(C_2H_5)_2O} 4AlH_3 \downarrow + 3LiCl \downarrow \quad (87)$$

But the AlH_3 formed was solvated in ether which could not be removed unless the decomposition to Al and H. Chizinsky et al. [354] reported the removal of ether from the solution by adding pentane or ligroin followed by the vacuum treatment of the precipitate. Apple and Frankel [355] reported the first method of non solvated AlH_3 by the bombardment of ultrapure aluminium target with hydrogen ions. However, AlH_3 polymorphs have typically been synthesized by organometallic methods. Recently it has been found that alane can be synthesized by cryomilling of $LiAlD_4$ and $AlCl_3$ without thermal decomposition [356,357]. Depending on the method and conditions of preparation, alane can be synthesized in six different forms [358]. Bower et al. [358] reported that β and γ forms of aluminium hydride were first formed which converted to most stable α-phase upon heating. Other known phases were identified as ά, δ, and ζ. Among the six polymorphic structure of AlH_3, the structure of α [359], ά [360], β [361] and γ [362] are known. The low stability of the δ and ζ phases is a major difficulty to perform their structure analysis. However, α-AlH_3 is the only structure of interest, particularly in the context of hydrogen storage materials as it meets the storage criteria specified by DOE.

The first report on the structure of α-AlH_3 and α-AlD_3 was made by Turley et al. [359] using XRD and neutron diffraction data. They suggested that both compounds crystallize in the trigonal space group $R\bar{3}c$ with six molecules in a hexagonal unit cell. On the basis of data proposed by Turley et al., recently Brinks et al. [360] re-examined a sample containing 2/3α and 1/3ά phase by Rietveld analysis. They suggested α-AlD_3 structure as a ReO_3 type structure with corner sharing AlD_6 rotated octahedra (Fig. 46).

In the same work [360] they discussed the structure of ά-AlD_3. It takes the β-AlF_3 structure with space group *Cmcm*, built up of corner sharing AlD_6 octahedra in an open structure with hexagonal holes of radius 3.9 Å (Fig. 47).

In a later study, Brinks et al. [361] reported the structure of β-AlD_3 using PND and synchrotron XRD data. The structure was found to be of the cubic pyrochlore type with space group $Fd\bar{3}m$ as shown in Fig. 48. It consists of corner sharing AlD_6 octahedra where each hydrogen is shared between 2 octahedra.

The structure of the γ phase has recently been studied by Brinks et al. [362] and Yartys et al. [363] using PND and synchrotron XRD. Studies revealed that γ-AlD_3 crystallizes with an orthorhombic unit cell in space group *Pnnm*. It consists of both corner and edge sharing AlD_6 octahedra where each hydrogen is shared between two octahedra (Fig. 49).

6.2. Thermodynamics and hydrogenation properties

The decomposition of α-AlH_3 occurs as follows [364]:

$$AlH_3 \rightarrow Al + \frac{3}{2}H_2 \quad (88)$$

The heat of decomposition of aluminium hydride samples was measured using a bomb calorimeter accommodating a small suspended heating oven containing the sample [365]. At 298 K, the calculated average enthalpy of formation was -11.4 ± 0.8 kJ / mol, absolute entropy was 30.0 ± 0.4 kJ/mol and Gibb's energy of formation was 45.4 ± 1.0 kJ/mol.

The thermodynamics of the α, β, and γ polymorphs were calculated using DSC. The total heat of $\beta \rightarrow \alpha$ transition and $\gamma \rightarrow \alpha$ is found to be 1.5 ± 0.4 kJ/mol and 2.8 ± 0.4 kJ/mol AlH_3. These transformations are exothermic and so can occur spontaneously at room temperature. The enthalpy of formation is found to be -10 kJ/mol AlH_3. It was demonstrated that a freshly synthesized nonsolvated AlH_3 desorbs about 10 wt% H_2 at temperature below 100 °C [365].

However, the above reaction occurs readily, but the reverse reaction is not easy to occur. About 2.5 GPa pressure of H_2 is required to rehydride it [366,367]. Another issue to use alane for practical application is its slow desorption kinetics. It has been shown that the kinetics is limited by nucleation and growth of the aluminium particles and not by diffusion through a surface oxide as was initially expected [368,369]. In addition, the decrease in the desorption temperature was also investigated and some solutions were proposed, by either utilizing additives such as alkali metal hydride [370] or particle size reduction using ball milling [371]. It

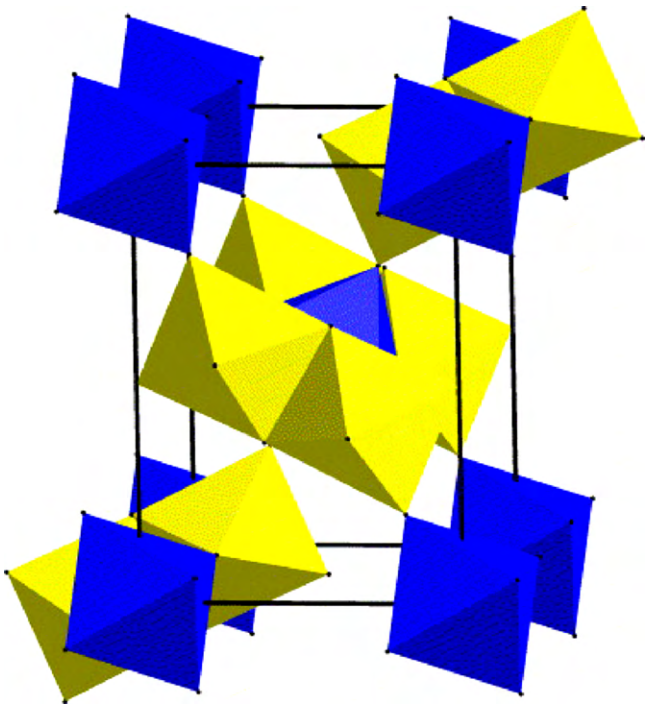

Fig. 49. The atomic arrangement of γ-AlD_3 in the unit-cell. The two different Al sites are illustrated by different colour of the octahedra. $Al1D_6$ octahedra are blue and Al_2D_6 octahedra are yellow [Reprinted from Ref. [362] with permission from Elsevier].

was found that doping of AlH_3 with small amount of LiH, NaH and KH results in accelerating H_2 desorption rates at low temperatures. This increase is explained due to the formation of alanate windows which provide a path for transport of H_2 from the alane phase.

A alternate approach for the regeneration of AlH_3 is adopted via a low temperature, low pressure, reversible reaction using Ti doped Al powder and triethylenediamine (TEDA) [368]. The reaction was proposed as follows:

$$Al_{(Ti)} + TEDA + 1.5H_2 \leftrightarrow Al_{(Ti)}H_3 - TEDA \quad (89)$$

Recently an effort has been made to increase the thermodynamic stability of AlH_3 hydride by partial Al substitution by means of MgH_2 [372], but no effect on the alane stabilization was obserbed. However, the activation energy was found to be increased as confirmed by DSC experiment.

7. Future prospects and challenges

Hydrogen storage in light weight complex hydride is an emerging and promising field of research for renewable energy, having potential to come up to the expectations of DOE for mobile applications. These materials can have large gravimetric and volumetric capacity to reversibly store a large amount of hydrogen, very light, low cost and simple to produce. Being a new field, there open big challenges to improve kinetics, low temperature release of hydrogen and fast charge discharge rates for mobile applications. Having a panoramic view on all the complex hydrides, alanates are found to be the most studied systems followed by borohydrides and amide. Among all alanates, $NaAlH_4$ seems to have potential to be a suitable hydrogen storage media but its comparatively low storage capacity ~5 wt% limits its use for the transportation sector, which requires the systems having capacities more than 10 wt%. But still it is good candidate for other mobile applications. $NaBH_4$ and $LiBH_4$, among the known borohydrides are most promising candidates which can be used for transportation applications due to their high hydrogen content (~10.8 and 13.4 wt%, respectively) at moderate conditions, but low dynamics of hydrogen release, is still a major problem associated with these systems. However, these materials have a good enough capacity margin to be doped by kinetics enhancing dopants. Other important and emerging hydrides are amides, i.e. M-N-H systems. There has been tremendous development with these materials in a very short span of time and considerable knowledge about their structure, thermodynamics and chemistry has been attained, but still they have a problem of material stability and slow kinetics. Most of amides are unstable upon heating at high temperature and release NH_3 which may be crucial for fuel cells. AlH_3 and $Al(BH_4)_3$ are very new materials which are relatively less studied but have great potential for creating a favorable position as to mobile storage applications.

One thing is sure, the technology has to be used judiciously for sample preparation so that maximum surface of materials be available for hydrogen absorption–desorption. Lot of work is under progress for sample preparation by ball milling in various atmospheres using various catalysts, but still this field is wide open for finding good catalyst which is very important for improving the hydrogen absorption–desorption kinetics. Surface area can be increased by creating hollow nano spheres having nano structured light weight hydride materials. Many other opportunities open up also there by using thin film technology under high and ultra high vacuum techniques. But both hollow spheres and thin films are yet to be explored extensively. The following listing summarizes challenges where work can be concentrated:

- Cost reduction and improvement in gravimetric hydrogen density whilst still operating at low temperatures (40–100 °C) and pressures (4–10 bars).
- New cheap synthetic processing routes to avoid lengthy and expensive solvent based synthesis and regeneration of novel light metal complex hydrides.
- An atomic and molecular level understanding of the physical and chemical processes involved in hydrogen storage and release.
- Understanding the effect of incorporated hydrogen on the electronic structure of the host lattice and the dynamics and energetics of hydrogen and its interaction with lattice defects in light weight complex hydrides.
- A fundamental understanding of the physical and chemical properties of light weight hydrides, including crystal structure, homogeneity ranges, thermodynamics and kinetics of hydrogenation–dehydrogenation processes and electronic structure.
- Understanding the critical role of dopants and the mechanisms of destabilization reactions in altering the nature of hydrogen bonding and achieving reasonable kinetics and reversibility of complex hydrides at temperatures of 80–150 K.
- A systematic investigation of the effect of size and curvature of nanomaterials on the thermodynamics of hydrogen storage. Studies on the benefits of nano-scale versions of hydride materials relative to their bulk counterparts, including shorter diffusion distances, new phases with better capacity, reduced heats of adsorption/desorption, faster kinetics, as well as new surface states capable of catalyzing hydrogen dissociation.

In short many challenges are wide open in this field and much work has to be done to make light weight complex hydrides useful for mobile applications, which will result in solving the greatest worldwide problem to reduce carbon emission and the concomitant global warming for better life on Planet Earth.

Acknowledgements

Author (I.P. Jain) is grateful to the Council of Scientific and Industrial Research (CSIR), Government of India, New Delhi for the financial support under Emeritus Scientist Scheme. One of us (Ankur Jain) is thankful to University Grants Commission, New Delhi for financial support in the form of Dr. D.S. Kothari Post Doctoral Fellowship Programme. Ms. Pragya Jain is thankful to Inter University Accelerator Centre (IUAC), New Delhi, India for Research Fellowship.

References

[1] W. Grochala, P.P. Edwards, Chem. Rev. 104 (2004) 1283–1315.
[2] T.E. Lipman, M.A. DeLucchi, Int. J. Vehicle Des. 17 (1996) 562.
[3] Martin Fleischmann, Stanley Pons, J. Electroanal. Chem. 261(1989) 301–308.
[4] (a) H.L. Chin, Z.S. Chen, C.P. Chou, Biotechnol. Prog. 19 (2003) 383;
(b) C.C. Wang, C.W. Chang, C.P. Chu, D.J. Lee, B.V. Chang, C.S. Liao, J. Biotechnol. 102 (2003) 83;
(c) V.C. Kalia, S. Lal, R. Ghai, M. Mandal, A. Chauhan, Trends Biotechnol. 21 (2003) 152;
(d) X. Zhao, I.P. Georgakaki, M.L. Miller, R. Mejia-Rodriguez, C.-Y. Chiang, M.Y. Darensbourg, Inorg. Chem. 41 (2002) 3917;
(e) J. Alper, Science 299 (2003) 1686.
[5] R.S. Irani, MRS Bull. 27 (2002) 680.
[6] Joachim Wolf, MRS Bull. 27 (2002) 684.
[7] http://www.sc.doe.gov/bes/hydrogen.pdf.
[8] Andreas Zuttel, Naturwissenschaften 91 (2004) 157–172.
[9] I.P. Jain, Chhagan Lal, Ankur Jain, Int. J. Hydrogen Energy 35 (2010) 5133.
[10] Shivani Agarwal, Annalisa Aurora, Ankur Jain, I.P. Jain, Amelia Montone, Int. J. Hydrogen Energy 34 (2009) 9157–9162.
[11] Ankur Jain, Shivani Agarwal, I.P. Jain, J. Alloys Comp. 480 (2009) 325–328.
[12] Ankur Jain, R.K.Jain, I.P.Jain, J. Power Sources 159 (2006) 132–134.
[13] Ankur Jain, R.K. Jain, Shivani Agarwal, I.P. Jain, Bull. Mater. Sci. 29 (2006) 67–72.
[14] A.C. Dillon, K.M. Jones, T.A. Bekkedahl, C.H. Kiang, D.S. Bethune, M.J. Heben, Nature 386 (1997) 377–379.
[15] G. Tibbetts Gary, P. Meisner Gregory, H. Olk Charles, Carbon 39 (2001) 2291–2301.
[16] Masashi Shiraishi, Taishi Takenobu, Masafumi Ata, Chem. Phys. Lett., 367 (2003) 633–636.
[17] C. Carpetis, W. Peschka, Int. J. Hydrogen Energy 5 (1980) 539–554.
[18] R.K. Agarwal, J.S. Noh, J.A. Schwarz, P. Davini, Carbon 25 (1987) 219–226.
[19] Andreas Züttel, Mater. Today, 6 (2003) 24-33.
[20] Borislav Bogdanovi, Manfred Schwickardi, J. Alloys Comp. 253–254 (1997) 1–9.
[21] A.F. Zhigach, D.S., Stasievich, The chemistry of hydrides, (Khimiya, Leningrad, 1969) [in Russian].
[22] J. Downs Anthony, R. Pulham Colin, Chem. Soc. Rev. 3 (1994) 175–184.
[23] M. Fichtner, O. Fuhr, O. Kircher, J. Alloys Comp. 356–357 (2003) 418–422.
[24] T.N. Dymova, N.G. Eliseeva, S.I. Bakum, Y.M. Dergachev, Dokl. Akad. Nauk. SSSR 215 (1974) 1369.
[25] A.E. Finholt, E.C. Jacobson, A.E. Ogard, P. Thompson, J. Am. Chem. Soc. 77 (1955) 4163.
[26] E.C. Ashby, Chem. Ind. (1962) 208–209.
[27] E.C. Ashby, G.J. Brendel, H.E. Redman, Inorg. Chem. 2 (1963) 499–504.
[28] H. Clasen, Angewandte Chemie 73 (1961) 322–331.
[29] L. Zaluski, A. Zaluska, J.O. Ström-Olsen, J. Alloys Comp. 290 (1999) 71–78.
[30] Ping Wang, Craig M. Jensen, J. Phys. Chem. B 108 (2004) 15827.
[31] Xiang-Dong Kang, Ping Wang, and Hui-Ming Cheng, J. Phys. Chem. C 111 (2007) 4879.
[32] Borislav Bogdanović, Michael Felderhoff, André Pommerin, Ferdi Schüth, Nick Spielkamp, Arne Stark, J. Alloys Comp. 471 (2009) 383–386.
[33] Borislav Bogdanović, Richard A. Brand, Ankica Marjanović, Manfred Schwickardi, Joachim Tölle, J. Alloys Comp. 302 (2000) 36–58.
[34] Ragaiy A. Zidan, Satoshi Takara, Allan G. Hee, Craig M. Jensen, J. Alloys Comp. 285 (1999) 119–122.
[35] G. Sandrock, K. Gross, G. Thomas, J. Alloys Comp. 339 (2002) 299–308.
[36] B. Bogdanović, M. Schwickardi, Appl. Phys. A 72 (2001) 221–223.
[37] A. Zaluska, L. Zaluski, J.O. Ström-Olsen, Appl. Phys. A 72 (2001) 157–165.
[38] K.J. Gross, G.J. Thomas, E. Mahzoub, G. Sandrock, Proc. 2001 DOE hydrogen program review, NREL/CP-570-30535.
[39] José M. Bellosta von Colbe, Michael Felderhoff, Borislav Bogdanović, Ferdi Schüth, Claudia Weidenthaler, Chem. Commun. (2005) 4732.
[40] J.W. Lauher, D. Dougherty, P.J. Herley, Acta Cryst. B35 (1979) 1454–1456.
[41] Ma Zhu, M.Y. Chou, J. Alloys Comp. 479 (2009) 678–683.
[42] V.K. Bel'skii, B.M. Bulychev, A.V. Golubeva, Russ. J. Inorg. Chem. 28 (1983) 1528.
[43] B.C. Hauback, H.W. Brinks, C.M. Jensen, K. Murphy, A.J. Maeland, J. Alloys Comp. 358 (2003) 142–145.
[44] Karl J. Gross, Steve Guthrie, Satoshi Takara, George Thomas, In-situ X-ray diffraction study of the decomposition of NaAlH4, J. Alloys Comp., 297 (2000) 270–281.
[45] (a) B. Bogdanović, M. Felderhoff, M. Germann, M. Härtel, A. Pommerin, F. Schüth, C. Weidenthaler, B. Zibrowius, J. Alloys Comp. 350 (2003) 246–255;
(b) Aline Léon, Oliver Kircher, Jörg Rothe, Maximilian Fichtner, Chemical State and Local Structure around Titanium Atoms in $NaAlH_4$ Doped with $TiCl_3$ Using X-ray Absorption Spectroscopy, J. Phys. Chem. B 108, (2004) 16372–16376;
(c) J. Ross Daniel, D. Halls Mathew, G. Nazri Abbas, F. Aroca Ricardo, Chem. Phys. Lett. 388 (2004) 430–435;
(d) H.W. Brinks, C.M. Jensen, S.S. Srinivasan, B.C. Hauback, D. Blanchard, K. Murphy, J. Alloys Comp. 376 (2004) 215–221.
[46] T.N. Dymova, S.I. Bakum, Russ. J. Inorg. Chem. 14 (1969) 1683.
[47] (a) P. Claudy, B. Bonnetot, G. Chahine, J.M. Letoffe, Thermochim. Acta 38 (1980) 75–88;
(b) Jean-Pierre Bastide, Bernard Bonnetot, Jean-Marie Létoffé, Pierre Claudy, Polymorphisme de l'hexahydroaluminate trisodique Na3AlH6, Mater. Res. Bull. 16 (1981) 91–96.
[48] E.C. Ashby, P. Kobetz, Inorg. Chem. 5 (1966) 1615–1617.
[49] J.A. Dilts, E.C. Ashby, Inorg. Chem. 11 (1972) 1230–1236.
[50] T.N. Dymova, Yu M. Dergachev, V.A. Sokolov, and N.A. Grechanaya, Dokl. Akad. Nauk SSSR, 224 (1975) 591, Engl. 556.
[51] German patent application 19526 434.7, 1995.
[52] D.L. Anton, J. Alloys Comp. 356–357 (2003) 400–404.
[53] R. Tom Walters, H. Scogin John, J. Alloys Comp. 379 (2004) 135–142.
[54] F. Schüth, B. Bogdanović, M. Felderhoff, Chem. Commun. (2004) 2249.
[55] C.M. Jensen, K.J. Gross, Appl. Phys. A 72 (2001) 213–219.
[56] X.D. Kang, P. Wang, X.P. Song, X.D. Yao, G.Q. Lu, H.M. Cheng, J. Alloys Comp. 424 (2006) 365–369.
[57] B. Bogdanović, M. Felderhoff, A. Pommerin, F. Schüth, N. Spielkamp, Adv. Mater. 18 (2006) 1198–1201.
[58] D. Pukazhselvan, M. Sterlin Leo Hudson, M.A. Bipin Kumar Gupta, O.N. Srivastava Shaz, J. Alloys Comp. 439 (2007) 243–248.
[59] A. Blomqvist, C. Moysés Araújo, P. Jena, R. Ahuja, Appl. Phys. Lett. 90 (2007) 141904.
[60] Yindee Suttisawat, Visara Jannatisin, Pramoch Rangsunvigit, Boonyarach Kitiyanan, Nongnuj Muangsin, Santi Kulprathipanja, J. Power Sources, 163 (2007) 997–1002.
[61] Gil-Jae Lee, Ji Woo Kim, Jae-Hyeok Shim, Young Whan Cho, Kyung Sub Lee, Scripta Mater., 56 (2007) 125–128.
[62] Yindee Suttisawat, Pramoch Rangsunvigit, Boonyarach Kitiyanan, Nongnuj Muangsin, Santi Kulprathipanja, Int. J. Hydrogen Energy, 32 (2007) 1277–1285.
[63] Yindee Suttisawat, Pramoch Rangsunvigit, Boonyarach Kitiyanan, Santi Kulprathipanja, Int. J. Hydrogen Energy, 33 (2008) 6195–6200.
[64] Tao Wang, Jun Wang, Armin D. Ebner, James A. Ritter, J. Alloys Comp., 450 (2008) 293–300.
[65] Mehraj-ud-din Naik, Sami-ullah Rather, Renju Zacharia, Chang Su So, Sang Woon Hwang, Ae Rhan Kim, Kee Suk Nahm, J. Alloys Comp., 471 (2009) L16–L22.
[66] J. Wang, A.D. Ebner, R. Zidan, J.A. Ritter, J. Alloys Comp. 391 (2005) 245–255.
[67] Gil-Jae Lee, Jae-Hyeok Shim, Young Whan Cho, Kyung Sub Lee, Int. J. Hydrogen Energy, 32 (2007) 1911–1915.
[68] A. Zaluska, L. Zaluski, J.O. Ström-Olsen, J. Alloys Comp. 298 (2000) 125–134.
[69] D. Pukazhselvan, Bipin Kumar Gupta, Anchal Srivastava, O.N. Srivastava, J. Alloys Comp., 403 (2005) 312–317.
[70] Polly A. Berseth, Andrew G. Harter, Ragaiy Zidan, Andreas Blomqvist, C. Moyses Araujo, Ralph H. Scheicher, Rajeev Ahuja, Puru Jena, Nano Lett. 9 (2009) 1501.
[71] P. Balde Cornelis, P.C. Hereijgers Bart, H. Bitter Johannes, P. de Jong Krijn, J. Am. Chem. Soc. 130 (2008) 6761–6765.
[72] A.E. Finholt, A.C. Bond Jr., H.I. Schlesinger, J. Am. Chem. Soc. 69 (1947) 1199–1203.
[73] J. Graetz, James Wegrzyn, James J. Reilly, J. Am. Chem. Soc. 130 (2008) 17790.
[74] J. Wang, D. Ebner Armin, A. Ritter James, J. Am. Chem. Soc. 128 (2006) 5949.
[75] Yoshitsugu Kojima, Yasuaki Kawai, Tetsuya Haga, Mitsuru Matsumoto, Akihiko Koiwai, J. Alloys Comp. 441 (2007) 189–191.
[76] Natalie Sklar, Benjamin Post, Inorg. Chem. 6 (1967) 669.
[77] B.C. Hauback, H.W. Brinks, H. Fjellvåg, J. Alloys Comp. 346 (2002) 184–189.
[78] D. Davis William, L.S. Mason, G. Stegeman, J. Am. Chem. Soc. 71 (1949) 2775.
[79] Martin B. Smith, George E. Bass Jr., J. Chem. Eng. Data 8 (1963) 342.
[80] T.N. Dymova, D.P. Aleksandrov, V.N. Konoplev, T.A. Silina, A.S. Sizareva, Russ. J. Coord. Chem. 20 (1994) 263.
[81] Jun Chen, Nobuhiro Kuriyama, Qiang Xu, Hiroyuki T. Takeshita, Tetsuo Sakai, J. Phys. Chem. B, 105 (2001) 11214.
[82] O.M. Løvvik, M. Opalka Susanne, W. Brinks Hendrik, C. Hauback Bjørn, Phys. Rev. B 69 (2004) 134117.
[83] Je-Wook Jang, Jae-Hyeok Shim, Young Whan Cho, Byeong-Joo Lee, J. Alloys Comp., 420 (2006) 286–290.
[84] W.E. Garner, E.W. Haycock, Proc. Roy. Soc. (London) A211 (1952) 335.
[85] V.I. Mikherva, M.I. Selivoknima, O.N. Kryukova, Proc. Acad. Sci. USSR Chem. Sec. 109 (1956) 489.
[86] Block Jacob, A.P. Gray, Inorg. Chem. 4 (1965) 305.
[87] M. McCarthy Jr., J.N. Maycook, V.R. Pai Verneker, J. Phys. Chem. 72 (1968) 4009–4014.
[88] V.I. Mikheeva, S.M. Arkhipov, Russ. J. Inorg. Chem. 12 (1967) 1066.

[89] Robert Ehrlich, Archie R. Young II., George Rice, Joseph Dvorak, Philip Shapiro, Harry F. Smith, J. Am. Chem. Soc. 88 (1966) 858.
[90] P. Balema Viktor, W. Dennis Kevin, K. Pecharsky Vitalij, Chem. Commun. (2000) 1665.
[91] V.P. Balema, V.K. Pecharsky, K.W. Dennis, J. Alloys Comp. 313 (2000) 69–74.
[92] V.P. Balema, J.W. Wiench, K.W. Dennis, M. Pruski, V.K. Pecharsky, J. Alloys Comp. 329 (2001) 108–114.
[93] Mirna Resan, Michael D. Hampton, Janice K. Lomness, Darlene K. Slattery, Int. J. Hydrogen Energy, 30 (2005) 1413–1416.
[94] D. Blanchard, H.W. Brinks, B.C. Hauback, P. Norby, Mater. Sci. Eng. B 108 (2004) 54–59.
[95] Xueping Zheng, Xuanhui Qu, Islam S. Humail, Ping Li, Guoqing Wang, Int. J. Hydrogen Energy 32 (2007) 1141–1144.
[96] Yoshitsugu Kojima, Yasuaki Kawai, Mitsuru Matsumoto, Tetsuya Haga, J. Alloys Comp. 462 (2008) 275–278.
[97] T. Sun, C.K. Huang, H. Wang, L.X. Sun, M. Zhu, Int. J. Hydrogen Energy 33 (2008) 6216–6221.
[98] E. Wiberg, R. Bauer, Z. Naturforsch. 5b (1950) 397.
[99] E. Wiberg, Angew. Chem. 65 (1953) 16.
[100] E. Wiberg, R. Bauer, Z. Naturforsch. 7b (1952) 131.
[101] A. Hertwig, German Patent 921, 986 (1955).
[102] Ethyl corp., British Patent 905, 985 (1962).
[103] J. Plesek, S. Hermanek, Collection Czech. Chem. Commun. 31 (1966) 3060.
[104] Eugene C. Ashby, Robert Donald Schwartz, B.D. James, Inorg. Chem. 9 (1970) 325.
[105] Maximilian Fichtner, Olaf Fuhr, J. Alloys Comp., 345 (2002) 286–296.
[106] Maximilian Fichtner, Jens Engel, Olaf Fuhr, Andreas Glöss, Oliver Rubner, Reinhart Ahlrichs, Inorg. Chem. 42 (2003) 7060.
[107] A. Fossdal, H.W. Brinks, M. Fichtner, B.C. Hauback, J. Alloys Comp. 404–406 (2005) 752–756.
[108] A. Fossdal, H.W. Brinks, M. Fichtner, B.C. Hauback, J. Alloys Comp. 387 (2005) 47–51.
[109] T.N. Dymova, N.N. Mal'tseva, V.N. Konoplev, A.I. Golovanova, D.P. Aleksandrov, A.S. Sizareva, Russ. J. Coord. Chem. 29 (2003) 385.
[110] M. Mamatha, B. Bogdanović, M. Felderhoff, A. Pommerin, W. Schmidt, F. Schüth, C. Weidenthaler, J. Alloys Comp. 407 (2006) 78–86.
[111] J. Wang, A.D. Ebner, J.A. Ritter, Adsorption 11 (2005) 811–816.
[112] Yoonyoung Kim, Eung-Kyu Lee, Jae-Hyeok Shim, Young Whan Cho, Kyung Byung Yoon, J. Alloys Comp. 422 (2006) 283–287.
[113] R.A. Varin, Ch. Chiu, T. Czujko, Z. Wronski, J. Alloys Comp. 439 (2007) 302–311.
[114] Heondo Jeong, Tae Hwan Kim, Ko Yeon Choo and In Kyu Song, Kor. J. Chem. Eng. 25 (2008) 268.
[115] Hiroyuki Morioka, Kenichi Kakizaki, Sai-Cheong Chung, Atsuo Yamada, J. Alloys Comp. 353 (2003) 310–314.
[116] B.C. Hauback, H.W. Brinks, R.H. Heyn, R. Blom, H. Fjellvåg, J. Alloys Comp. 394 (2005) 35–38.
[117] J.P. Bastide, J. Elhajri, P. Claudy, A. Elhajbi, Synt. React. Inorg. Metal Org. Chem. 25 (1995) 1037.
[118] M.E. Arroyo y de Dompablo, G. Ceder, J. Alloys Comp. 364 (2004) 6–12.
[119] P. Vajeeston, P. Ravindran, A. Kjekshus, H. Fjellvåg, J. Alloys Comp. 363 (2004) L8–L12.
[120] Jose R. Ares, Kondo-Francois Aguey-Zinsou, Fabrice Leardini, Isabel Jímenez Ferrer, Jose-Francisco Fernandez, Zheng-Xiao Guo, Carlos Sánchez, J. Phys. Chem. C 113 (2009) 6845.
[121] V.P. Tarasov, S.I. Bakum, A.V. Novikov, Russ. J. Inorg. Chem. 46 (2001) 409.
[122] V.P. Tarasov, S.I. Bakum, A.V. Novikov, Russ. J. Inorg. Chem. 45 (2000) 1890.
[123] W. Schwab, K. Wintersberger, Z. Naturforsch. 8b (1953) 690.
[124] A.E. Finholt, Glen D. Barbaras, Geraldine K. Barbaras, Grant Urry, Thomas Wartik, H.I. Schlesinger, J. Inorg. Nuc. Chem. 1 (1955) 317–325.
[125] T.N. Dymova, Russ. J. Inorg. Chem. 15 (1970) 1201.
[126] Maximilian Fichtner, Christoph Frommen, Olaf Fuhr, Inorg. Chem. 44 (2005) 3479.
[127] M. Schwarz, A. Haiduc, H. Stil, P. Paulus, H. Geerlings, J. Alloys Comp. 404–406 (2005) 762–765.
[128] N.N. Mal'tseva, A.I. Golovanova, T.N. Dymova, D.P. Aleksandrov, Russ. J. Inorg. Chem. 46 (2001) (1793).
[129] H. Noeth, M. Schmidt, A. Treitl, Chem. Ber. 128 (1995) 999.
[130] O.M. Løvvik, Phys. Rev. B 71 (2005) 144111.
[131] Christopher Wolverton, Vidvuds Ozoliš, Phys. Rev. B 75 (2007) 064101.
[132] A. Klaveness, P. Vajeeston, P. Ravindran, H. Fjellvåg, A. Kjekshus, J. Alloys Comp. 433 (2007) 225–232.
[133] M. Mamatha, C. Weidenthaler, A. Pommerin, M. Felderhoff, F. Schüth, J. Alloys Comp. 416 (2006) 303–314.
[134] V. Iosub, T. Matsunaga, K. Tange, M. Ishikiriyama, Int. J. Hydrogen Energy 34 (2009) 906–912.
[135] Pierre Claudy, Bernard Bonnetot, Jean-Pierre Bastide, Létoffé Jean-Marie, Mater. Res. Bull. 17 (1982) 499–150.
[136] J. Huot, S. Boily, V. Güther, R. Schulz, J. Alloys Comp. 283 (1999) 304–330.
[137] H.W. Brinks, B.C. Hauback, C.M. Jensen, R. Zidan, J. Alloys Comp. 392 (2005) 27–30.
[138] O.M. Løvvik, O. Swang, Europhys. Lett. 67 (2004) 607–613.
[139] J. Graetz, Y. Lee, J.J. Reilly, S. Park, T. Vogt, Phys. Rev. B 71 (2005) 184115.
[140] X.Z. Ma, E. Martinez-Franco, M. Dornheim, T. Klassen, R. Bormann, J. Alloys Comp. 404–406 (2005) 771–774.
[141] A. Fossdal, H.W. Brinks, J.E. Fonneløp, B.C. Hauback, J. Alloys Comp. 397 (2005) 135–139.
[142] Y. Nakamura, A. Fossdal, H.W. Brinks, B.C. Hauback, J. Alloys Comp. 416 (2006) 274–278.
[143] J.P. Bastide, P. Claudy, J.M. Letoffe, Jilali El Hajri, Rev. Chim. Min. 24 (1987) 190–198.
[144] M.H. Sørby, H.W. Brinks, A. Fossdal, K. Thorshaug, B.C. Hauback, J. Alloys Comp. 415 (2006) 284–287.
[145] Ewa Ronnebro, Eric H. Majzoub, J. Phys. Chem. B110 (2006) 25686–25691.
[146] B.M. Bulychev, K.N. Semenenko, K.B. Bitsoev, Koord. Khim. 4 (1978) 374.
[147] H. Grove, H.W. Brinks, R.H. Heyn, F.-J. Wu, S.M. Opalka, X. Tang, B.L. Laube, B.C. Hauback, J. Alloys Comp. 455 (2008) 249–254.
[148] Hilde Grove, Hendrik W. Brinks, Ole M. Løvvik, Richard H. Heyn, Bjørn C. Hauback, J. Alloys Comp. 460 (2008) 64–68.
[149] B.D. James, M.G.H. Wallbridge, Prog. Inorg. Chem. 11 (1970) 99.
[150] U. Bilici, Second International Boron Symposium, vol. 23–25, 2004, pp. 119–125.
[151] Çetin Çakanyıldırım, Metin Gürü, Int. J. Hydrogen Energy 33 (2008) 4634–4639.
[152] Cooper HBH. Production of alkali metal borohydrides. US Patent No: 3473899; 1969.
[153] Yoshitsugu Kojima, Tetsuya Haga, Int. J. Hydrogen Energy 28 (2003) 989–993.
[154] J.M. Adams, Metal Boron Compounds & Boranes, Interscience Publishers, 1964.
[155] A.M. Soldate, J. Am. Chem. Soc. 69 (1947) 987.
[156] S.C. Abrahams, J. Kalnajs, J. Chem. Phys. 22 (1954) 434.
[157] W.H. Stockmayer, C.C. Stephenson, J. Chem. Phys. 21 (1953) 1311.
[158] R. Lindsay Davis, H.L. Kennard Colin, J. Solid State Chem. 59 (1985) 393–396.
[159] P. Fischer, A. Zuttel, Proceeding of EPDIC-8, Trans. Tech. Publication Ltd., 2002.
[160] S. Kumar Ravhi, L. Cornelius Andrew, Appl. Phys. Lett. 87 (2005) 261916.
[161] C. Moysïes Araïujo, A. Blomqvist, R. Ahuja, J. Phys.: Condens. Matter. 20 (2008) 122202.
[162] H.I. Schlesinger, C. Brown Herbert, A.E. Finholt, R. Gilbreath James, R. Hoekstra Henry, K. Hyde Earl, J. Am. Chem. Soc. 75 (1953) 215.
[163] Donald D. Wagman, William H. Evans, Vivian B. Parker, Richard H. Schumm, Iva Halow, Sylvia M. Bailey, Kenneth L. Churney, Ralph L. Nuttall, J. Phys. Chem. Ref. Data 18 (1989) 1807.
[164] Y. Marrero-Alfonso Eyma, R. Gray Joshua, A. Davis Thomas, A. Matthews Michael, Int. J. Hydrogen Energy 32 (2007) 4717–4722.
[165] J.C. Ingersoll, N. Mani, J.C. Thenmozhiyal, A. Muthaiah, J. Power Sources 173 (2007) 450–457.
[166] Palanichamy Krishnan, Tae-Hyun Yang, Won-Yong Lee, Chang-Soo Kim, J. Power Sources 143 (2005)17–23.
[167] J.S. Zhang, W.N. Delgass, T.S. Fisher, J.P. Gore, J. Power Sources 164 (2007) 772–781.
[168] B.H. Liu, Z.P. Li, J. Power Sources 187 (2009) 527–534.
[169] Y. Shang, R. Chen, Energy Fuels 20 (2006) 2142–2148.
[170] Yinghong Shang, Rui Chen, Energy Fuels 20 (2006) 2149–2154.
[171] Steven C. Amendola, Stefanie L. Sharp-Goldman, M. Saleem Janjua, Michael T. Kelly, Phillip J. Petillo, Michael Binder, J. Power Sources 85 (2000)186–189.
[172] C. Amendola Steven, L. Sharp-Goldman Stefanie, M. Saleem Janjua, C. Spencer Nicole, T. Kelly Michael, J. Petillo Phillip, Binder Michael, Int. J. Hydrogen Energy 25 (2000) 969–975.
[173] Yoshitsugu Kojima, Ken-ichirou Suzuki, Kazuhiro Fukumoto, Megumi Sasaki, Toshio Yamamoto, Yasuaki Kawai, Hiroaki Hayashi, Int. J. Hydrogen Energy 27 (2002) 1029–1034.
[174] Dong Hua, Yang Hanxi, Ai Xinping, Cha Chuansin, Int. J. Hydrogen Energy 28 (2003)1095–1110.
[175] Ying Bai, Chuan Wu, Feng Wu, Baolian Yi, Mater. Lett. 60 (2006) 2236–2239.
[176] Lluís Soler, Jorge Macanás, Maria Muñoz, Juan Casado, Int. J. Hydrogen Energy 32 (2007) 4702–4710.
[177] R. Peña-Alonso, A. Sicurelli, E. Callone, G. Carturan, R. Raj, J. Power Sources 165 (2007) 315–323.
[178] Yeji Lee, Youngmi Kim, Harim Jeong, Misook Kang, J. Ind. Eng. Chem. 14 (2008) 655–660.
[179] U.B. Demirci, O. Akdim, P. Miele, J. Power Sources 192 (2009) 310–315.
[180] J.F. Mao, X.B. Yu, Z.P. Guo, H.K. Liu, Z. Wu, J. Ni, J. Alloys Comp. 479 (2009) 619–623.
[181] H.I. Schlesinger, C. Brown Herbert, J. Am. Chem. Soc. 62 (1940) 3429–3435.
[182] H.I. Schlesinger, C. Brown Herbert, R. Hoekstra Henry, R. Rapp Louis, J. Am. Chem. Soc. 75 (1953) 199–204.
[183] D. Goerrig, German Patent (1958)1077644.
[184] O. Friedrichs, F. Buchter, A. Borgschulte, A. Remhof, C.N. Zwicky, Ph. Mauron, M. Bielmann, A. Züttel, Acta Mater. 56 (2008) 949–954.
[185] P.M. Harris, E.P. Meibohm, J. Am. Chem. Soc. 69 (1947) 1231–1232.
[186] J-Ph. Soulié, G. Renaudin, R. Černý, K. Yvon, J. Alloys Comp. 346 (2002) 200–205.
[187] Kazutoshi Miwa, Nobuko Ohba, Shin-ichi Towata, Yuko Nakamori, Shin-ichi Orimo, Phys. Rev. B 69 (2004) 245120.
[188] E.M. Fedneva, V.L. Alpatova, V.I. Mikheeva, Russ. J. Inorg. Chem. 9 (1964) 826.
[189] A. Züttel, P. Wenger, S. Rentsch, P. Sudan, Ph. Mauron, Ch. Emmenegger, J. Power Sources 118 (2003) 1–7.
[190] D.S. Stasinevich, G.A. Egorenko, Russ. J. Inorg. Chem. 13 (1968) 341–343.
[191] A. Züttel, S. Rentsch, P. Fischer, P. Wenger, P. Sudan, Ph. Mauron, Ch. Emmenegger, J. Alloys Comp. 356–357 (2003) 515–520.
[192] Yuko Nakamori, Shin-ichi Orimo, J. Alloys Comp. 370 (2004) 271–275.
[193] K. Miwa, N. Ohba, S. Towata, Y. Nakamori, S. Orimo, J. Alloys Comp. 404–406 (2005) 140–143.

[194] John J. Vajo, Sky L. SkeithFlorian Mertens, J. Phys. Chem. B 109 (2005) 3719–3722.
[195] Ming Au, Arthur Jurgensen, J. Phys. Chem. B 110 (2006) 7062–7067.
[196] Yoshitsugu Kojima, Ken-ichirou Suzuki, Yasuaki Kawai, J. Power Sources 155 (2006) 325–328.
[197] Yao Zhang, Wan-Sheng Zhang, Ai-Qin Wang, Li-Xian Sun, Mei-Qiang Fan, Hai-Liang Chu, Jun-Cai Sun, Tao Zhang, Int. J. Hydrogen Energy 32 (2007)3976–3980.
[198] Z.Z. Fang, X.D. Kang, H.B. Dai, M.J. Zhang, P. Wang, H.M. Cheng, Scripta Mater. 58 (2008) 922–925.
[199] Seon-Ah Jin, Jae-Hyeok Shim, Young Whan Cho, Kyung-Woo Yi, Oleg Zabara, Scripta Mater. 58 (2008) 963–965.
[200] R. Köster, K. Ziegler, Angew. Chem. 69 (3) (1957) 94.
[201] (a) V.N. Konoplev, V.M. Bakulina, Izv. Akad. Nauk. SSR, Ser. Khim. 1 (1971) 159;
(b) V.N. Konoplev, Russ. J. Inorg. Chem. 25 (1980) 964.
[202] Yuko Nakamori, Kazutoshi Miwa, Akihito Ninomiya, Haiwen Li, Nobuko Ohba, Shin-ichi Towata, Andreas Züttel, Shin-ichi Orimo, Phys. Rev. B 74 (2006) 045126.
[203] Krzysztof Chłopek, Christoph Frommen, Aline Léon, Oleg Zabara, Maximilian Fichtner, J. Mater. Chem., 33 (2007) 3496–3503.
[204] V.N. Konoplev, V.M. Bakulina, Russ. Chem. Bull. 20 (1971) 136.
[205] P. Vajeeston, P. Ravindran, A. Kjekshus, H. Fjellvåg, Appl. Phys. Lett. 89 (2006) 071906.
[206] R. Černý, Y. Filinchuk, H. Hagemann, K. Yvon, Angew. Chem. Int. Ed. 46 (2007) 5765–5767.
[207] Jae-Hyuk Her, Peter W. Stephens, Yan Gao, Grigorii L., Soloveichik, Job Rijssenbeek, Matthew Andrus, Ji-Cheng Zhao, Acta Cryst. B63 (2007) 561–568.
[208] Lyci George, Vadym Drozd, Surendra K. Saxena, Elisa Gil Bardaji, Maximilian Fichtner, J. Phys. Chem. C, 113 (2009) 486–492.
[209] V. Ozolins, E.H. Majzoub, C. Wolverton, Phys. Rev. Lett. 100 (2008) 135501.
[210] H.-W. Li, K. Kikuchi, Y. Nakamori, K. Miwa, S. Towata, S. Orimo, Scripta Mater. 57 (2007) 679–682.
[211] T. Matsunaga, F. Buchter, P. Mauron, M. Bielman, Y. Nakamori, S. Orimo, N. Ohba, K. Miwa, S. Towata, A. Züttel, J. Alloys Comp. 459 (2008) 583–588.
[212] H.-W. Li, K. Kikuchi, Y. Nakamori, N. Ohba, K. Miwa, S. Towata, S. Orimo, Acta Mater. 56 (2008) 1342–1347.
[213] Grigorii L. Soloveichik, Yan Gao, Job Rijssenbeek, Matthew Andrus, Sergei Kniajanski, Robert C. Bowman Jr., Son-Jong Hwang, Ji-Cheng Zhao, Int. J. Hydrogen Energy, 34 (2009) 916–928.
[214] E. Wiberg, R.Z. Hartwimmer, Z. Naturforsch. 10b (1955) 295.
[215] E. Wiberg, H. Noth, R.Z. Hartwimmer, Z. Naturforsch. 10b (1955) 292.
[216] V.I. Mikheeva, L.V. Titov, Zh. Neorg. Khim. 9 (1964) 789.
[217] Kazutoshi Miwa, Masakazu Aoki, Tatsuo Noritake, Nobuko Ohba, Yuko Nakamori, Shin-ichi Towata, Andreas Züttel, Shin-ichi Orimo, Phys. Rev. B 74 (2006) 155122.
[218] Gagik Barkhordarian, Thomas Klassen, Martin Dornheim, Rüdiger Bormann, J. Alloys Comp., 440 (2007) L18–L21.
[219] Y. Nakamori, H.-W. Li, K. Kikuchi, M. Aoki, K. Miwa, S. Towata, S. Orimo, J. Alloys Comp. 446–447 (2007) 296–300.
[220] Ewa Rönnebro, Eric H. Majzoub, J. Phys. Chem. B, 111 (2007) 12045–12047.
[221] F. Buchter, Z. Łodziana, A. Remhof, O. Friedrichs, A. Borgschulte, Ph. Mauron, A. Zuttel, D. Sheptyakov, G. Barkhordarian, R. Bormann, K. Chłopek, M. Fichtner, M. Sørby, M. Riktor, B. Hauback, S. Orimo, J. Phys. Chem. B 112 (2008) 8042.
[222] Yaroslav Filinchuk, Ewa Rönnebro, Dhanesh Chandra, Acta Mater. 57 (2009) 732–738.
[223] M.D. Riktor, M.H. Sørby, K. Chłopek, M. Fichtner, F. Buchter, A. Züttel, B.C. Hauback, J. Mater. Chem. 17 (2007) 4939.
[224] N.S. Kedrova, N.N. Mal'tseva, Russ. J. Inorg. Chem. 22 (1977) 973.
[225] P. Vajeeston, P. Ravindran, H. Fjellvåg, J. Alloys Comp. 446–447 (2007) 44–47.
[226] M. Aoki, K. Miwa, T. Noritake, N. Ohba, M. Matsumoto, H.-W. Li, Y. Nakamori, S. Towata, S. Orimo, Appl. Phys. A 92 (2008) 601–605.
[227] Jae-Hun Kim, Seon-Ah Jin, Jae-Hyeok Shim, Young Whan Cho, Scripta Mater., 58 (2008) 481–483.
[228] Jae-Hun Kim, Jae-Hyeok Shim, Young Whan Cho, J. Power Sources, 181 (2008) 140–143.
[229] V.I. Mikheeva, N.N. Maltseva, L.S. Alekseeva, Zh. Neorg. Khim. 13 (1968) 1303.
[230] H.I. Schlesinger, Univ. of Chicago, Navy Contract No. N 173-S-9820, 1945–1946.
[231] J. Marks Tobin, R. Kolb John, Chem. Rev. 77 (1977) 263.
[232] Eun Jeon, YoungWhan Cho, J. Alloys Comp., 422 (2006) 273.
[233] Sesha Srinivasan, Diego Escobar, Yogi Goswami, Elias Stefanakos, Int. J. Hydrogen Energy, 33 (2008) 2268.
[234] Sesha Srinivasan, Diego Escobar, Michael Jurczyk, Yogi Goswami, Elias Stefanakos, J. Alloys Comp., 462 (2008) 294.
[235] P. Choudhury, R. Venkat, Bhethanabotla, Elias Stefanakos, Phys. Rev. B 77 (2008) 134302.
[236] S. Kumar Ravhi, L. Cornelius Andrew, J. Alloys Comp. 476 (2009) 5.
[237] G. Renaudin, S. Gomes, H. Hagemann, L. Keller, K. Yvon, J. Alloys Comp. 375 (2004) 98.
[238] P. Vajeeston, P. Ravindran, A. Kjekshus, H. Fjellvåg, J. Alloys Comp. 387 (2005) 97.
[239] J. van Setten Michiel, A. de Wijs Gilles, Phys. Rev. B 77 (2008) 165115.
[240] Toyoto Sato, Kazutoshi Miwa, Yuko Nakamori, Kenji Ohoyama, Hai-Wen Li, Tatsuo Noritake, Masakazu Aoki, Shin-ichi Towata, Shin-ichi Orimo, Phys. Rev. B, 77 (2008) 104114.
[241] Kazutoshi Miwa, Nobuko Ohba, Shin-ichi Towata, Yuko Nakamori, Andreas Züttel, Shin-ichi Orimo, J. Alloys Comp., 446–447 (2007) 310.
[242] T. Hayashi, K. Tobita, Y. Nakamori, S. Orimo, J. Nucl. Mater. 386–388 (2009) 119.
[243] E. Anne Nickels, Martin Owen Jones, William I. F. David, Simon R. Johnson, Rebecca L. Lowton, Marco Sommariva, Peter P. Edwards, Angew. Chem. 47 (2008) 2817.
[244] Xiao-Bing Xiao, Wei-Yang Yu and Bi-Yu Tang, J. Phys.: Condens. Matter. 20 (2008) 445210.
[245] Leo Seballos, Jin Z. Zhang, Ewa Rönnebro, Julie L. Herberg, E.H. Majzoub, J. Alloys Comp. 476 (2009) 446.
[246] Gay Lussac, L.J. Thernard, Ann. Phys. 32 (1809) L.
[247] A.W. Titherley, J. Am. Soc., Trans. 65 (1894) 504.
[248] F.W. Dafert, R. Miklanz, Manotsh. Chem. 31 (1910) 981.
[249] O. Ruff, H. Geoges, Ber. Dtsh. Chem. Ges. 44 (1911) 502.
[250] S. Orimo, Y. Nakamori, J.R. Eliseo, A. Züttel, C.M. Jensen, Chem. Rev. 107 (2007) 4111–4132.
[251] P. Chen, Z. Xiong, J. Luo, J. Lin, K.L. Tan, Nature 420 (2002) 302–304.
[252] L. Shaw, W. Osborn, T. Markmaitree, X. Wan, J. Power Sources 177 (2008) 500–505.
[253] R. Juza, Opp. K. Z. Anorg. Allg. Chem. 266 (1951) 313.
[254] H. Von, R. Jacobs, Z. Juza, Anorg. Allg. Chem. 391 (1972) 271.
[255] Kazutoshi. Miwa, Nobuko Ohba, Shin-ichi Towata, Phys. Rev. B 71 (2005) 195109.
[256] S. Orimo, Y. Nakamori, G. Kitahara, K. Miwa, N. Ohba, T. Noritake, S. Towata, Appl. Phys. A 79 (2004) 1765–1767.
[257] Y. Song, Z.X. Guo, Phys. Rev. B 74 (2006) 195120.
[258] J.B. Yang, X.D. Zhou, Q. Cai, W.J. James, W.B. Yelon, Appl. Phys. Lett. 88 (2006) 041914.
[259] S. Chellappa Raja, D. Chandra, M. Somayazulu, S.A. Gramsch, R.J. Hemley, J. Phys. Chem. B 111 (2007) 10785–10789.
[260] T. Noritake, H. Nozaki, M. Aoki, S. Towata, G. Kitahara, Y. Nakamori, S. Orimo, J. Alloys Compd. 393 (2005) 264.
[261] K. Ohoyama, Y. Nakamori, S. Orimo, K. Yamada, J. Phys. Soc. Jpn. 74 (2005) 483.
[262] R.A. Forman, J. Chem. Phys. 55 (1971) 1987.
[263] M.P. Balogh, C.Y. Jones, J.F. Herbst Jr., L.G. Hector, M. Kundrat, J. Alloys Compd. 420 (2006) 326.
[264] P. Chen, Z. Xiong, J.Z. Luo, J.Y. Lin, K.L. Tan, J. Phys. Chem. B 107 (2003) 10967–10970.
[265] Y.H. Hu, E. Ruckenstein, J. Phys. Chem. A 107 (2003) 9737–9739.
[266] T. Ichikawa, S. Isobe, N. Hanada, H. Fujii, J. Alloys Compd. 365 (2004) 271.
[267] T. Ichikawa, N. Hanada, S. Isobe, H.Y. Leng, H. Fujii, J. Alloys Compd. 404–406 (2005) 435–438.
[268] J.H. Yao, C. Shang, K.F. Aguey-Zinsou, Z.X. Guo, J. Alloys Compd. 432 (2007) 277–282.
[269] T. Ichikawa, N. Hanada, S. Isobe, H. Leng, H. Fujii, J. Phys. Chem. B 108 (2004) 7887–7892.
[270] L. Shaw, R. Ren, T. Markmaitree, W. Osborn, J. Alloys Compd. 448 (2008) 263.
[271] J.Z. Hua, J.H. Kwaka, Z. Yanga, W. Osbornb, T. Markmaitreeb, L.L. Shawb, J. Power Sources 181 (2008) 116–119.
[272] V.H. Jacobs, R. Juza, Z. Anorg. Allg. Chem. 370 (1969) 254–261.
[273] A.P. Terentiew, Z. Anorg. Allg. Chem. 162 (1927) 349–353.
[274] Y. Nakamori, G. Kitahara, S. Orimo, J. Power Sources 138 (2004) 309–312.
[275] M.H. Sørby, Y. Nakamura, H.W. Brinks, T. Ichikawa, S. Hino, H. Fujii, B.C. Hauback, J. Alloys Compd. 428 (2007) 297.
[276] Wang, J. Phys. Chem. C 112 (2008) 18264–18269.
[277] H.Y. Leng, T. Ichikawa, S. Hino, N. Hanada, S. Isobe, H. Fujii, J. Phys. Chem. B 108 (2004) 8763–8765.
[278] J.J. Hu, Z.T. Xiong, G.T. Wu, P. Chen, J. Power Sources 159 (2006) 120.
[279] J.J. Hu, G.T. Wu, Y.F. Liu, Z.T. Xiong, P. Chen, J. Phys. Chem. B 110 (2006) 14688.
[280] Y. Kojima, Y. Kawai, Chem. Commun. 19 (2004) 2210–2211.
[281] Y. Kojima, Y. Kawai, N. Ohba, J. Power Sources 159 (2006) 81–87.
[282] T.M. Kahmer (Publication Manager), W.F. McClune (Editor-in-Chief), S.N. Kabekkodu (Editor of Calculated Patterns), H.E. Clark (Staff Scientist), Powder Diffraction File, International Centre for Diffraction Data (JCPDS), Pennsylvania, USA, 2004.
[283] H. Leng, T. Ichikawa, S. Hino, N. Hanada, S. Isobe, H. Fujii, J. Power Sources 156 (2006) 166–170.
[284] S. Hino, T. Ichikawa, H. Leng, H. Fujii, J. Alloys Comp. 398 (2005) 62–66.
[285] R. Juza, H. Schumacher, Z. Anorg. Allg. Chem. 324 (1963) 278.
[286] J. Senker, H. Jacobs, M. Muller, W. Press, H.M. Mayer, R.M. Ibberson, Z. Anorg Allg. Chem. 625 (1999) 2025.
[287] W.F. Luo, J. Alloy. Compd. 381 (2004) 284–287.
[288] W. Luo, S. Sickafoose, J. Alloys Compd. 407 (2006) 274–281.
[289] Z.T. Xiong, G.T. Wu, J.J. Hu, P. Chen, Adv. Mater. 16 (2004) 1522–1525.
[290] Z.T. Xiong, J.J. Hu, G.T. Wu, P. Chen, W.F. Luo, K. Gross, J. Wang, J. Alloys Compd. 398 (2005) 235–239.
[291] T. Ichikawa, K. Tokoyoda, H. Leng, H. Fujii, J. Alloys Compd. 400 (2005) 245–248.
[292] W. Luo, J. Alloys Compd. 385 (2004) 316.
[293] J. Rijssenbeek, Y. Gao, J. Hanson, Q. Huang, C. Jones, B. Toby, J. Alloys Compd. 454 (2008) 233.
[294] Y. Wang, M.Y. Chou, Phys. Rev. B 76 (2007) 014116.
[295] I. Velikokhatnyi Oleg, N. Kumta Prashant, Mater. Sci. Eng. B 140 (2007) 114–122.

[296] Z. Maa, M.Y. Chou, J. Appl. Phys. 104 (2008) 083519.
[297] K. Gross, W. Luo, Presentation at MRS annual meeting, Boston, November 2004.
[298] J. Yang, A. Sudik, C. Wolverton, J. Alloys Compd. 430 (2007) 334–338.
[299] S.V. Alapati, J.K. Johnson, D.S. Sholl, J. Phys. Chem. B 110 (2006) 8769.
[300] A.R. Akbarzadeh, V. Ozolins, C. Wolverton, Adv. Mater. 19 (2007) 3233.
[301] W. Osborn, T. Markmaitree, L.L. Shaw, J. Power Sources 172 (2007) 376–378.
[302] Y. Liu, K. Zhong, M. Gao, J. Wang, H. Pan, Q. Wang, Chem. Mater. 20 (2008) 3521–3527.
[303] K. Toyokoda, S. Hino, T. Ichikawa, K. Okamoto, H. Fujii, J. Alloys Compd. 439 (2007) 337–341.
[304] H. Wu, J. Am. Soc. 130 (2008) 6515–6522.
[305] P. Chen, Presented at A Variety of Metal–N–H Systems for Hydrogen Storage, Session P14: Focus Session: Hydrogen Storage I: Media, Los Angeles, CA, March 2005.
[306] Z.T. Xiong, G.T. Wu, J.J. Hu, P. Chen, presented at Symp. P Materials for Rechargeable Batteries, Hydrogen Storage and Fuel Cells; 3rd Int. Conf. on Materials for Advanced Technologies (ICMAT 2005) and 9th Int. Conf. on Advanced Materials (ICAM 2005), Singapore, July 2005.
[307] Z.T. Xiong, G.T. Wu, J.J. Hu, P. Chen, Catal. Today 120 (2007) 287.
[308] Z.T. Xiong, G.T. Wu, J.J. Hu, P. Chen, J. Power Sources 159 (2006) 167.
[309] L. Jun, Z.Z. Fang, J. Phys. Chem. B 109 (2005) 20830–20834.
[310] Z.T. Xiong, G.T. Wu, J.J. Hu, Y. Lui, P. Chen, W. Luo, J. Wang, Adv. Funct. Mater. 17 (2007) 1137–1142.
[311] (a) T.C. Bissot, R.W. Parry, J. Am. Chem. Soc. 77 (1955) 3481;
(b) G. Kodama, R.W. Parry, J.C. Carter, J. Am. Chem. Soc. 81 (1959) 3534;
(c) C.E. Nordman, C. Reimann, J. Am. Chem. Soc. 81 (1959) 3538;
(d) G.E. Ryschkewitsch, J. Am. Chem. Soc. 82 (1960) 3290;
(e) D.F. Gaines, R. Schaeffer, J. Am. Chem. Soc. 86 (1964) 1505;
(f) K.W. Böddeker, S.G. Shore, R.K. Bunting, J. Am. Chem. Soc. 88 (1966) 4396;
(g) R. Komm, R.A. Geanangel, R. Liepins, Inorg. Chem. 22 (1983) 1684;
(h) C.W. Yoon, L.G. Sneddon, J. Am. Chem. Soc. 128 (2006) 13992;
(i) H.V.K. Divyabalanage, R.P. Shrestha, Angew. Chemie. Int. Ed. 46 (2007) 8995;
(j) F.H. Stephens, Ammonia Borane: Dalton Trans. (2007) 2613–2626.
[312] S.G. Shore, R.W. Parry, J. Am. Chem. Soc. 77 (1955) 6084.
[313] Mayer Erwin, Inorg. Chem. 12 (1973) 1954.
[314] S.G. Shore, R.W. Parry, J. Am. Chem. Soc. 80 (1958) 12.
[315] S.G. Shore, R.W. Parry, J. Am. Chem. Soc. 80 (1958) 8.
[316] M.G. Hu, J.M. Van Paasschen, R.A. Geanangel, J. Inorg. Nucl. Chem. 39 (1977) 2147.
[317] V.P. Sorokin, B.I. Vesmina, N.S. Klimova, Zh. Neorg. Khim. 8 (1963) 66.
[318] S.G. Shore, Dissertation, Univ. of Michigan.
[319] R.M. Adams, J. Beres, A. Dodds, A.J. Morabito, Inorg. Chem. 10 (1971) 2072.
[320] S.G. Shore, K.W. Boddeker, Inorg. Chem. 3 (1964) 914.
[321] P.V. Ramachandran, P.D. Gagare, Inorg. Chem. 46 (2007) 7810.
[322] D.J. Heldebrant, A. Karkamkar, J.C. Linehan, T. Autrey, Energy Environ. Sci. 1 (2008) 156.
[323] E.L. Lippert, W.N. Lipscomb, J. Am. Chem. Soc. 78 (1956) 503.
[324] E.W. Hughes, J. Am. Chem. Soc. 78 (1956) 502.
[325] V.P. Sorokin, B.V. Vesnina, N.S. Klimovc, Russ. J. Inorg. Chem. 8 (1963) 32.
[326] C.F. Hoon, E.C. Reynhardt, J. Phys. C: Solid State Phys. 16 (1983) 6129–6136.
[327] W.T. Klooster, T.F. Koetzle, P.E.M. Siegbahn, T.B. Richardson, R.H. Crabtree, J. Am. Chem. Soc. 121 (1999) 6337.
[328] R. Custelcean, J.E. Jackson, Chem. Rev. 101 (2001) 1963–1980.
[329] J. Li, F. Zhao, F. Jing, J. Chem. Phys. 116 (2002) 25.
[330] R. Custelcean, Z.A. Dreger, J. Phys. Chem. B 107 (2003) 9231–9235.
[331] R.D. Suenram, L.R. Thorne, Chem. Phys. Lett. 78 (1981) 157–160.
[332] L.R. Thorne, R.D. Suenram, F.J. Lovas, J. Chem. Phys. 78 (1983) 167.
[333] A. Gutowska, L. Li, Y. Shin, Chongmin M. Wang, Xiaohong S. Li, John C. Linehan, R. Scott Smith, Bruce D. Kay, Benjamin Schmid, Wendy Shaw, Maciej Gutowski, Tom Autrey, Angew. Chemie. Int. Ed. 44 (2005) 3578.
[334] F. Baitalow, J. Baumann, G. Wolf, K. Jaenicke-Rößler, G. Leitner, Thermochim. Acta 391 (2002) 159–168.
[335] G. Wolf, J. Baumann, F. Baitalow, F.P. Hoffmann, Thermochim. Acta 343 (2000) 19–25.
[336] M. Bowden, T. Kemmitt, W. Shaw, N. Hess, J. Linehan, M. Gutowski, Mater. Res. Soc. Symp. Proc. 927 (EE–02–04) (2006) 0927.
[337] M.E. Bluhm, M.G. Bradley, R. Butterick III, U. Kusari, L.G. Sneddon, J. Am. Chem. Soc. 128 (2006) 7748–7749.
[338] J.S. Wang, R.A. Geanangel, Inorg. Chim. Acta 148 (1988) 185–190.
[339] F. Cheng, H. Ma, Y. Li, J. Chen, Inorg. Chem. 46 (2007) 788–794.
[340] H. Stephens Frances, R. Tom Baker, H. Matus Myrna, J. Grant Daniel, A. Dixon David, Angew. Chem. Int. Ed. 46 (2007) 746.
[341] C.A. Jaska, K. Temple, A.J. Lough, I. Manners, J. Am. Chem. Soc. 125 (2003) 9424.
[342] M.C. Denney, V. Pons, T.J. Hebden, D.M. Heinekey, K.I. Goldberg, J. Am. Chem. Soc. 128 (2006) 12048.
[343] J. Keaton Richard, M. Blacquiere Johanna, R. Tom Baker, J. Am. Chem. Soc. 129 (2007) 1844.
[344] S.D. Benedetto, M. Carewska, C. Cento, P. Gislon, M. Pasquali, S. Scaccia, P.P. Prosini, Thermochim. Acta 441 (2006) 184–190.
[345] D.J. Heldebrant, A. Karkamkar, N.J. Hess, M. Bowden, S. Rassat, F. Zheng, K. Rappe, T. Autrey, Chem. Mater. 20 (2008) 5332–5336.
[346] S. Hausdorf, F. Baitalow, G. Wolf, Florian O.R.L. Mertens, Int. J. Hydrogen Energy 33 (2008) 608–614.
[347] D. Neiner, A. Karkamkar, J.C. Linehan, B. Arey, T. Autrey, S.M. Kauzlarich, J. Phys. Chem. C 113 (2009) 1098–1103.
[348] P.A. Storozhenko, R.A. Svitsyn, V.A. Ketsko, Russ. J. Inorg. Chem. 50 (2005) 980.
[349] M. Chandra, Q. Xu, J. Power Sources 156 (2006) 190–194.
[350] M. Chandra, Q. Xu, J. Power Sources 159 (2006) 855.
[351] Q. Xu, M. Chandra, J. Power Sources 159 (2006) 855.
[352] M. Chandra, Q. Xu, J. Power Sources 168 (2007) 135.
[353] T. Umegaki, J.M. Yan, X.B. Zhang, H. Shioyama, N. Kuriyama, Q. Xu, Int. J. Hydrogen Energy 34 (2009) 2303–2311.
[354] George Chizinsky, Gordon G. Evans, Thomas R. P. Gibb Jr., M. John Rice Jr., J. Am. Chem. Soc.77 (1955) 3164–3165.
[355] M. Appel, J.P. Frankel, J. Chem. Phys. 42 (1965) 3984.
[356] Sabrina Sartori, Susanne M. Opalka, Ole Martin Løvvik, Matylda N. Guzik, Xia Tang, Bjørn C. Hauback, J. Mater. Chem., 18 (2008) 2361.
[357] Sabrina Sartori, Andreas Istad-Lem, Hendrik W. Brinks, Bjørn C. Hauback, Int. J. Hydrogen Energy 34 (2009) 6350–6356.
[358] Frank M. Brower, Norman E. Matzek, Paul F. vReigler, Harold W. Rinn, Charles B. Roberts, Donald L. Schmidt, John A. Snover, Kazuji Terada, J. Am. Chem. Soc. 98 (976) 2450–2453.
[359] W. Turley June, W. Rinn Harold, Inorg. Chem. 8 (1969) 18.
[360] W. Brinks Hendrik, Istad-Lem Andreas, C. Hauback Bjørn, J. Phys. Chem. B 110 (2006) 25833–25837.
[361] H.W. Brinks, W. Langley, C.M. Jensen, J. Graetz, J.J. Reilly, B.C. Hauback, J. Alloys Comp. 433 (2007) 180–183.
[362] H.W. Brinks, C. Brown, C.M. Jensen, J. Graetz, J.J. Reilly, B.C. Hauback, J. Alloys Comp. 441 (2007) 364–367.
[363] Volodymyr A. Yartys, Roman V. Denys, Jan Petter Maehlen, Christoph Frommen, Maximilian Fichtner, Boris M. Bulychev, Hermann Emerich, Inorg. Chem. 46 (2007) 1051–1055.
[364] Graetz Jason, J. Reilly James, J. Alloys Comp. 424 (2006) 262–265.
[365] G.C. Sinke, L.C. Walker, F.L. Oetting, D.R. Stull, J. Chem. Phys. 47 (1967) 2759.
[366] B. Baranowski, M. Tkacz, Z. Physk. Chem. N.F. 135 (1983) 27.
[367] K. Konovalov Sergei, M. Bulychev Boris, Inorg. Chem. 34 (1995) 172–175.
[368] Graetz Jason, J. Reilly James, J. Phys. Chem. B 109 (2005) 22181–22185.
[369] I.M.K. Ismail, T. Hawkins, Thermochim. Acta 439 (2005) 32–43.
[370] Gary Sandrock, James Reilly, Jason Graetz, Wei-Min Zhou, John Johnson, James Wegrzyn, J. Alloys Comp. 421 (2006) 185–189.
[371] S. Orimo, Y. Nakamori, T. Kato, C. Brown, C.M. Jensen, Appl. Phys. A 83 (2006) 5.
[372] V. Iosub, T. Matsunaga, K. Tange, M. Ishikiriyama, K. Miwa, J. Alloys Comp. 484 (2009) 426–430.